THE

LONDON, EDINBURGH, AND DUBLIN

PHILOSOPHICAL MAGAZINE

AND

JOURNAL OF SCIENCE.

[SEVENTH SERIES.]

NOVEMBER 1937.

LXVI. *The Determination of Specific Heats by an Eddy Current Method.*—Part II. *Experimental.*

By W. J. THOMAS, *B.Sc., Ph.D., and* R. M. DAVIES, *D.Sc., F.Inst.P., University College of Wales, Aberystwyth* *.

CONTENTS.

SECTION 1.

General Description of the Method.

THE general principles underlying the method have already been discussed in Section 1 of Part I. of this work. It has been shown (equation (1.10)) that the specific heat s of the material of the core of the coil is given by

$$s = \frac{(W-W_0).t}{JM\Theta_c} = \frac{I^2(R-R_0).t}{JM\Theta_c} \quad . \quad . \quad (1.1)$$

* Communicated by the Authors.

where

Θ_c=temperature rise of the specimen (corrected for radiation losses, etc.) in time t,

M=mass of the specimen,

I=virtual value of the coil current (assumed constant),

W, W_0=power expended in the coil with and without the core respectively,

R, R_0=effective resistance of the coil with and without the core respectively,

J=electrical equivalent of heat.

If Θ_c be measured in °C., t in seconds, M in grammes, W and W_0 in international watts, I in international amperes, R and R_0 in international ohms, then J=4·1835 $\pm$0·0007 international joule calorie $\frac{-1}{15}$, and the specific heat s is thus given in terms of the 15° C. calorie.

Thus the determination of s requires the determination of

(*a*) the mass of the specimen,

(*b*) the corrected temperature rise Θ_c of the specimen,

(*c*) the change in power $(W-W_0)$ or, alternatively, $I^2(R-R_0)$,

(*d*) the time interval t.

Before proceeding to describe the details of the experiment, it will be convenient to discuss and consider in a general way the requirements for the measurements of these quantities.

With regard to measuring the temperature rise in the specimen, it is obvious that a thermocouple method will be most convenient. The null method, employing a potentiometer system, was found to be unsatisfactory, as the maximum temperature attained by the specimen had to be estimated, and was thus liable to error. This difficulty was overcome by employing a deflexion method, since the rise of temperature can be followed much better with this method than with the null method. The experimental arrangements are described in Section 2(*c*).

Turning next to the measurement of the change in power in the coil $(W-W_0)$ or $I^2(R-R_0)$, it has been shown in Section 2 (*b*) (vi.) of Part I. of this work that both the virtual value and the frequency of the current

should be as high as possible ; it is also desirable that the source of alternating current should yield a steady output.

Preliminary experiments were carried out with a motor generator as a source of alternating current, and although ample power was available the output was unsteady, and, in addition, the frequency was too low. For these reasons it was decided to use a valve oscillator, and a combined oscillator and amplifier, described in Section 2 (*a*), was built; this is capable of delivering 25 watts, and its performance has been found to be satisfactory in every way.

In order to measure the change in power expended in the coil a moving coil dynamometer was first built ; this consisted of a fixed " current " coil and a moving " voltage " coil suspended by a phosphor bronze strip, but since the ratio $\left(\frac{W-W_0}{W_0}\right)$ is a small fraction of the order of 0·05 it soon became clear that the usual deflexion method was not sensitive enough. A null method was then adopted in which the couple acting on the " voltage " coil due to the alternating current was neutralized by a couple due to a direct current passing through another fixed " current " coil and also through another " voltage " coil wound on the same former as the alternating current " voltage " coil. This method again proved to be too insensitive. Finally, it was decided to measure the effective resistance of the coil and the current passing through it, and this was found to be sufficiently sensitive and accurate. This method will be described in detail in Section 2 (*d*).

The time interval t was at first observed by means of a stop-clock, but this was later replaced by a chronograph method of timing ; by means of this time intervals can be determined to within 1/15 second.

Section 2.

Experimental Arrangements.

(a) *The Valve Oscillator and Amplifier.*

Following the publication of an article [1] describing a high-efficiency two-stage amplifier, a combined oscillator and amplifier (fig. 1) based upon this article was built. The oscillator itself is a dynatron oscillator, which has

been found to be satisfactory and to be simpler in design than the ordinary grid-coupled triode system.

In fig. 1 V_1 represents a screen grid valve (Mazda, S.G. 215), LC an oscillatory circuit, L being a coil consisting of about 1300 turns of 28 S.W.G. copper wire, and C a variable mica condenser whose value ranges from 0·005 microfarads to 3·5 microfarads. The potentiometer R_1 (50,000 ohms) and the resistance R_2 (100,000 ohms) serve to vary the potentials on the anode and the screen grid until the condition for maintained oscillation is obtained.

Fig. 1.

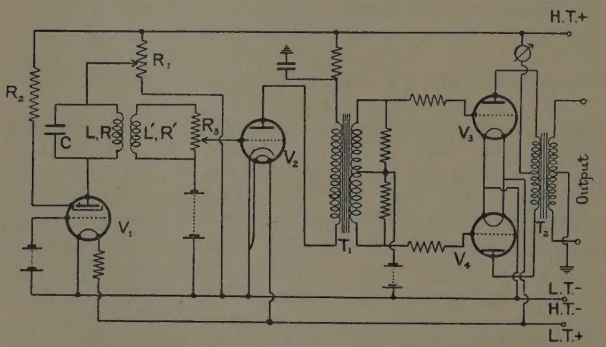

The valve oscillator.

The output of the dynatron, obtained from the coupling coil L′, consisting of about 2000 turns of 28 S.W.G. copper wire, is fed into a potentiometer R_3 (500,000 ohms), and the controlled potential is applied to the grid of an indirectly heated triode V_2 (Osram ML4). The magnified signal then passes through the primary of a push-pull transformer T_1 (1 : 3·5 ratio), the two secondaries of which supply the grids of the valves V_3 and V_4 (Osram PX 25 A) which are in a modified push-pull arrangement. The anodes of these valves are connected to a push-pull output transformer T_2, designed to suit the impedance of the external load.

The anode voltages are supplied by a battery of accumulators whose voltage is 400 volts. This voltage is, in the case of the valves V_3 and V_4, applied to the anodes

through the centre-tapped primary of the transformer T_2. In the case of the valve V_2 the potential applied to the anode is 200 volts, a resistance (10,000 ohms) being connected in the anode lead to effect a voltage drop of 200 volts. The filament currents are supplied from two large capacity accumulators connected in series. The necessary negative grid-bias voltages are supplied by means of dry batteries. The grid-bias voltages used are : $-4{\cdot}5$ volts for V_1, -15 volts for V_2, and -120 volts for V_3 and V_4.

(b) *The Coil and Associated Apparatus.*

It has been shown in Section 2 (*b*) (ii.) of Part I. of this work that it is necessary that the coil in which the specimen is inserted should have a large number of turns per unit length and, at the same time, as large a current as possible should be passed through the coil. These two quantities are not independent, and they are largely determined by the constants of the output transformer on the valve oscillator as indicated in the preceding section. A considerable amount of preliminary work was carried out with a view to finding the optimum size and shape of the coil and the optimum wire diameter ; it was found that for specimens whose lateral dimensions were of the order of the optimum dimensions (see Sections 2 and 3 of Part I. of this work) satisfactory results were obtained with a multi-layer solenoid consisting of 500 to 1000 turns of 28 S.W.G. copper wire, the internal diameter of the solenoid being about 5 cm. to cm., and its winding length about 10 cm. to 15 cm.

It was soon realized that it would be necessary to maintain the temperature of the coil constant by dispersing, in some way or other, the heat generated by the alternating current flowing in the coil. Two undesirable effects follow if this heat is not dispersed by some means :

(*a*) There is a gradual increse in the value of the resistance of the coil, due to the gradual rise in its temperature, and hence it is impossible to determine (as shown in Section 2 (*d*)) the change in resistance of the coil due to the insertion of the specimen with any reasonable accuracy.

(*b*) Heat is transferred by convection etc. to the specimen, thus causing a rise in temperature which is

not accounted for by the measured change in power in the coil.

Fig. 2.

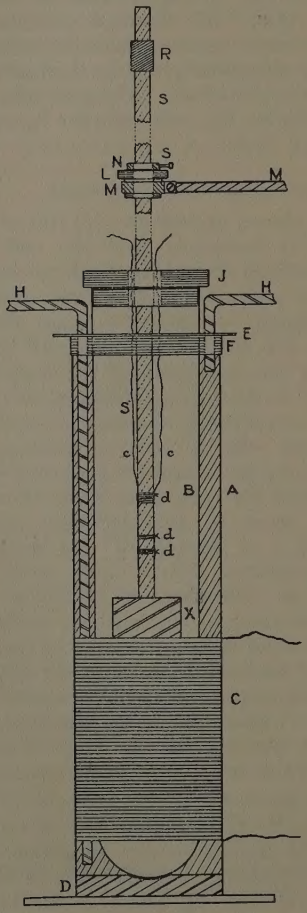

The coil arrangement.

In connexion with (*a*) an additional difficulty arises from the fact that, in general, there is a change in the

value of the alternating current passing through the coil when a specimen is inserted in the coil; this is due to the change in the magnitude and nature of the load imposed on the valve oscillator by the coil. This brings about a change in the temperature of the coil, and this is naturally followed by a change in its resistance. These difficulties were solved by adopting the jacket arrangement shown in fig. 2, and by keeping the value of the alternating current flowing through the coil constant whether the specimen is inserted or not.

The coil C, whose winding length is about 13 cm., consists of 700 turns of 28 S.W.G. copper wire; it is wound on the lower end of a glass jar A, whose length is about 46 cm. and whose outside diameter is 5·6 cm. The direct current resistance of the coil is 21·87 ohms, and its effective a.c. resistance for the frequencies used in the present work has the same value; the inductance of the coil is about 13 millihenries. The length of the jar A has been chosen so that the effective a.c. resistance of the coil C is unaltered if the specimen is removed from the upper end of the jar to a considerable distance away. This jar forms the external wall of a water-jacket, the inner wall of the jacket being another glass tube B, whose diameter is 3·8 cm., and which is closed at its lower end. This inner tube is kept fixed in a central position inside the outer jar by inserting its lower end into a cavity bored in a rubber stopper D, which is squeezed tightly into the bottom of the jar. The upper end of the inner tube passes through a brass annulus E, this being soldered to a short brass tube F which fits over the outer surface of the jar. The inlet and outlet tubes, H, also pass through holes drilled in this annulus, and all contacts between the brass and glass surfaces are made watertight by sealing them with white sealing-wax.

The specimen, X, is attached to the lower end of an ebonite rod S, about 30 inches long, in the manner indicated in fig. 3. The rod, whose diameter is 5/16 inch, is turned at its lower end, a, to a diameter of $\frac{1}{8}$ inch over a length of about $\frac{1}{4}$ inch. A hole, a', is drilled in the specimen, so that the portion a of the rod will fit tightly into it and thus hold the specimen rigidly to the rod. b represents the "hot" junction of the thermo-couple, and a hole is drilled in the specimen to

accommodate this. Care is always needed to ensure that there is good thermal contact between the junction *b* and the specimen when the rod is inserted in the specimen. The thermocouple leads *c*, shown dotted, lie in grooves cut in the lower portion of the rod, and are held in position by means of thread, *d*, tied round the rod.

Reverting to fig. 2, the rod passes through an ebonite cap J, which is a slack fit in the upper end of the tube B ; the rod also passes through a short piece of ebonite

Fig. 3.

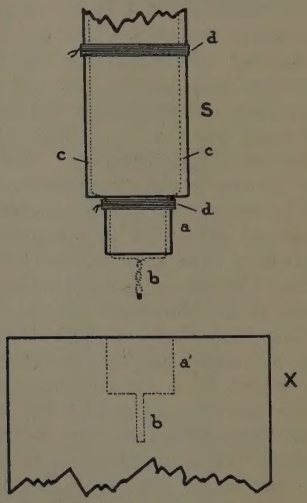

Method of supporting the specimen.

tube L, held in position by means of a clamp M. The tube L, together with the cap J, form two bearings which limit the motion of the rod and the specimen to vertical motion along the axis of the tube ; the rod can be fixed in any desired position by means of a brass ring and screw arrangement N. A piece of thick rubber tubing, R, fits tightly over the rod near its upper end, and its position is adjusted so that when the arrangement N is released the rod S drops, and its motion is arrested when the specimen is well inside the coil. The thermocouple leads pass through two holes in the cap J, and they

can move freely through these holes as the rod S is moved up and down.

Another glass water-jacket (not shown in the figure) surrounds the outside of the coil, and water from an electrically regulated thermostat is pumped through the two jackets, thus maintaining the coil at a constant temperature of approximately 20° C. The present arrangement avoids the difficulties described at the beginning of this section, and, in addition, it ensures that when the specimen is inserted in the coil the temperature of its surroundings is constant and known. This latter point is important in calculating the correction for heat losses for the specimen (see Section 3).

The advantage of this arrangement, in addition to that of temperature control, is that the specimen always assumes the same position inside the coil when N is released. The value of this will be made clear in Section 4.

(c) *The Measurement of Temperature.*

The temperature measurements were carried out with a Manganin-Eureka thermocouple made with wires of 26 S.W.G. The variable temperature, or "hot," junction of the thermocouple was formed by spot welding the two wires in a carbon arc. The remaining ends of the thermocouple wires are soldered to the bared ends of two lengths of rubber-covered copper-wire. These ends are waxed into two glass tubes about 4 inches long, these tubes being tied together to form the constant temperature, or "cold," junction of the couple. The "cold" junction was kept during calibration, and subsequent temperature measurements, in a water-bath immersed in the electrically regulated thermostat from which is taken the water supply for the jackets of Section 2(*b*).

As indicated in Section 1, it was found necessary to use a deflexion method for measuring temperatures by means of the thermocouple. For this purpose the thermocouple is connected in series with a moving coil galvanometer and a resistance box, the resistance of the latter being adjusted so that the galvanometer is critically damped; let the total resistance of this circuit be R_t ohms.

In the course of preliminary experiments the galvanometer scale was calibrated directly by finding the galvanometer deflexions, δ, corresponding to known differences of temperature, θ, between the " hot " and " cold " junctions. It was found, however, that the calibration curves obtained in this way varied from time to time. This variation was traced to the effects of fluctuations in room-temperature on the thermocouple-galvanometer circuit. Let e be the thermocouple e.m.f. (in volts) corresponding to a given temperature difference θ between the " hot " and " cold " junctions ; e is, naturally, independent of room-temperature. The galvanometer deflexion δ produced by e is equal to $e/k\mathrm{R}_t$, where k is the sensitivity of the galvanometer in amperes per scale division ; k and R_t are both affected by changes in room-temperature.

This source of error can be avoided by determining the e.m.f. or (e, θ) calibration curve of the thermocouple, and by determining or eliminating the value of $k\mathrm{R}_t$ before and after each experiment, *i. e.*, by calibrating the galvanometer before and after each experiment.

In determining the (e, θ) calibration curve of the thermocouple the e.m.f. of the thermocouple was determined by a potentiometer method ; temperatures were measured, using a Beckmann thermometer calibrated at the N.P.L. It was found that the relation between e.m.f. and temperature difference was linear within the range used.

Two independent calibrations gave the values 39·97 and 39·92 microvolts per °C. for e_1, the thermocouple e.m.f. per unit temperature difference between the junctions. The two calibrations thus agree to within 0·13 per cent., and in the calculation of results the mean value of e_1 (39·95 microvolts per °C.) was used.

The rise in temperature of the specimen during an experiment is usually of the order of 2° C. In order to determine this rise the thermocouple is connected, as shown in fig. 4, in series with the sensitive reflecting galvanometer G_1, the resistance r_1 (0·1 ohm), and a variable resistance R_3 of the order of 100 ohms. The value of R_3 is adjusted so that the galvanometer is critically damped, the correct value being determined in a preliminary experiment. The total resistance of this circuit is $\mathrm{R}_t = r_1 + \mathrm{R}_3 + \mathrm{G}$, where G is the resistance of the

galvanometer G_1, and if δ is the galvanometer deflexion the e.m.f. e of the thermocouple is equal to $k\delta R_1$, where k is the galvanometer sensitivity.

In order to find the temperature difference θ corresponding to the galvanometer deflexion δ it has been shown that it is necessary to calibrate the galvanometer G_1 by determining or eliminating the value of the product kR_1, and this may be done by means of the circuit shown in fig. 5. It is seen that the circuit consists of a potentiometer circuit $E_1 r_1 R_1 R_2$, together with the circuit of fig. 4

Fig. 4.

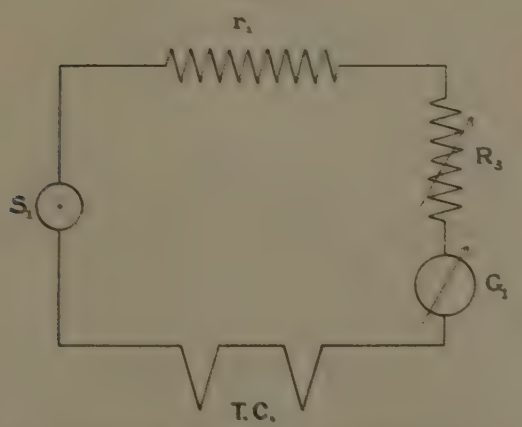

The thermocouple circuit used for temperature measurements.

and a key S_2 which is used to short-circuit the thermocouple TC during this part of the experiment. After short-circuiting TC, in order to eliminate R_1, the resistance R_3 is increased by an amount equal to the sum of r_1 and the resistance of the thermocouple and its leads (7·5 ohms). The following procedure is then adopted :

(i.) The current i_2 in the circuit $S_1 S_2 G_1 R_3$ is adjusted by varying R_1 and R_2, R_1 being kept constant and the key K_3 being open ; i_2 is adjusted so that the deflexion δ' of the galvanometer spot (from the extreme right to the extreme left position) when i_2 is reversed by means of X is very nearly equal to the deflexion δ obtained

in the course of the experiment. Then if i_1 is the current in the main circuit $E_1 r_1 R_1 R_2$

$$i_2 = i_1 r_1 / R_l = k\delta'/2. \quad . \quad . \quad . \quad . \quad . \quad (2.1)$$

(ii.) The current i_1 in the main circuit $E_1 r_1 R_1 R_2$ is found by balancing against the standard cell C. In this part of the experiment K_3 is closed and S_1 open, and the ratio of R_1 to R_2 is varied, their sum being kept constant

Fig. 5.

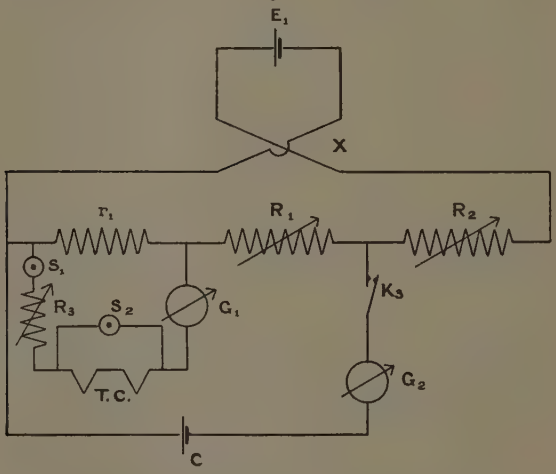

Circuit for the calibration of the galvanometer.

and equal to its previous value, until balance is shown by the galvanometer G_2.

If R_1' is the value of R_1 at balance, and E is the e.m.f. of the standard cell,

$$E = i_1(R_1' + r_1). \quad . \quad . \quad . \quad . \quad . \quad (2.2)$$

Thus equation (2.1) becomes

$$i_2 = \frac{k\delta'}{2} = \frac{E r_1}{R_l(R_1' + r_1)}$$

and

$$e = k R_l \delta = 2 . \frac{\delta}{\delta'} . \frac{E r_1}{(R_1' + r_1)} . \quad . \quad . \quad . \quad (2.3)$$

Thus e is determined in terms of the deflexions δ and δ', the e.m.f. E of the standard cell and the known resistances r_1 and R_1'.

For example, in one calibration

$$\delta' = 9{\cdot}97_3 \text{ cm.}, \quad E = 1{\cdot}0178_6 \text{ volt}, \quad r_1 = 0{\cdot}1000 \text{ ohm},$$

$$R_1' = 2494{\cdot}36 \text{ ohms},$$

from which

$$e = 8{\cdot}184_9 \times \delta \text{ microvolts.} \quad . \quad . \quad . \quad (2.4)$$

It should be added that δ and δ' are usually of the order of 100 millimetres, and that it is possible to read δ and δ' to within about 0·05 millimetre by means of a magnifying lens. In addition, since δ and δ' are very nearly equal any possible deviations from a linear relation between current and galvanometer deflexion are eliminated.

(d) *The measurement of the change in power expended in the coil.*

For the reasons given in Section 1 it was decided to measure the coil current I and the change $(R - R_0)$ in effective coil resistance rather than to measure directly the change in power $(W - W_0)$.

The change $(R - R_0)$ in the effective coil resistance is best measured by means of an a.c. bridge described in Section 2(*d*) (i.). As regards the measurement of the current I, it is clear that the value of I which appears in equations (1.10) of Part I. and (1.1) of Part II. is the r.m.s. value, and for this reason it is best to measure I by means of an a.c. meter which measures r.m.s. values rather than by means of a meter which measures peak or mean values. For this reason it was decided to use a vacuo-junction galvanometer system for the measurement of the current, since such a system, if calibrated with direct current, will indicate true r.m.s. values whatever be the wave-form of the alternating current. The experimental details of this measurement are described in Section 2(*d*) (ii.).

(i.) *The measurement of the change in effective coil resistance.*

The effective resistance of the coil and changes in its effective resistance can be measured by means of an

equal-arm Rayleigh bridge (fig. 6), in which P and Q represent the ratio arms.

The coil RL, described in Section 2 (*b*), is connected in series with a shunted vacuo-junction T, which is used to measure the current through the coil as described in Section 2 (*d*) (ii.); the heater resistance of the vacuo-junction is 3 ohms, while the value of the shunt is 0·25 ohm. RL and T form the third arm of the bridge, whilst the remaining arm consists of a Tinsley variable Self-Inductor R_1L_1 (range 5·5–140 millihenries), connected in series with a variable resistance S, which is shunted by another variable resistance *s*.

Fig. 6.

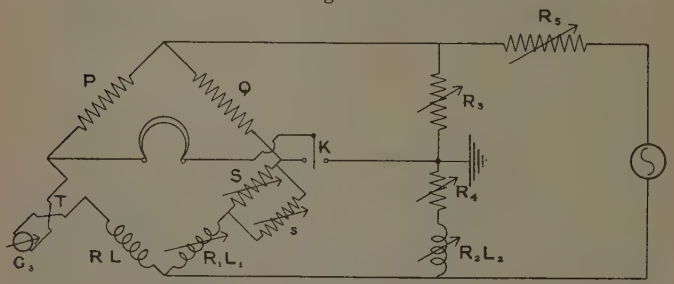

The Rayleigh bridge.

In order to eliminate earth capacity effects the Wagner earthing device is employed, and, as shown in the diagram, the appropriate form for the Rayleigh bridge consists of a variable resistance R_3 in one arm and a variable self-inductance R_2L_2 in series with a variable resistance R_4 in the other. The junction of the two arms is earthed. The range of L_2 is from 44 to 600 millihenries. K is a two-way key by means of which the telephones can be brought into the main bridge or into the auxiliary bridge at will. Exact balance is obtained by alternately balancing the main and auxiliary bridges two or three times.

In order to maintain the current through the coil constant a variable resistance R_5 is inserted between the bridge and the source. Since it is only the *change* in the effective resistance of the coil that is required the values of the resistance of the vacuo-junction T and that of the variable inductance R_1L_1 need not be known

provided that they remain constant ; the only resistances which need be known are S and s.

If R_0 and R be the values of the effective resistance of the coil without and with the specimen respectively, and if r_0 and r be the corresponding values of the net resistance of S and s at balance, then

$$(R-R_0)=(r-r_0). \quad . \quad . \quad . \quad . \quad . \quad (2.5)$$

In deducing this equation it is assumed that the resistance T of the vacuo-junction, together with its shunt, remains constant. In general the resistance of a vacuo-junction depends on the current which flows through it, and this might give rise to considerable error in the present experiment if the current through the vacuo-junction were allowed to vary and if the vacuo-junction were unshunted. Actually the shunt resistance is considerably less than the vacuo-junction resistance, so that changes in the vacuo-junction resistance have little effect on the value of T ; in addition the current through the vacuo-junction is kept constant. It is therefore justifiable to assume that the resistance of the vacuo-junction together with its shunt remains constant.

It is also assumed that the resistance R_1 of the variable self-inductance remains constant during an experiment ; this self-inductance is wound with copper-wire, and hence the value of R_1 will depend on the room-temperature and on the current flowing through it. Since the time required for an experimental run is about 15 minutes there will be little variation in room-temperature in this period ; furthermore, the current through the inductance remains constant, since the current through the coil RL is kept constant. It is therefore justifiable to assume that R_1 is constant.

(ii.) *The measurement of current.*

As stated above, the r.m.s. value of the current through the coil is measured by means of a vacuo-junction galvanometer system, the system being calibrated by means of a direct current. In the course of preliminary experiments it was found that the calibration of the vacuo-junction circuit varied on account of such causes as fluctuations in room-temperature ; in order to avoid

such variations it was decided to calibrate the circuit before each separate specific heat determination. The procedure adopted was to pass a direct current through the heater of the vacuo-junction until a certain predetermined deflexion was obtained ; the direct current giving this deflexion was then measured by a potentiometer method in terms of resistances and the e.m.f. of a standard cell. In the subsequent specific heat determination the current through the coil RL of fig. 6 is adjusted by means of the rheostat R_5 until the deflexion is exactly equal to that used in the direct current calibration. When this procedure is adopted the r.m.s. value of the alternating current is equal to the direct current used in calibration, and the vacuo-junction and associated galvanometer may be regarded as transfer instruments used to determine an alternating current in terms of direct current standards. It should be added that some vacuo-junctions give unequal deflexions on reversal of a direct current passing through the heater ; preliminary experiment showed that the vacuo-junction used in the present work did not suffer from this defect, and hence it was possible to perform the calibration without reversing the direct current used for calibration. The vacuo-junction was protected from the effects of draughts by being placed in a box packed with cotton-wool.

The circuit used for the direct current calibration is shown in fig. 7, in which $E_1 r_1 R_1 R_2$, G_2, and C represent respectively the potentiometer circuit, galvanometer, and standard cell shown in fig. 5. T represents the vacuo-junction and G_3 its associated galvanometer ; by means of the double-pole double-throw switch, K_2, T can be connected either in the RL arm of the a.c. bridge of fig. 6 or in the calibrating circuit of fig. 7. E_2 is a 4-volt accumulator which supplies the direct current used for calibrating T and G_3 ; this current can be varied by means of the rheostat R_4, consisting of a wire rheostat in series with a carbon rheostat, the former being used for coarse adjustment and the latter for fine adjustment. This portion of the circuit includes a four-terminal resistance r_2 whose value is $1{\cdot}993_5$ ohm. The method of carrying out the calibration is as follows —

(i.) The key K_2 is switched over to its left-hand position, the double-pole double-throw key K_1 is switched

over to its right-hand position, the tapping key K_3 being open. The current through the vacuo-junction T is then adjusted by means of R_4 until the deflexion of the galvanometer G_3 is equal to some predetermined value. Let I be the current in this circuit under these conditions.

(ii.) The potential drop Ir_2 across r_2 due to the current I is then balanced against the p.d. between the points A and B in the potentiometer circuit. This balance

Fig. 7.

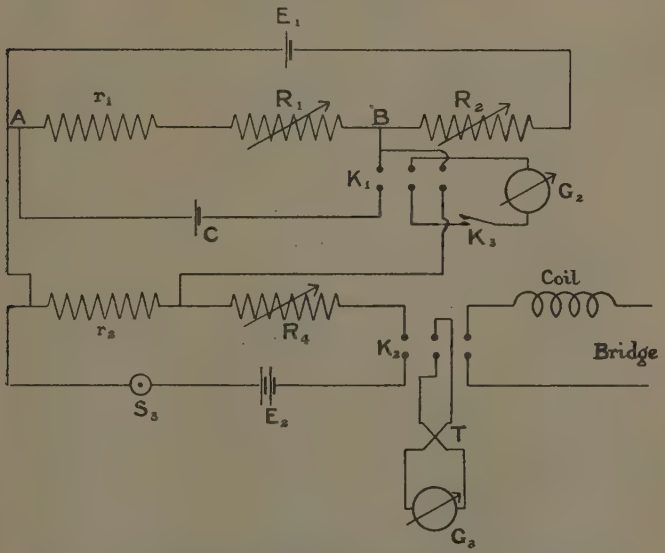

Circuit for the calibration of the vacuo-junction and galvanometer by direct current.

condition is attained by varying the ratio of R_1 to R_2, the galvanometer G_2 being used to indicate balance. If i' be the current in the main potentiometer circuit at balance, then

$$Ir_2 = i'(R_{1a} + r_1), \quad . \quad . \quad . \quad . \quad (2.6)$$

where R_{1a} is the value of R_1 under these conditions.

(iii.) Finally, the value of the current i' is determined by balancing the p.d. between A and B against the standard cell C. To do this the key K_2 is placed in its

neutral position and K_1 in its left-hand position. Balance is obtained by varying the ratio of R_1 to R_2, their sum being kept constant and equal to its value in stage (ii.) above.

Let R_{1b} be the value of R_1 when this balance is obtained, then

$$E = i'(R_{1b}+r_1), \quad . \quad . \quad . \quad . \quad . \quad (2.7)$$

where E is the e.m.f. of the standard cell. From equations (2.6) and (2.7) it follows that

$$I = \frac{E}{r_2} \cdot \frac{(R_{1a}+r_1)}{(R_{1b}+r_1)}, \quad . \quad . \quad . \quad . \quad . \quad (2.8)$$

or, in terms of the numerical values of E, r_1, and r_2,

$$I = \frac{1{\cdot}0178_6}{1{\cdot}9935} \cdot \frac{(R_{1a}+0{\cdot}1)}{(R_{1b}+0{\cdot}1)}$$

$$= 0{\cdot}5119_9 \cdot \frac{(R_{1a}+0{\cdot}1)}{(R_{1b}+0{\cdot}1)}. \quad . \quad . \quad . \quad (2.9)$$

In practice it is convenient to group together the separate circuits shown in figs. 5 and 7.

Section 3.

The Correction for Heat Losses from the Specimen.

During the early stage of this work considerable difficulty was experienced in the accurate evaluation of the correction for heat losses due to radiation etc. from the specimen to its surroundings. If the initial temperature of the specimen is approximately the same as that of its surroundings, the "cooling" correction proves to be of the same order of magnitude as the observed rise of temperature; this is due to the fact that the rate of rise of temperature during the experiment is very small, being usually of the order of 0·002° C. per second. The correction may be reduced to a small value if the specimen is heated over a range of temperature extending equally on either side of the temperature of the surroundings. The transfer of heat from the surroundings to the specimen in the first half of the experiment is then nearly equal to the loss of heat from the specimen during the second half. The correction is deduced in the following manner: fig. 8 represents

the relation between the temperature, θ, of the specimen during an experimental run, and time t. The point A (t_1, θ_1) represents the instant at which the specimen is introduced into the coil ; the point B (t_2, θ_2) represents the instant at which the current through the coil is switched off, and C (t_3, θ_3) an instant after the specimen has been allowed to cool for a period.

Fig. 8.

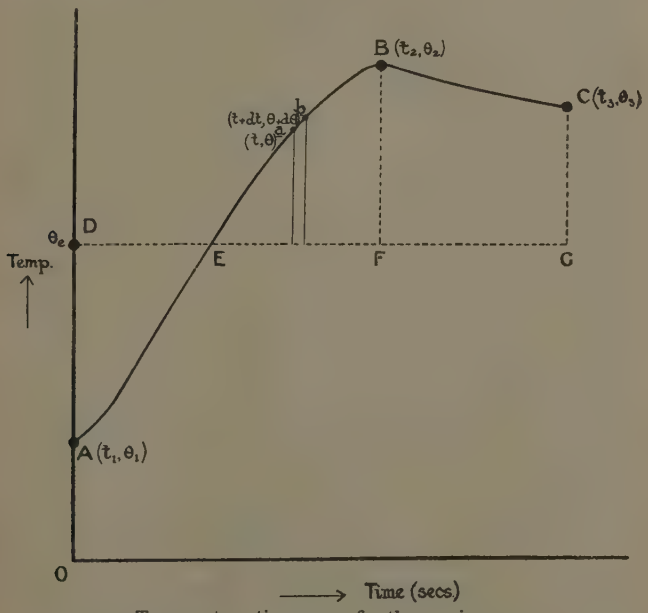

Temperature-time curve for the specimen.

The temperature θ_e of the surroundings of the specimen is kept constant (as described in Section 2 (*b*) by means of the water-jacket system which surrounds the specimen ; experiment shows that θ_e becomes equal to the temperature of the thermostat (20·0° C.) within about half an hour of starting the flow of water through the jackets. The relation of θ_e with time is thus given by a straight line DG of ordinate θ_e parallel to the t-axis.

If A_1=(area BEF)−(area DEA),

A_2=area BCGF;

the corrected rise of temperature, Θ_c, is given by

$$\Theta_c=(\theta_2-\theta_1)+\frac{A_1}{A_2}(\theta_2-\theta_3). \quad . \quad . \quad . \quad (3.1)$$

The correction term vanishes if the area DEA of fig. 8 is equal to the area BEF. If the relation between θ and t during the " heating " period were linear, then the correction term would vanish if $(\theta_2-\theta_e)$ is equal to $(\theta_e-\theta_1)$; actually the relation is not linear. With practice it is, however, possible after a preliminary run to gauge the maximum temperature θ_2 so that the two areas DEA and BEF are very nearly equal. In all the experimental results given in Section 6 the cooling correction is small, its maximum value being about 2 per cent. of the uncorrected temperature rise $(\theta_2-\theta_1)$.

In actual practice it is found to be more convenient to plot galvanometer scale readings as ordinate rather than temperature; the above result for the cooling correction is still valid, since it has been shown in Section 2 (*c*) that the galvanometer deflexions are proportional to the difference of temperature between the " hot " and " cold " junctions of the thermocouple. For the purpose of evaluating Θ_c the times corresponding to different scale readings are obtained from the chronograph tape, and from these readings the (scale reading, time) curve is drawn. The galvanometer scale reading corresponding to the enclosure temperature, θ_e, is obtained for each experimental run by placing the bare " hot " junction of the thermocouple in the position which will be occupied by the specimen during the run. The scale reading so obtained differs usually by about a millimetre from the zero of the galvanometer on open circuit, showing that there is little difference between the temperature of the " cold " junction (*i. e.* of the thermostat) and the temperature of the surroundings of the specimen.

The values of the areas DEA and BEF are in practice determined by means of a planimeter.

By following this procedure the observed temperature rise and the cooling correction are evaluated in terms of galvanometer scale readings; for the purpose of calculating specific heats these readings are converted to degrees Centigrade by the calibration process described in Section 2 (*c*).

In the majority of the experiments the enclosure temperature was 20° C., and the temperature rise of the specimen was of the order of 2° C. (corresponding approximately to 10 cm. deflexion on the galvanometer scale).

Section 4.

Experimental Procedure.

After the valve oscillator, the thermostat, and the water-jackets have had sufficient time to become steady the galvanometer used for temperature measurement is calibrated (see Section 2 (*c*)). This is followed by calibration of the vacuo-junction with its associated galvanometer (see Section 2 (*d*) (ii.)). The vacuo-junction is then switched into the bridge arm (*v.* figs. 6 & 7), the output from the source is switched into the bridge, and the main and auxiliary bridges are balanced, the specimen being placed at some distance from the coil. The current through the bridge is adjusted so that the vacuo-junction galvanometer indicates the deflexion for which it has been calibrated.

In the meantime the "hot" junction of the thermocouple has been placed in the position later occupied by the specimen, and the galvanometer reading corresponding to the enclosure temperature is taken (see Section 3). The specimen is then mounted on the ebonite rod carrying the thremocouple leads (fig. 3). Generally the temperature of the specimen at this stage is 2° C. or 3° C. below the enclosure temperature; if necessary, the specimen is warmed or cooled by ether until this temperature difference is obtained.

The rod carrying the specimen is then adjusted so that, when released, the specimen will take up a convenient position within the coil. With the specimen in this position the bridge is balanced, the current through the coil being once more adjusted so that the deflexion of the vacuo-junction galvanometer is identical with its deflexion in the calibration experiment.

The specimen is then raised to the upper end of inner water-jacket; meanwhile the temperature of the specimen gradually increases, and the movement of the galvanometer spot indicating the temperature of the specimen is followed. The specimen is dropped into position

within the coil when its temperature is about 1° C. below that of its surroundings, *i. e.*, when the galvanometer deflexion is about 5 cm. to the left of zero. The instant at which the specimen is dropped is registered on the chronograph tape, and the galvanometer scale reading at the same instant is recorded; any slight adjustments which may be necessary in the coil current and in the bridge balance are made as quickly as possible. During the " heating " period the movement of the thermo-couple galvanometer spot is followed, and the instants at which it passes certain scale divisions are registered on the chronograph tape; at the same time the coil current and the bridge balance are checked periodically. When the desired maximum temperature of the specimen is reached the oscillator is switched off; the instant of switching off is registered on the chronograph tape, and the galvanometer scale reading at this instant is recorded.

The specimen is then allowed to cool *in situ*, and the motion of the galvanometer spot during the " cooling " period is observed just as in the " heating " period.

When the " cooling " period is completed the specimen is removed and the effective resistance of the coil without the specimen is redetermined; in most cases this effective resistance remains constant, within the limits of experimental error, throughout an experiment. Generally the effective resistance of the coil with the specimen inserted will also remain constant, but in some instances there is a slight gradual change, due to the changes in the resistivity and permeability of the specimen owing to its change of temperature; in such cases it is legitimate to take the arithemetic mean of the initial and final values, since the change with time is small and is practically linear.

Section 5.

Description of the Specimens investigated.

The main purpose of the present work was to examine the accuracy and scope of the method rather than to obtain values for the specific heats of any particular substances.

In connexion with the accuracy of the method the number of independent measurements involved in a

single specific heat determination is comparatively large, and this may lead to a large systematic error in the final result. The best test of the presence or absence of such a systematic error would be given by the determination by the present method of the specific heat of a number of specimens whose specific heats have already been determined accurately by some standard method. By the courtesy of Professor R. T. Dunbar, of the University College, Cardiff, it was possible to carry out a test of this nature, using specimens of copper, aluminium, and iron, whose specific heats had been determined to a high degree of accuracy by Dr. Ezer Griffiths [2] at Cardiff in 1912 (specimens nos. 1, 2, 3, below). As shown in Section 6 there is satisfactory agreement between the values given by Griffiths and the values obtained by the present method.

In connexion with the scope of the method the specimens investigated fall into three categories :—

(1) Metals and alloys used in the form of a homogeneous plate or cylinder, the lateral dimensions of the plate or cylinder having approximately the optimum values indicated in Sections 2 and 3 of Part I. of this work. The substances used in this way were :

(*a*) Ferro-magnetic substances :—Iron, nickel, " monel," " glowray," 48 per cent. nickel iron, " dullray."

(*b*) Non-magnetic substances of comparatively low resistivity, ρ :—Copper ($\rho \doteqdot 1{\cdot}7$ microhm cm.), aluminium ($\rho \doteqdot 3{\cdot}2$ microhm cm.).

(*c*) Non-magnetic substances of comparatively high resistivity :—Antimony ($\rho \doteqdot 40$ microhm cm.).

(2) Metals and alloys used according to the " composite cylinder " method of Section 3 (*e*) of Part I. of this work. In order to test the accuracy of this method the specific heat of a square-section cast specimen of antimony was first determined directly. This specimen was then " turned " into a cylinder, reduced in diameter, and used with a hollow copper cylinder to form a composite cylinder ; the specific heat of antimony was again determined, using this composite cylinder. The results given by the two methods are in excellent agreement (see Section 6). In addition the specific heat of a cast

sample of bismuth ($\rho \doteqdot 119$ microhm cm.) was determined by the composite cylinder method.

(3) Liquids used according to the " composite cylinder " method. The method was employed to determine the specific heat of water.

For this a hollow copper cylinder closed at one end is employed, and the water is contained in this. The " hot " junction of the thermocouple is inserted in a hole drilled in the copper, this hole being of such diameter that the junction fits tightly into it. The cylinder is thus supported by means of the thermocouple leads. The ebonite rod, S (fig. 2), is replaced in this experiment by a glass tube of the same outside diameter as the ebonite rod, drawn out to a capillary at its lower end, this capillary being immersed in the water. The upper end of the glass tube is connected to an arrangement whereby air can be forced through the tube, emerging as bubbles through the water in the cylinder. The water is thus kept well stirred throughout the experiment, to ensure uniformity of temperature throughout.

The rate of bubbling must of necessity be slow in order to avoid evaporation of the water.

A description of the substances investigated, together with their mechanical and thermal treatment, is appended below. The specimens of nickel and nickel alloys were presented to the laboratory by Messrs. Henry Wigg'n and Co., Ltd., and in the case of the annealed specimens the annealing was carried out by the donors before sending the specimens. The particulars regarding the compositions of the copper, aluminium, and iron specimens are obtained from the work of Dr. Ezer Griffiths [2].

(1) *Copper.*

Purity :—Cu = 99·95 per cent. Remaining 0·05 per cent. consists of Pb, Fe, and a very little SiO_2.

(2) *Aluminium.*

Purity :—99·90 per cent. aluminium with traces of iron.

(3) *Iron.*

Purity :—

S = 0·021 per cent., Cu = 0·040 per cent.
P = 0·005 ,, ,, O = 0·015 ,, ,,
C = 0·012 ,, ,, N = 0·0026 ,, ,,
Mn = 0·036 ,, ,, H = 0·0005 ,, ,,

Silicon trace ; Fe (by difference) = 99·87 per cent.

(4) *Nickel.*

Purity :—99·5 per cent. nickel.

Heat treatment :—

9 in. square billet, heated to about 1150° C., hot rolled to $\frac{3}{4}$ in.—re-heated, hot rolled to $\frac{1}{4}$ in., annealed sample heated to about 1150° C.

(5) 48 *per cent. Nickel Iron.*

Composition :—48 per cent. nickel, balance iron.

Heat treatment :—$7\frac{1}{2}$ in. billet, heated and rolled as for nickel.

(6) "*Dullray.*"

Composition :—33–35 per cent. nickel, 3–5 per cent. chromium, balance iron.

Heat treatment :—$7\frac{1}{2}$ in. square billet, heated and rolled as for nickel.

(7) "*Monel.*"

Composition :—67 per cent. nickel, 23 per cent. copper, 2–3 per cent. impurities.

Heat treatment :—4 in. billet, heated and rolled as for nickel.

(8) "*Glowray.*"

Composition :—65 per cent. nickel, 15 per cent. chromium, 20 per cent. iron.

Heat treatment :—$7\frac{1}{2}$ in. billet, heated to about 1250° C., hot rolled to 6 in., re-heated, hot rolled to 0·3 in., re-heated, hot rolled to $\frac{1}{4}$ in.

(9) *Antimony.*

Purity :—Unknown.

(10) *Bismuth.*

Purity :—Unknown.

TABLE I.

Experiment no.	Frequency.	Current (amps.).	Change in resistance (ohms).	Change in power (watts).	Corrected rise of temp. (°C.).	Time (seconds).	Specific heat.
			Copper.—Mass of specimen = 74·884 gm.				
1.....	1775	0·2221	$1·196_9$	0·05902	1·827	892·0	0·0917
2.....	1775	0·1971	$1·194_4$	0·04640	1·157	713·8	0·0914
3.....	1887	0·1944	$1·220_7$	0·04634	1·547	958·2	0·0916
4.....	1887	0·2156	$1·053_5$	0·04897	1·650	966·5	0·0915
5.....	1980	0·2020	$1·259_7$	0·05143	1·903	1063·5	0·0917
6.....	1980	0·1959	$1·258_7$	0·04829	1·460	869·2	0·0917
			Aluminium.—Mass of specimen = 36·638 gm.				
1.....	1775	0·1839	$1·706_5$	0·05771	1·374	780·9	0·2140
2.....	1775	0·1886	$1·701_5$	0·06051	1·736	939·7	0·2138
3.....	1887	0·1891	$1·790_0$	0·06399	1·710	877·0	0·2141
4.....	1887	0·1829	$1·765_4$	0·05908	1·611	894·1	0·2139
5.....	1980	0·1831	$1·813_6$	0·06081	1·591	857·0	0·2136
6.....	1980	0·1889	$1·818_4$	0·06487	1·667	841·4	0·2136
			Iron.—Mass of specimen = 26·039 gm.				
1.....	1775	0·2229	$1·288_1$	0·06400	1·724	314·6	0·1072
2.....	1775	0·1944	$1·310_0$	0·04951	1·885	445·4	0·1074
3.....	1887	0·1913	$1·437_7$	0·05262	1·852	412·1	0·1074
4.....	1887	0·1963	$1·444_1$	0·05563	1·459	306·3	0·1072
5.....	1980	0·1943	$1·565_0$	0·05910	1·947	384·6	0·1072
6.....	1980	0·1885	$1·572_4$	0·05584	1·777	372·1	0·1073

Section 6.

Experimental Results.

A number of independent experiments were carried out for each specimen, the frequency and coil current being varied as much as possible. All values of the specific heats relate to a temperature of 20° C.

In the case of the specimens of copper, aluminium, and iron used by Griffiths the experimental data and the results are summarized in Table I.

The mean values of the results, together with their probable errors (according to the method of least squares), and the results obtained by Griffiths for the specific heat at 20° C., are as follows :—

Table I. (*a*).

Specimen.	Griffiths.	Present Work.
Copper	$0{\cdot}0918_3$	$0{\cdot}0916_2 \pm 0{\cdot}00004$
Aluminium.	$0{\cdot}2132_7$	$0{\cdot}2138_2 \pm 0{\cdot}00006$
Iron	$0{\cdot}1074_2$	$0{\cdot}1072_9 \pm 0{\cdot}00003$

Table II.

Substance.	Mass of specimen (gm.).	Individual results.	Mean value.
Nickel (U)	61·365	$0{\cdot}1074_5$, $0{\cdot}1075_4$, $0{\cdot}1073_8$, $0{\cdot}1074_6$	$0{\cdot}1075 \pm 0{\cdot}00002$
Nickel (A)	51·192	$0{\cdot}1073_2$, $0{\cdot}1072_3$, $0{\cdot}1073_9$, $0{\cdot}1072_9$	$0{\cdot}1073 \pm 0{\cdot}00002$
48 per cent. nickel iron (U).	48·686	$0{\cdot}1131_4$, $0{\cdot}1132_0$, $0{\cdot}1129_5$, $0{\cdot}1129_5$	$0{\cdot}1131 \pm 0{\cdot}00004$
48 per cent. nickel iron (A).	50·074	$0{\cdot}1125_0$, $0{\cdot}1125_1$, $0{\cdot}1126_9$, $0{\cdot}1121_9$	$0{\cdot}1125 \pm 0{\cdot}00007$
" Dullray " (U)	49·071	$0{\cdot}1127_5$, $0{\cdot}1125_2$, $0{\cdot}1124_9$, $0{\cdot}1124_7$	$0{\cdot}1126 \pm 0{\cdot}00004$
" Dullray " (A)	49·441	$0{\cdot}1142_2$, $0{\cdot}1146_2$, $0{\cdot}1144_3$, $0{\cdot}1143_3$	$0{\cdot}1144 \pm 0{\cdot}00006$
" Monel " (U)	29·894	$0{\cdot}1080_5$, $0{\cdot}1077_4$, $0{\cdot}1078_8$	$0{\cdot}1079 \pm 0{\cdot}00006$
" Monel " (A)	39·062	$0{\cdot}1070_5$, $0{\cdot}1071_6$, $0{\cdot}1072_8$, $0{\cdot}1074_8$	$0{\cdot}1072 \pm 0{\cdot}00006$
" Glowray " (U)	32·789	$0{\cdot}1115_4$, $0{\cdot}1112_8$, $0{\cdot}11140_0$	$0{\cdot}1114 \pm 0{\cdot}00005$
Antimony	69·779	$0{\cdot}0522_2$, $0{\cdot}0520_7$, $0{\cdot}0522_4$, $0{\cdot}0520_9$	$0{\cdot}0521 \pm 0{\cdot}00006$

Note :—U = Unannealed specimen.
A = Annealed specimen.

The individual values of the specific heat obtained by the direct method, together with the mean value and the probable error, are given in Table II.

TABLE III.

Composite Cylinder Method.

	Individual results.	Mean value.
Specimen :—Antimony.		
Water equivalent of the copper cylinder. (Mass = 27·477 gm.).	2·7622, 2·7609, 2·7691	2·764
Water equivalent of the composite cylinder. (Mass = 53·232 gm.).	4·1020, 4·1054, 4·0997, 4·1031	4·102
Specific heat of antimony. (Mass = 25·755 gm.).	$0·0519_6$, $0·0520_7$, $0·0518_7$, $0·0519_8$	$2·764 \pm 0·00003$
Specimen :—Bismuth.		
Water equivalent of the copper cylinder. (Mass = 31·627 gm.).	2·9090, 2·9070, 2·9155	2·910
Water equivalent of the composite cylinder. (Mass = 74·376 gm.).	4·2258, 4·2358, 4·2308	4·231
Specific heat of bismuth. (Mass = 42·749 gm.).	$0·0307_7$, $0·0310_0$, $0·0308_8$	$0·0308_8 \pm 0·00004$
Specimen :—Water.		
Water equivalent of the copper cylinder. (Mass = 29·953 gm.).	2·7550, 2·7532, 2·7608	2·756
Water equivalent of the composite cylinder. (Mass (*a*) = 32·674 gm. (*b*) = 32·620 gm.).	(*a*) 5·5238 (*b*) 5·4568, 5·4653	(*a*) 5·524 (*b*) 5·461
Specific heat of water. (Mass (*a*) = 2·721 gm. (*b*) = 2·667 gm.).	(*a*) $1·017_3$ (*b*) $1·012_9$, $1·016_0$	$1·015 \pm 0·00009$

Turning next to the values of the specific heats obtained by the "composite cylinder" method, the individual results, together with the mean values, are given in Table III.

Section 7.

Discussion of the Results.

(a) *Accuracy of the Results.*

In estimating the accuracy of the results given by this method equation (1.1) shows that the expression for s involves :

(i.) the square of the current, I, through the coil ;
(ii.) the change in resistance, $(R-R_0)$, of the coil due to insertion of the specimen ;
(iii.) the time t for which the specimen is heated by eddy currents ;
(iv.) the mass M of the specimen ;
(v.) the corrected rise of temperature, Θ_c, of the specimen.

(i.) In evaluating I there are two possible sources of error—the error in adjusting the galvanometer deflexion to the value to be used in an experiment, and the error in measuring the direct current corresponding to this deflexion. By means of a magnifying lens it is possible to read the position of the galvanometer spot to within 0·05 millimetre, and since the deflexion is usually of the order of 9 cm. this corresponds to an error of about 0·005 in 9, *i. e.*, 0·06 per cent. in the deflexion. Since I^2 is proportional to the deflexion, the percentage error in I^2 is also *0·06* per cent. The error in measuring the direct current corresponding to a given deflexion is due partly to incorrect balancing of the potentiometer (see Section 1 (*b*)), and partly to inaccuracies in the resistance boxes forming the potentiometer. The discrimination of the potentiometer balance is of the order of 1 in 10,000, whereas the overall accuracy of the resistance boxes is about 1 in 2000. The percentage error in the measurement of the direct current is thus about 0.05 per cent., the corresponding error in I^2 being about *0·1* per cent.

(ii.) The a.c. bridge of fig. 6 can be balanced to within 0·1 ohm on the shunt s used for fine adjustment. An uncertainty of 0·1 ohm in s corresponds to an uncertainty of about 0·001 ohm in the resistance of the coil. The change, $(R-R_0)$, in the resistance of the coil is of the order of 1·5 ohm, and thus the error in the evaluation of $(R-R_0)$ is of the order of 0·001 in 1·5, *i. e.*, about *0·07* per cent.

(iii.) The time interval, t, between two points on the chronograph tape can be estimated to within 0·05 second ; the minimum value of t used in the experiments was about 200 seconds, and thus the error in t will not exceed *0·03* per cent.

(iv.) The error in the measurement of the mass, M, of the specimen is negligible.

(v.) As shown in Section 2 (*c*) in order to evaluate Θ_c the temperature rise of the specimen is determined in terms of the galvanometer deflexion (cm.), and then converted into ° C. by means of equation (2.3).

In determining the rise in temperature of the specimen in terms of the galvanometer deflexion there are two possible sources of error :—

(*a*) The estimation of the deflexion of the galvanometer spot during the " heating " period. This deflexion is of the order of 8 cm., and can be estimated to within 0·01 cm. ; thus the error due to incorrect estimation is 1 in 800, *i. e.*, *0·12* per cent.

(*b*) The error in evaluating the cooling correction, which arises from the inaccuracy in determining the reading on the galvanometer scale corresponding to the temperature of the surroundings of the specimen, θ_e. This can be determined to within 0·05 cm. of the correct value, and for a typical set of results in which the cooling correction is large, calculation shows that an uncertainty of 0·05 cm. in this quantity is equal to an uncertainty of 0·012 cm. in the value of the correction. The rise in temperature in this example was approximately 8·5 cm., so that the error in Θ_c, due to inaccuracy in the determination of θ_e is 1 in 700, *i. e.*, *0·14* per cent.

In evaluating the factor of equation (2.3) there are two possible sources of error :—

(*c*) The estimation of the deflexion of the galvanometer spot. The deflexion estimated is of the order of 10 cm., and, as stated in (i.) above, this deflexion can be estimated to within 0·005 cm., so that the maximum error in the estimation is 1 in 2000, *i. e.*, *0·05* per cent.

(*d*) The error arising partly from incorrect balancing of the potentiometer and partly due to inaccuracies in the

resistance boxes forming the potentiometer (see i.) above). This results in a maximum error of about *0·05* per cent. in the value of the above factor.

Thus the maximum error in the evaluation of θ is about *0·35* per cent.

Hence, assuming that all the errors are additive, the inaccuracy of any individual result is about **0·6** per cent.

Referring to the results given in Section 6, the following table gives the maximum discrepancy for the results obtained by the direct method for some of the specimens:—

Specimen.	Maximum discrepancy.
Copper	0·39 per cent.
Aluminium	0·23 per cent.
Iron	0·28 per cent.
Nickel (unannealed) ..	0·19 per cent.
Nickel (annealed) ...	0·19 per cent.

Turning next to the results obtained by the "composite cylinder" method, as previously stated the accuracy of this method was tested by determinations of the specific heats of antimony directly, and by the "composite cylinder" method. The results are given in Tables II. and III. The mean value obtained directly was $0{\cdot}0521_3$, whereas the mean value given by the "composite cylinder" method was $0{\cdot}0519_8$; the difference is about 0·3 per cent., and the agreement is satisfactory. Considering next the determination of the specific heat of water, the maximum discrepancy between the three results is 0·4 per cent., but the mean value is about 1·5 per cent. too large: this is to be attributed to the difficulty of obtaining uniform temperature throughout the system with the small quantities employed, and thus the method cannot be regarded as satisfactory for liquids, although the results quoted for antimony show that it is satisfactory for badly conducting solids.

It is to be expected, however, that the results obtained by the "composite cylinder" method should be less accurate than those obtained directly, since the specific heat of the cylinder core is calculated from the *difference* between the water equivalent of the composite cylinder

and that of the copper sheath. This is shown by the following table :—

Specimen.	Maximum discrepancy.
Antimony	0·40 per cent.
Bismuth	0·75 per cent.
Water	0·40 per cent.

Turning next to the absolute accuracy of the results, Table I. (*a*), giving the experimental results obtained by Griffiths and by the present method, is of interest. It is seen that the discrepancy between these two sets of results is about 0·2 per cent. for copper, about 0·25 per cent. for aluminium, and about 0·1 per cent. for iron. The excellent agreement between the two sets of results shows that the absolute accuracy of the method is satisfactory.

In addition to its use in the determination of specific heats at room-temperature the method can be adapted for use at high temperatures, and the extension of the method in this direction is now being investigated in this laboratory.

In conclusion, the authors wish to acknowledge their indebtedness to Vice-Principal Gwilym Owen for his constant interest and valuable suggestions in the course of the work, to Professor R. T. Dunbar and to Dr. Ezer Griffiths, F.R.S., for their courtesy in connexion with the standard specimens of copper, aluminium, and iron, and to Messrs. Henry Wiggin and Co., Ltd., for their gift of nickel and nickel-alloys ; one of the authors (W. J. T.) is also indebted to the University of Wales for a postgraduate studentship which enabled the work to be carried out.

8. *References.*

(1) ' Wireless World,' March 15th (1935).
(2) Griffiths, Phil. Trans. of the Royal Soc. of London, Series A, vol. ccxiii. (1913).

LXVII. *On the Relation between Thrust and Torque Distribution and the Dimensions and the Arrangement of Propeller-blades.* *By* H. Reissner, *Berlin* †.

1. *State of Knowledge.—Outline and Scope of the Problem.*

A. Betz and L. Prandtl ‡ have shown that the theory of the vortex sheet left behind the trailing edge of an aerofoil and of the induced supplementary current produced by the vortices can also be applied to the theory of the action of propeller blades.

Th. Troller §, following a suggestion of Th. v. Karman, has worked out the induced velocities for helical sheets with appropriate (or probable) vortex distributions by means of the Biot-Savart integrals, and has compared them with Prandtl's ‡ approximate solution for the edge effect of the Betz rigid helicoid for minimum induced resistance.

The exact solution of this problem, utilizing the helical symmetry of the rigid moving vortex sheets, has been given by S. Goldstein ‖ by means of a series of particular integrals, the mathematical difficulty consisting in the continuous transition from the inner to the outer field.

Of further work mention must be made of the papers of C. N. H. Lock ¶ and D. Yeatman ††, the former extending Prandtl's approximate substitution of a rigid grating for the helical rigid sheet to a grating of parallel plane sheets of prescribed potential discontinuity; the latter paper bringing forth very complete calculations from Goldstein's formulæ and comparison with recent experiments.

† Communicated by the Author.

‡ "Schraubenpropeller mit geringstem Energieverlust," A. Betz; with an Appendix by L. Prandtl. *Nachr. d. K. Ges. d. Wiss. z. Gott. Math.-Phys. Kl.* (1919).

§ "Aerodynam. Theorie und Entwurf von Luftschrauben," Th. Troller. *Abhdlgen. aus d. Aerodynamischen Inst. Aachen.* (1932). Also *Z. A. M. M.* (1928).

‖ "On the Vortex Theory of Screw Propellers," S. Goldstein. Proc. Roy. Soc. A, cxxiii. pp. 440–465 (1929).

¶ "An Application of Prandtl Theory to an Air-screw," C. N. H. Lock. R. & M. p. 1521 (1932).

†† Tables for Use in an Improved Method of Air-screw Strip Theory Calculus. R. & M. p. 1674 (1934).

Notwithstanding all this very valuable pioneering work named above, I have tried in this paper to advance further towards a rational theory which would give the interdependent relation between circulation, thrust, and torque along the blades on the one hand, and dimensions, angle settings, number of blades, and inflow velocity on the other.

Such a theory, furnishing an integral equation, exists for the much simpler two-dimensional problem † of the purely translational motion of the aerofoils of aeroplanes by bringing together and equalizing the circulation, induced velocity, changed angle of attack, and lift distribution at the centre line of the aerofoil, with the circulation and induced velocity produced by the plane trailing vortex sheet.

The analogous three-dimensional problem of the screw propeller seems not to have been attacked yet, partly perhaps on account of the unwieldy appearance of the three-dimensional Biot-Savart Integral and partly because the methods appropriate for the induction of a rigid sheet are not adapted for an arbitrary distribution of vorticity in non-rigid helical sheets.

A certain connexion to these questions and a resemblance to the starting point of this paper is to be found in a paper by H. Lamb ‡, which treats the magnetic field of an electric helical stream-line. A paper by S. Kawada § also must be quoted. Lamb develops the Biot-Savart integral at some convenient points in a trigonometrical series along the circumference, making use of the helical symmetry and comparing the coefficients, which are functions of the radius, with solutions of the potential problem. In the inner field he finds they are Bessel functions of the first kind; in the outer field Bessel functions of the second kind.

S. Kawada § has published a formula for the velocities induced by a circulation of constant magnitude along the blade. He expresses the solution in the inner field by a

† See also the work of L. Prandtl, A. Betz, M. Munk, B. Eck, E. Trefftz, H. Glauert, C. Wieselsberger, I. Lotz, Hueber, R. Fuchs in Aerodynamik,' Berlin, ii. ' Theorie der Luftkräfte,' von R. Fuchs. Also Th. v. Karman, *Z. A. M. M.* pp. 56–61 (1935).

‡ " The Magnetic Field of a Helix," H. Lamb. Proc. Cambr. Phil. Soc. xxi. pp. 477–481 (1923).

§ " Induced Velocity by Helical Vortices," S. Kawada. Journ. of Aeron. Sciences, p. 86 (1936).

term linear in the angular coordinate and by an infinite trigonometric series of Bessel functions, while outside the blade radii a series of Bessel functions alone continues the solution. The author does not say so, but it is easily seen that the vortex system producing this flow of constant circulation consists of the helical vortex lines running through the blade tips and an axial straight vortex line of the combined infinite strength of the helical lines.

The starting point chosen here is the (non-homogeneous) Laplace-Poisson differential equation for the velocity potential produced by a source distribution of helical symmetry, but otherwise arbitrarily prescribable.

It is shown first that a source distribution linear along the circumference between each pair of neighbouring blades allows a very simple one-term solution for an otherwise arbitrary source distribution, but is of necessity connected with discontinuous functions of potential and of radial velocity along the blade-centre lines. The next step then is to find a solution produced by the same source distribution, but not involving the discontinuity sheets. This solution, found by harmonic analysis, when subtracted from the first gives the flow induced by a set of helical sheets of radially prescribable discontinuity, viz., by a circulation function arbitrarily prescribable along the blade centre lines and zero outside.

The circulation, arbitrary during this process, becomes definite when it is taken into account that the circulation gives the lift distribution, which again depends on the width and the angle of attack of the blade section, and also, finally, that this angle depends on the induced velocity.

In this manner a second equation between circulation and induced velocity is obtained, from which, in principle, either the circulation, lift, and induced velocity can be determined from the blade width, angle setting, and number of blades or (simpler) inversely the width and angle function of the blades can be determined for a given circulation and lift function and number of blades.

Another way of looking at the question of how the circulation may be distributed is given by a maximum problem. In fact, as the thrust and torque of a propeller as functions of circulation, induced velocity and profile resistance can be given by equations ; it may be asked, for instance, which distributions of circulation and induced

velocity give maximum thrust for a given torque if the functional relation between them found before is observed. Betz has announced the simple theorem that neglecting the profile resistance the induced velocity for minimum induced resistance is the same as induced by a rigid sheet, and Goldstein has given a very remarkable analysis leading to the corresponding circulation. Here a more general integral equation, which takes into account the profile resistance and is of a structure different from the Biot-Savart integral and from the series solution of Goldstein, is developed.

The theory is here obtained in its simplest form inasmuch as it replaces the blades by lines, *i. e.*, by the front

Fig. 1.

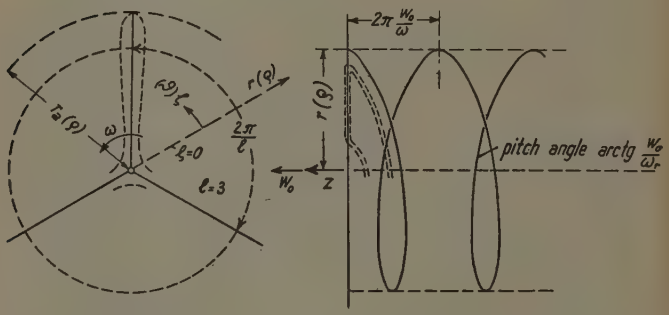

edges of the infinitely thin trailing vortex sheets, and does not consider the contraction of the propeller jet. A generalization taking account of the thickness and width of the blade and perhaps also of the contraction will be necessary later on.

The electromagnetic analogy between the velocity field created by helical vortex lines and the magnetic field generated by helical electric currents was the reason for quoting the paper of Lamb, although this paper was concerned with an electromagnetic topic.

This analogy might perhaps lead to the following convenient method of testing the hydrodynamic theory of the air-screw where it has been mathematically developed, and of investigating and enlarging the con-

sequences of theoretical conceptions where mathematical treatment has so far been too difficult.

Take a frame of a helical surface and on it an assembly of isolated electric wire circuits of horseshoe shape, of which some are shown on fig. 1. Send through each wire an electric current of strength proportional to a prescribed vortex strength of a small strip of the vortex sheet.

Then the magnetic field could be determined (surveyed) for instance, by means of galvanometers, and would then yield a complete description of the corresponding field of induced velocities.

The wires might be arranged, not only on cylindrical helices, as mathematical treatment has been forced to assume until now, but also on helical lines of converging radius and changing pitch so as further to refine the theory of the air-screw.

2. *The First Relation between Circulation Function and Induced Velocities.*

The calculation of velocities induced by a vortex sheet might be effected by Biot-Savart's (three-dimensional) integral, but we avoid geometric inconveniences and apparent singularities of the integrand, if we here prefer to make use of the differential equation of potential flow produced by a certain distribution of sources and sinks equivalent to the vortex sheets.

This may be formulated in the following way :—

The continuity equation for the field of the velocity vector $\mathbf{c}$ containing a source density $q(x, y, z)$ is given by

$$\operatorname{div} \mathbf{c} = -q. \quad . \quad . \quad . \quad . \quad . \quad . \quad (1)$$

Assuming that the velocity vector is derived from a potential $\phi = \operatorname{grad} \mathbf{c}$, we have

$$\nabla^2 \phi = -q, \quad . \quad . \quad . \quad . \quad . \quad . \quad (1a)$$

or in cylindrical coordinates r, θ, z (fig. 1).

$$\frac{1}{r}\frac{\partial}{\partial r}\left(r\frac{\partial \phi}{\partial r}\right) + \frac{1}{r^2}\frac{\partial^2 \phi}{\partial \theta^2} + \frac{\partial^2 \phi}{\partial z^2} = -q(r, \theta, z).$$

Taking into consideration only a state of flow of helical symmetry as in the papers of Lamb, Betz, Goldstein, and Kawada, we put for a helical surface traced out by the

centre line of a blade rotating with angular velocity ω and proceeding with axial velocity w_0 (fig. 1)

$$\theta - \frac{\omega}{w_0} z = \zeta, \quad \frac{\partial}{\partial z} = -\frac{\partial}{\partial \zeta}\frac{\omega}{w_0}, \quad \frac{\partial}{\partial \theta} = \frac{\partial}{\partial \zeta}, \quad \frac{\omega r}{w_0} = \rho. \quad (2)$$

We thus arrive at the two-dimensional equation :

$$\frac{1}{\rho}\frac{\partial}{\partial \rho}\left(\rho \frac{\partial \phi}{\partial \rho}\right) + \frac{\partial^2 \phi}{\partial \zeta^2}(1+\rho^{-2}) = -\frac{{w_0}^2}{\omega^2} q(\rho, \zeta). \quad (1b)$$

First part of the Solution.—For reasons connected with the convergence of the development, and in order not to miss the constant term for the axial and tangential velocities, we make use of a very simple solution ϕ_0

Fig. 2.

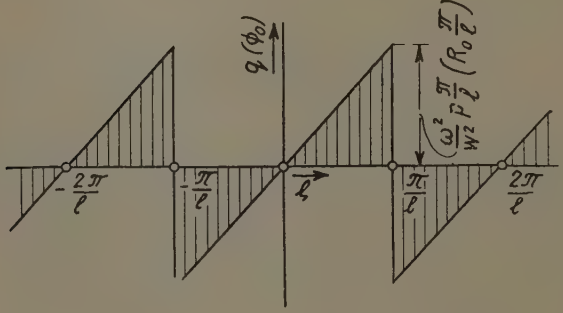

giving the required discontinuity distribution along the blade centre lines, but containing, in addition, undesirable source distributions which will later be removed by a Fourier expansion.

Thus we write for the angular spaces between adjacent blade centre lines

$$-\frac{\pi}{l}, \quad +\frac{\pi}{l}, \quad \frac{3\pi}{l} \cdots \frac{(2l-3)\pi}{l} \quad \text{(fig. 1)},$$

$$\phi_0 = \zeta R_0(\rho), \quad \frac{{w_0}^2}{\omega^2} q(\rho) = -\zeta p(\rho) \quad \text{(fig. 2)},$$

p giving a (positive) source density on the leading edge of the blade and a (negative) sink density on the trailing edge, and R_0 and p being functions of ρ only.

(1 *b*) then transforms into

$$\frac{1}{\rho}\frac{d}{d\rho}\left(\rho\frac{dR_0}{d\rho}\right)=p(\rho), \quad . \quad . \quad . \quad . \quad . \quad (3)$$

furnishing the solution

$$R_0=c_1\ln\rho+c_2+\int_0^{\rho}\frac{d\xi}{\xi}\int_0^{\xi}d\psi\,\psi p(\psi). \quad . \quad . \quad (3a)$$

The constants of integration c_1 and c_2 must be zero, since the velocities must be zero at infinity and finite at the axis, so that we have

$$\phi_0=\zeta\int_0^{\rho}\frac{d\xi}{\xi}\int_0^{\xi}d\psi\,\psi p(\psi), \quad . \quad . \quad . \quad . \quad (3b)$$

and for the velocities belonging to this potential

$$\left.\begin{aligned} u^{(0)}&=\frac{\partial\phi_0}{\partial r}=\frac{\omega}{w_0}\zeta\rho^{-1}\int_0^{\rho}d\psi\,\psi p(\psi),\\ v^{(0)}&=\frac{1}{\rho}\frac{\partial\phi_0}{\partial\theta}=\frac{\omega}{w_0}\rho^{-1}\int_0^{\rho}\frac{d\xi}{\xi}\int_0^{\xi}d\psi\,\psi p(\psi),\\ w^{(0)}&=\frac{\partial\phi_0}{\partial z}=-\frac{\omega}{w_0}\int_0^{\rho}\frac{d\xi}{\xi}\int_0^{\xi}d\psi\,\psi p(\psi). \end{aligned}\right\} \quad . \quad (4)$$

ϕ_0 and the radial velocity component change discontinuously at the radii

$$-\frac{\pi}{l}, \quad +\frac{\pi}{l}, \quad \frac{3\pi}{l} \ldots . \frac{(2l-3)\pi}{l},$$

while the tangential velocities $v^{(0)}$ and the axial velocities $w^{(0)}$ are continuous across these radii and are constant on each circumference, being functions of ρ only.

Thus the circulation Γ is connected with the potential discontinuity in the following way :

$$\Gamma=\Delta\phi_0=\frac{2\pi}{l}R_0=\frac{2\pi}{l}\int_0^{\rho}\frac{d\xi}{\xi}\int_0^{\xi}d\psi\,\psi p, \quad . \quad . \quad (5a)$$

Hence we find for the vortex strength

$$E=\Delta u^{(0)}=\frac{d\Gamma}{dr}=\frac{2\pi}{l}\frac{\omega}{w_0}\rho^{-1}\int_0^{\rho}d\psi\,\psi p. \quad . \quad . \quad (5b)$$

Looking at the complete circumference $\zeta=2\pi$ the flow appears to be generated both by a source distribution

$$\frac{w_0^2}{\omega^2}q=-\zeta p_1=-\left(\zeta-\frac{2\pi}{l}\right)p_1;$$

$$=-\left(\zeta-\frac{4\pi}{l}\right)p_1\ldots-\zeta\left(-\frac{2(l-1)\pi}{l}\right),$$

and also by discontinuities E resp. Γ on the radii

$$-\frac{\pi}{l},\quad+\frac{\pi}{l},\quad\frac{3\pi}{l}\ldots\frac{(2l-3)\pi}{l},$$

that is, on the helical sheets corresponding to these radii.

The values of circulation and vortex strength will not be changed by the superposition of other purely irrotational motions.

It is important to remark that the source distribution q can be chosen as a function of the radial coordinate ρ in such a way as to give any desired discontinuity function or circulation Γ, since by (3) and (5 *a*)

$$p=\frac{l}{2\pi}\frac{1}{\rho}\frac{d}{d\rho}\left(\rho\frac{d\Gamma}{d\rho}\right).\quad\ldots\quad(3c)$$

In this first part of the solution the circulation at any radius is created only by the sources inside this radius.

Remark.—There are other single-term solutions valid in each *half* sector, giving any desired circulation function Γ and joinable so as to fulfil all the necessary symmetry and continuity conditions.

They can be given in the form (k meaning an arbitrary constant)

$$\phi_k=\pm\tfrac{1}{2}\Gamma\frac{e^{\pm k\zeta}-1}{e^{k\frac{\pi}{l}}-1},$$

$$q=\pm(q_k e^{\pm k\zeta}-q_0),$$

where

$$q_k=-\frac{\omega^2}{2w_0^2}\frac{1}{e^{k\frac{\pi}{l}}-1}\left[\frac{1}{\rho}\frac{d}{d\rho}\left(\rho\frac{d\Gamma}{d\rho}\right)+\Gamma(1+k^2\rho^{-2})\right],$$

$$q_0=-\frac{\omega^2}{2w_0^2}\frac{1}{e^{k\frac{\pi}{l}}-1}\frac{1}{\rho}\frac{d}{d\rho}\left(\rho\frac{d\Gamma}{d\rho}\right).$$

On this discontinuous solution of (1 *b*) could be superimposed a continuous solution generated by the same source distribution, but of opposite sign, in the same way as in (1 *c*), below.

By choosing an advantageous value of k the convergence of the expansion might perhaps be improved, but the constant term in the axial and tangential velocity, giving the limiting state of flow for an infinite number of blades, would not appear explicitly.

Second part of the Solution.—As stated above, we must now make the three-dimensional source distribution $q=-\frac{\omega^2}{{w_0}^2}p\zeta$ disappear, retaining nevertheless the discontinuities $\Delta\phi_0=\Gamma$ and $\Delta u^\circ=\mathrm{E}$ of the potential and of the radial velocity respectively.

This will be effected by superimposing a *continuous* solution of (1 *b*) arising from the above introduced source density q by developing them trigonometrically as follows :—

We put

$$\phi\equiv\phi_1=\sum_{n=1}^{n=\infty}\mathrm{R}_n\sin(nl\zeta), \quad . \quad . \quad . \quad . \quad (6)$$

which disappears both at the radii of symmetry

$$0, \quad \frac{2\pi}{l}, \quad \frac{4\pi}{l}, \ldots \frac{2(l-1)\pi}{l},$$

and at the radii of the blade centre lines

$$-\frac{\pi}{l}, \quad +\frac{\pi}{l}, \quad \frac{3\pi}{l} \ldots \frac{(2l-3)\pi}{l}.$$

Then introducing the abbreviation

$$nl\rho=\sigma_n,$$

(1 *b*) takes the form

$$\frac{1}{\sigma_n}\frac{d}{d\sigma_n}\left(\sigma_n\frac{d\mathrm{R}_n}{d\sigma_n}\right)-\mathrm{R}_n\left(1+\frac{(nl)^2}{{\sigma_n}^2}\right)$$

$$=-\frac{l}{\pi(nl)^2}p\int_{-\frac{\pi}{l}}^{+\frac{\pi}{l}}\zeta\sin(nl\zeta)\,d\zeta$$

$$=(-1)^n\frac{2p}{(nl)^3}. \quad . \quad . \quad . \quad . \quad . \quad (1c)$$

The solution is given by Bessel Functions of imaginary argument of the first and second kind $I_{nl}(nl\rho)$, $K_{nl}(nl\rho)$ (in the notation of Watson).

We introduce the integration constants $f_n^{(1)}$ and $f_n^{(2)}$ and make use of the general relation between the two integrals $I_{nl}(nl\rho)$ and $K_{nl}(nl\rho)$ of the homogeneous differential equation conjugate to (1 *c*)

$$I_{nl}(\sigma_n)\frac{dK_{nl}(\sigma_n)}{d\sigma_n}-K_{nl}(\sigma_n)\frac{dI_{nl}(\sigma_n)}{d\sigma_n}=-\frac{1}{\sigma_n}, \quad . \quad (1\,d)$$

and find the solution of (1 *c*) in the form

$$R_n=(-1)^n\frac{2}{(nl)^3}\Big[f_n^{(1)}I_{nl}(\sigma_n(+f_n^{(2)}K_{nl}(\sigma_n) +I_{nl}(\sigma)_n\int_0^{\sigma_n}d\tau_n K_{nl}(\tau_n)\tau_n p -K_{nl}(\sigma_n)\int_0^{\sigma_n}d\tau_n I_{ul}(\tau_n)\tau_n p\Big]. \quad (7)$$

The constants $f_n^{(1)}$ and $f_n^{(2)}$ can be determined from the conditions that the velocities disappear at infinity and remain finite at the axis, which are fulfilled by making

$$(R_n)_{\rho=0}=0, \quad (R_n)_{\rho\to\infty}=0.$$

This gives, since $p=0$ for $\rho>\rho_a$,

$$f_n^{(2)}=0, \quad f_n^{(1)}=-\int_0^{\sigma_{n,a}}d\tau_n K_{nl}(\tau_n)\tau_n p,$$

and therefore

$$R_n=-(-1)^n\frac{2}{(nl)^3}\Big[K_{nl}(\sigma_n)\int_0^{\sigma_n}d\tau_n I_{nl}(\tau_n)\tau_n p +I_{nl}(\sigma_n)\int_{\sigma_n}^{\sigma_{n,a}}d\tau_n K_{nl}(\tau_n)\tau_n p\Big], \quad (8\,a)$$

or

$$R_n=-(-1)^n\frac{2}{nl}\Big[K_{nl}(nl\rho)\int_0^{\rho}d\xi I_{nl}(nl\xi)\xi p +I_{nl}(nl\rho)\int_{\rho}^{\rho a}d\xi\, K_{nl}(nl\xi)\xi p\Big]. \quad (8\,b)$$

It is remarkable that the field given by (3 *b*) and (8 *a*) or (8 *b*) splits automatically into an inner and an outer

domain, the circle of division moving with the circle at which the potential is to be calculated.

The velocities arising out of the potential ϕ_1 may be derived in the following form :

$$\left.\begin{aligned} u^{(1)} &= \frac{\omega}{w_0} \sum_{n=1}^{\infty} \frac{d\mathrm{R}_n}{d\rho} \sin(nl\zeta), \\ v^{(1)} &= \frac{\omega}{w_0} \rho^{-1} \sum_{n=1}^{\infty} nl\mathrm{R}_n \cos(nl\zeta), \\ w^{(1)} &= -\frac{\omega}{w_0} \sum_{n=1}^{\infty} nl\mathrm{R}_n \cos(nl\zeta). \end{aligned}\right\} \quad . \quad . \quad . \quad (9)$$

What is needed in the following investigations is the induced velocity component c^*, supposed to be small in the direction perpendicular to the undisturbed velocity c_0 at the radii

$$\zeta = \frac{\pi}{l}, \quad \frac{3\pi}{l}, \cdots \frac{(2l-1)\pi}{l}.$$

This induced velocity must be composed of half the values of the induced velocity components v_1 and w_1, as only half of the helical vortex sheet—that is, the sheet only from $z=0$ to $z=\infty$ —is actually present.

Thus we get

$$c^* = \frac{1}{2}\left[w_1 \frac{\omega r}{c_0} - v_1 \frac{w_0}{c_0}\right],$$

and as c_0 (in view of the positive direction of z) is negative,

$$\frac{c^*}{c_0} = -\frac{1}{2w_0(1+\rho^2)}[(w^{(0)}+w^{(1)})\rho - (v^{(0)}+v^{(1)})].$$

Using now formulæ (4) and (9) for the angles

$$\zeta = \frac{\pi}{l}, \quad \frac{3\pi}{l}, \cdots \frac{(2l-1)\pi}{l},$$

this expression leads to

$$\frac{c^*}{c_0} = \frac{\omega}{2{w_0}^2\rho}\left[\mathrm{R}_0 + \sum_{n=1}^{\infty} (-1)^n nl\mathrm{R}_n\right],$$

or, on account of (8 *b*),

$$\frac{c^*}{c_0} = \frac{\omega}{2{w_0}^2\rho}\left[\mathrm{R}_0 - 2\sum_{n=1}^{\infty} \mathrm{K}_{nl}(nl\rho)\int_0^{\rho} d\xi\, \mathrm{I}_{nl}(nl\xi)\xi p + \mathrm{I}_{nl}(nl\rho)\int_{\rho}^{\rho_a} d\xi\, \mathrm{K}_{nl}(nl\xi)\xi p\right]. \quad (10)$$

Now, by (5 *a*), the circulation is proportional to R_0

$$R_0 \frac{2\pi}{l} = \Gamma,$$

and by (3 *c*),

$$p = \frac{l}{2\pi} \frac{1}{\rho} \frac{d}{d\rho} \left(\rho \frac{d\Gamma}{d\rho} \right). \quad . \quad . \quad . \quad . \quad (3c)$$

By insertion in (10) this equation becomes

$$\frac{c^*}{c_0} = \frac{\omega l}{4\pi\rho w_0^2} \Big[\Gamma - 2 \sum_{n=1}^{\infty} K_{nl}(nl\rho) \int_0^{\rho} I_{nl}(nl\xi) d\left(\xi \frac{d\Gamma}{d\xi} \right) + I_{nl}(nl\rho) \int_{\rho}^{\rho_a} K_{nl}(nl\xi) d\left(\xi \frac{d\Gamma}{d\xi} \right) \Big], \quad (10a)$$

which, by integration by parts, can of course appear in different forms.

For numerical treatment it is convenient to replace $d\left(\xi \frac{d\Gamma}{d\xi} \right)$ by the equivalent source density gradient p and to introduce the following dimensionless quantities :

$$\Gamma^* \equiv \Gamma \frac{l\omega}{w_0^2},$$

$$p^* = \frac{1}{\xi} \frac{d}{d\xi} \left(\xi \frac{d\Gamma^*}{d\xi} \right).$$

Then (10 *a*) may be written

$$\frac{c^*}{c_0} = \frac{1}{4\pi\rho} \Big[\Gamma^* - 2 \sum_{n=1}^{\infty} K_{nl}(nl\rho) \int_0^{\rho} I_n(nl\xi) p^* \xi \, d\xi + I_{nl}(nl\rho) \int_{\rho}^{\rho_a} K_{nl}(nl\xi) p^* \xi \, d\xi \Big]. \quad (10b)$$

Equations (10 *a*) and (10 *b*) give the induced relative velocity and with it the induced resistance of the blades produced by the trailing helical discontinuity sheet of arbitrarily prescribable distribution of circulation Γ or vorticity $\frac{d\Gamma}{dr}$.

For the special case of the Betz propeller of minimum

induced resistance—that is, for c^* produced by a rigid axially moving helical surface—we must have

$$\frac{c^*}{c_0} = k \frac{\rho}{1+\rho^2},$$

and the circulation Γ creating this motion has to fulfil the following integral equation :

$$k \frac{\rho^2}{1+\rho^2} = \Gamma - 2 \sum_{n=1}^{\infty} \mathrm{K}_{nl}(nl\rho) \int_0^{\rho} \mathrm{I}_{nl}(nl\xi) d\left(\xi \frac{d\Gamma}{d\xi}\right) + \mathrm{I}_{nl}(nl\rho) \int_{\rho}^{\rho a} \mathrm{K}_{nl}(nl\xi) d\left(\xi \frac{d\Gamma}{d\xi}\right). \quad (10c)$$

The solution of this equation has, of course, to conform with Goldstein's † solution.

3. *The Second Relation between Circulation Function and Induced Velocities, containing Blade Dimensions, Angle Setting, Lift Coefficient, and Profile Resistance.*

We make use of the following proposition of Prandtl, fundamental for the three-dimensional theory of the aerofoil.

The lift $d\mathrm{A}$ and the profile drag $d\mathrm{W}$ for an element $t\,dx$ of an aerofoil is determined by the density μ of the air, by the local velocity c, the local effective angle of incidence i, and the lift and drag coefficients c_a and c_w of the profile taken for infinite aspect ratio (fig. 3).

This proposition is expressed by the formulæ

$$\left.\begin{aligned} d\mathrm{A} &= \frac{\mu}{2} c^2 c_a t\, dx, \\ d\mathrm{W} &= \beta\, d\mathrm{A}, \qquad \beta = \frac{c_w}{c_a}, \end{aligned}\right\}, \quad . \quad . \quad . \quad (11)$$

where the lift force $d\mathrm{A}$ is perpendicular to the local velocity and contains the induced resistance and the profile resistance proper $d\mathrm{W}$ acts in the direction of the local velocity and

$$\beta = \frac{c_w}{c_a}$$

is called the profile fineness.

Below a certain critical angle of incidence which we suppose here is not reached, the lift coefficient is, with

† "On the Vortex Theory of Screw Propellers," S. Goldstein. Proc. Roy. Soc. A, cxxiii. pp, 4:0–465 (1929).

sufficient exactness, a linear function of the angle of incidence, which may be reckoned from the angle of no lift, viz. :

$$c_a = c_a' i, \quad c_a' \equiv \frac{dc_a}{di} \dagger, \quad . \quad . \quad . \quad . \quad (12)$$

and the fineness β of the profile changes so slowly with the angle that we may put β a constant with regard to i, but changing with the form and surface of the profile.

Fig. 3.

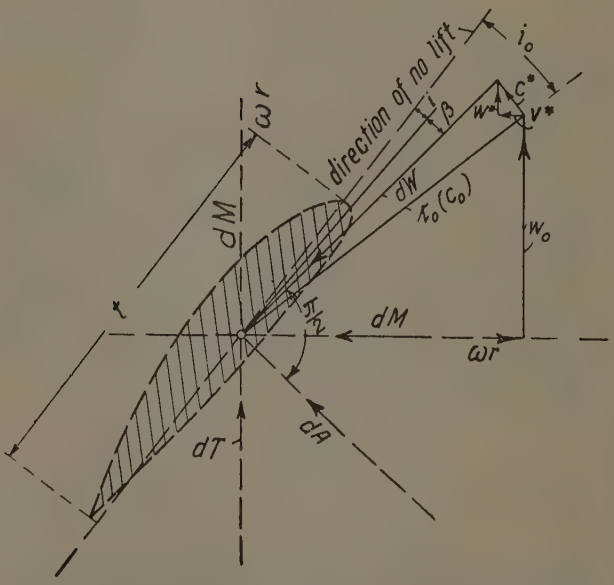

Introducing, furthermore, the proposition of Joukowski-Prandtl concerning the relation between circulation Γdx and lift dA,

$$dA = \mu c \Gamma \, dx,$$

which shows that the circulation function and the lift distribution are proportional, with the factor

$$\mu c = \mu w_0 \sqrt{1+\rho^2},$$

† It is well known that, furthermore, c_a is diminished by the profile resistance.

we get the well-known law

$$\Gamma = \frac{c}{2} t c_a = \frac{c}{2} t c_a' i, \quad . \quad . \quad . \quad . \quad . \quad (13)$$

or $\quad dA = \mu c \Gamma \, dr, \quad r \equiv x, \quad c^2 \sim c_0^2 = w_0^2 + \omega^2 r^2.$

Finally, the effective angle i of incidence or attack can be derived from the "undisturbed" angle between the line of no lift and the direction of the relative flow at infinity by representing the induced and the profile resistance as rotations of the line of lift.

According to fig. 3 we have, then,

$$i = i_0 - \frac{c^*}{c} - \beta, \quad . \quad . \quad . \quad . \quad . \quad . \quad (14)$$

and the second leading equation between circulation and induced velocity, which, moreover, contains also the fineness of the profile β, the lift derivative c_a', and the width of blade t takes the form

$$\Gamma = \frac{w_0}{2} \sqrt{1+\rho^2}\, t c_a' \left(i_0 - \frac{c^*}{c} - \beta \right). \quad . \quad . \quad (13a)$$

It will be useful to replace Γ, t, and A by the following dimensionless quantities, corresponding to the number l of all blades :

the "specific" circulation (as already defined)

$$\Gamma^* = \Gamma \frac{l\omega}{w_0^2};$$

the "specific" blade width

$$t^* = t l c_a' \frac{\omega}{2 w_0};$$

the "specific" lift function

$$\frac{dA^*}{d\rho} = \frac{dA}{d\rho} \frac{l\omega^2}{\mu w_0^4}. \quad \Bigg\} \quad . \quad . \quad . \quad . \quad . \quad (14)$$

Equations (13) then take the form

$$\left.\begin{aligned} \Gamma^* &= t^* i \sqrt{1+\rho^2}, \\ \frac{dA^*}{d\rho} &= \Gamma^* \sqrt{1+\rho^2} = t^* i (1+\rho^2). \end{aligned}\right\} \quad . \quad . \quad . \quad (13b)$$

4. *Thrust and torque of the propeller expressed by the circulation function and the induced velocities. Complete set of equations between circulation, induced velocity, blade width, profile lift derivative, profile resistance, and angle setting of the profile.*

According to fig. 3 and formula (11) the distributions of thrust T and torque M along the blade are the following :

$$dT = dA\frac{\omega r - v^*}{c} - dW\frac{w_0 + w^*}{c}$$

$$= dAc^{-1}[\omega r - v^* - \beta(w_0 + w^*)],$$

$$dM = r\left[dA\frac{w_0 + w^*}{c} + dW\frac{\omega r - v^*}{c}\right]$$

$$= rd\,Ac^{-1}[w_0 + w^* + \beta(\omega r - v^*)].$$

As the induced velocity components v^* and w^* have, up to small quantities of higher order, the values

$$v^* = \frac{c^*}{c} w_0, \quad w^* = \frac{c^*}{c}\omega r,$$

we obtain the following formulæ by integrating over the l blade lengths, by neglecting products of small quantities like βv^* and βw^*, by introducing again the dimensionless variable $\rho = \frac{\omega r}{w_0}$, and by using formulæ (13), (13 *a*), and (13 *b*).

$$\left.\begin{aligned} T^* &= \int_0^{\rho_a} d\rho\, \Gamma^*\left[\rho - \left(\frac{c^*}{c} + \beta\right)\right], \\ M^* &= \int_0^{\rho_a} d\rho\, \rho\Gamma^*\left[1 + \rho\left(\frac{c^*}{c} + \beta\right)\right]. \end{aligned}\right\} \dagger \quad (15)$$

† Betz, annunciating his theorem of the rigid sheet, solves the following problem of minimum induced resistance for prescribed thrust : —Work of resistance

$$W^* = M^* - T^* = \int d\rho\Gamma^* \frac{c^*}{c}(1+\rho^2),$$

work of thrust $T^* = \int d\rho\Gamma^*\rho$, leaving out the term $\frac{c^*}{c}$ of the first of equations (15) variation, $\delta[W^* - \lambda T^*] = 0$.

Observing this inconsistency in regard to quantities of the second order the author is doubtful if *the theorem of the right helical sheet does* not *require a correction*. This doubt does not arise in regard to the corresponding theorem of the aerofoil in translational motion, where small quantities of the second order are retained consistently.

In these the following further dimensionless quantities have been introduced, namely,

the "specific" thrust . . . $T^* = T \frac{\omega^2}{\mu w_0^4}$,

and the "specific" torque $M^* = M \frac{\omega^3}{\mu w_0^5}$.

All the dimensionless quantities introduced, except ρ_a, differ from the customary quantities in that they do not contain the diameter of the propeller.

Remark on Approximate Theories.—Instead of equations (10 *a* or *b*) some approximate propeller theories use a relation between the circulation Γ and a certain mean value c_m^* of the induced velocity, which may be explained either as induced by an infinite number of blades or, as I prefer to look at it, as the mean of the induced velocities between each pair of adjacent blades.

The relation is obtained by following a circuit round a blade section, considering that only the circumferential part behind the blade contributes to the value of the circulation, and that the *mean* value of the induced velocity from the front to the trailing edge must be taken.

In this way (looking at fig. 3) one gets

$$\frac{c_m^*}{c} = \frac{\Gamma^*}{4\pi\rho} \quad \text{or} \quad \Gamma^* = 4\pi\rho \frac{c^*}{c} \frac{c_m^*}{c^*}, \quad . \quad . \quad . \quad (16)$$

of which the first relation (in view of the definitions (14)) coincides with the first term of the right side of (10 *b*), and the other terms give the correction due to the finite number of blades.

For the Betz propeller of minimum induced resistance

$$\frac{c^*}{c} = k\frac{\rho}{1+\rho^2}, \quad \Gamma^* = 4\pi k \frac{\rho^2}{1+\rho^2} \frac{c_m^*}{c^*}, \quad . \quad . \quad (17)$$

where k is an arbitrary constant to be determined by the value either of the thrust or of the torque. $\frac{c_m^*}{c^*}$ being the quotient between mean and local induced velocity, it follows that the induction by the trailing (free) vortex sheet is missing in this approximation and must be approximated separately.

This is what Prandtl did in his well-known formula, viz.:

$$\frac{c_m^*}{c^*} = \frac{2}{\pi} \operatorname{arc\,cos}\, e^{-\frac{l}{2}\left(1-\frac{r}{r^2}\right)\sqrt{1+\rho^2}}, \quad . \quad . \quad (18)$$

obtained by substituting a grating of parallel rigid half infinite sheets for the rigid helical sheet.

The approximate theories have hitherto superimposed this effect after the completion of the calculations of thrust and torque by the formulæ (15), but it seems more rational to incorporate the value of $\frac{c_m^*}{c^*}$ of formula (18) in the integrals of equation (15), as will be shown in another paper.

Approximately then (10 *a*) may be replaced by (16) and (18); furthermore, Γ^* may be eliminated by (16) from equations (15), which then contain only the one variable function $\frac{c^*}{c}$, *i. e.*, the induced velocity distribution.

After that it is easy to satisfy the *condition of maximum thrust* T* *for given torque* M* and given speed w_0 and angular velocity ω, for which $\frac{c^*}{c}$ and Γ^* are given by the formulæ

$$\frac{c^*}{c} = \frac{1}{4}\frac{\rho(1-\lambda)}{1+\lambda\rho^2} - \beta = \frac{\Gamma^*}{4\pi\rho}\frac{c^*}{c_m^*}, \quad . \quad . \quad . \quad (19)$$

where the Lagrangian factor λ is to be determined from the given value of the torque M*, and $\frac{c_m^*}{c^*}$, the ratio of the mean and local induced velocity, has been assumed not to influence the position and value of maximum thrust and not to be allowed to vary, and must be taken from Prandtl's formula (18).

5. *Signification and possible use of the four equations* (15), (10 *a*), *and* (13 *a*, *b*) *of the Propeller Problem.*

Before proceeding further it may be stated that equations (10 *a*) and (13 *a*, *b*) correspond exactly to the equations determining the lift and induced velocity distribution of aeroplane wings.

In the same manner as with aeroplane wings there are three ways of attacking the propeller problem.

a. The *first* and seemingly simplest *way* of getting results from the four equations (15), (10 *a*), (13 *a*, *b*) is to choose a succession of plausible and desirable distributions of Γ^*—that means also plausible and desirable distributions of lift along the blade—for instance (fig. 4)

$$\Gamma^* = g\rho^p(\rho_a{}^q - \rho^q), \quad . \quad . \quad . \quad . \quad . \quad (20)$$

which makes Γ^* zero at $\rho = 0$ and $\rho = \rho_a$ (as it should), and can be varied by taking a succession of values of p and q.

Then, from (10 *a*), we would get the corresponding distributions of the induced velocity $\frac{c^*}{c}$; putting further

Fig. 4.

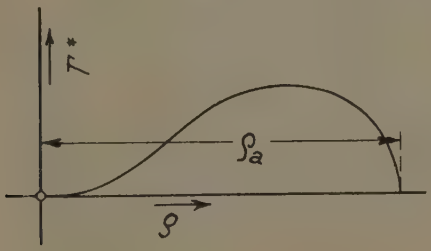

Γ^* and $\frac{c^*}{c}$ into (15) we can first determine the constant g by the given value of the torque M* and then the thrust T*.

Finally, from (13 *a*, *b*), the corresponding blade angles i_0 can be determined for an appropriate shape tc_a' of the blade, or the shape tc_a' can be taken from (13 *a*) for a given pitch distribution i_0.

By repeating this procedure for several values of the exponents p and q and several blade length numbers ρ_a, one is able to choose the relatively best propeller.

As the simplest procedure, requiring only integrations and summations of appropriately given terms, is furthermore the most suitable for showing the possibilities and limitations of the general method of solution, it may be discussed a little further and illustrated by a numerical example.

Starting from (10 *b*) we use for the Bessel Functions the approximate expressions of J. W. Nicholson †, which, introducing as independent variable,

$$u = \sqrt{\xi^2+1},$$

take the form

$$\left.\begin{aligned} I_{nl}(nl\xi) &= \frac{1}{\sqrt{2nl\pi}}\frac{1}{\sqrt[4]{u}}\left[e^u\sqrt{\frac{u-1}{u+1}}\right]^{nl}, \\ K_{nl}(nl\xi) &= \sqrt{\frac{\pi}{2nl}}\frac{1}{\sqrt[4]{u}}\left[e^u\sqrt{\frac{u-1}{u+1}}\right]^{-nl}, \end{aligned}\right\} \quad . \quad (22)$$

and which here are sufficiently exact for an argument of about $nl\xi > 4$, which for a number of blades $l=3$ and a radial dimensionless abscissa $\xi=2$ would mean $n>1$, so that expressions (22) can be used throughout.

The following abbreviations are useful :

$$e^u\sqrt{\frac{u-1}{u+1}} \equiv U_1, \quad p^*\sqrt{u} \equiv U_2.$$

Then (10 *b*) takes the form

$$\frac{c^*}{c} = \frac{1}{4\pi\rho}\left[\Gamma^* - \frac{1}{l\sqrt{u}}\sum_{n=1}^{\infty}\frac{1}{n}\left[U_1^{-n}\int_0^{u=\sqrt{\rho^2+1}} U_1^n\,du\,U_2 + U_1^n\int^{u_a}\left[U_1^{-n}\,du\,U_2\right]\right]. \quad (10f)$$

The first term gives the relative velocity induced at a point ρ by the circulation at the same point, the first series gives the velocities at the point ρ induced by the circulations at the points inside of ρ, and the second series the velocity at ρ induced by the circulations at the points outside ρ.

As regards the convergence of the series in (10 *f*) it is at least of the order $\Sigma\frac{1}{n^2}$ for the following reasons :—

The mean value $U_{2,m}$ of U_2, which might be put outside the respective integral as a factor as n increases, approaches its value at the limit ρ for both integrals, because with n

† "The Approximate Calculation of Bessel Functions of Imaginary Argument." Phil. Mag. xx. pp. 938–43 (1910).

The expressions (22) are supplemented for higher approximation by further terms, which are not needed here.

increasing the functions, U_1^n and U_1^{-n} are more and more concentrated at the point ρ. This results from the fact that the function U_1 is for the influential part of the abscissæ of the type e^{cu} and U_1^{-1} of the type $e^{-c(u_a-u)}$ with a very close approximation. Therefore, after integration and multiplication, the exponential functions cancel each other, and there remains only another factor $\frac{1}{n}$ to be multiplied with the one standing outside the bracket in (10 *f*).

For a *numerical example* the following data and functions will be chosen (as liable to appear in propeller practice) :

$$\rho_a = 3{\cdot}04 \text{ corresponding to } u_a = 3{\cdot}2,$$

$$\Gamma^* = g\rho^5(\rho_a - \rho), \quad . \quad . \quad . \quad . \quad . \quad (20a)$$

Fig. 5.

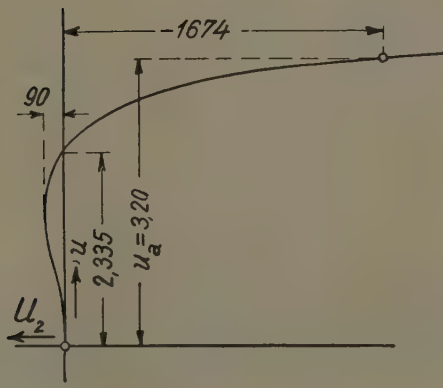

and, following from (3 *c*),

$$p^*\sqrt{u} = g\sqrt{u}(u^2-1)[25\rho_a\sqrt{u^2-1} - 36(u^2-1)]. \quad (3d)$$

The function Γ^* gives the lift distribution ; it has, inside the interval of the blade centre line, the character of fig. 4, and is zero outside.

The function $U_2 = p^*\sqrt{u}$ derived from it appears as in fig. 5.

In the table on p. 766 we give only the figures of the first series terms, from which further terms can be easily derived.

It is not intended here to give a full calculation of the distribution of the induced relative velocities $\frac{c^*}{c}$ along the radius. It may suffice here to compute this value for one point ρ, which will be chosen at the radius where the strength of the fictitious generating sources p^*, and with it the function U_2, change sign. The table shows that this is the point

$$u = 2{\cdot}335, \quad \rho = 2{\cdot}11, \quad \frac{r}{r_a} = \frac{\rho}{\rho_a} = \frac{2{\cdot}11}{3{\cdot}04} = 0{\cdot}695.$$

The choice of this point, which is about at the centre of thrust pressure, makes the calculation a bit clearer

u.	ξ.	Γ^*/g.	U_2.	U_1.	U_2U_1.	U_2U_1.
1	0	0	0	0	0	
1·01	0·142	$1{\cdot}66.10^{-4}$	0·203	$0{\cdot}73.10^{-2}$	$0{\cdot}148.10^{-2}$	27·85
1·1	0·458	0·052	6·00	0·281	1·685	21·35
1·4	0·980	1·865	45·15	4·57	206·7	9·87
1·8	1·50	11·60	90·0	34·01	3060	2·65
2·0	1·73	—	100·1	77·5	7750	1·29
2·2	1·96	31·30	60·4	169·1	10200	0·357
2·335	2·11	38·90	0	279	0	0
2·4	2·18	42·46	− 44·3	354	−15710	−0·125
2·5	2·291	—	− 123·8	508	$-6{\cdot}29.10^4$	−0·244
2·7	2·508	53·0	− 310·0	1030	$-3{\cdot}19.10^5$	−0·301
3·1	2·93	22·75	−1320	4020	$-5{\cdot}3.10^6$	−0·328
3·2	3·04	0	−1674	5639	$-9{\cdot}42.10^5$	−0·297

without otherwise being of any advantage, the terms of each series being then all of one sign.

On computing by a graphical method the values of the integrals appearing in $(10\,f)$ up to $n = 6$, and estimating an upper limit of the remainder R by assuming convergence like $\Sigma \frac{1}{n^2}$, beginning with the 6th term $(10\,f)$, yields the following result :

$$\left(\frac{c^*}{c}\right)_{\rho=2{\cdot}11} = \frac{g}{4.2{\cdot}11\pi}\left[38{\cdot}9 - \frac{1}{l\sqrt{2{\cdot}335}}(+15{\cdot}850 \quad -66{\cdot}70)\right.$$
$$3{\cdot}170 \quad 9{\cdot}05$$
$$0{\cdot}996 \quad 2{\cdot}26$$
$$0{\cdot}4055 \quad 0{\cdot}997$$
$$0{\cdot}1925 \quad 0{\cdot}489$$
$$\left.0{\cdot}0771 \quad 0\ 275\right]$$
$$+\ldots\ldots -\ldots\ldots$$

$$= \frac{g}{4.2\cdot11\pi}\left[38\cdot9+\frac{1}{l\sqrt{2}.335}(59\cdot18+\mathrm{R})\right].$$

The last member of the series is $0\cdot275-0\cdot0771=0\cdot198$.

Now we put $0\cdot198=\frac{a}{6^2}$, then $a=7\cdot13$ and

$$\mathrm{R}=7\cdot13\left[\frac{\pi^2}{6}-\sum_1^6\frac{1}{n^2}\right]=1\cdot07,$$

from the well-known value of $\sum_1^\infty\frac{1}{n^2}$.

Putting the number of blades $l=3$ we get

$$\left(\frac{c^*}{c}\right)_{\rho=2\cdot11}=\frac{g}{2}(5\cdot875+1\cdot95+0\cdot035).$$

The factor g is determined by the total value of thrust expected; the first figure gives the self-induced relative velocity and the rest give the correction due to the tip loss, which in this rather great distance from the tip would be only about one-third of the self-induction, but would become greater on approaching the tip of the blade.

Increasing the number l of blades makes the tip loss correction smaller and smaller, till at $l=\infty$ the self-induction alone is left and coincides with the inflow given by the relation (16) of the approximate theory.

b. The second method of attacking the problem consists in taking the induced velocity $\frac{c^*}{c}$ from (13*b*) and (14) as a function of the circulation Γ^* and putting its value into (10 *a*) so as to obtain an integral equation for Γ^* alone, depending on the prescribed distributions of i_0 and tc_a'.

To this end (13 *b*, 14) may be written

$$\frac{c^*}{c}=i_0-\beta-\frac{\Gamma^*}{t^*\sqrt{1+\rho^2}},$$

and (10 *a*) then becomes

$$\Gamma^*=\Gamma_0^*+2\,\frac{\frac{t^*\sqrt{1+\rho^2}}{4\pi\rho}\sum_{n=1}^{\infty}\mathrm{K}_{nl}(nl\rho)\int_0^{\rho}\mathrm{I}_{nl}(nl\xi)d\left(\xi\frac{d\Gamma^*}{d\xi}\right)}{1+\frac{t^*\sqrt{1+\rho^2}}{4\pi\rho}}$$
$$+\mathrm{I}_{nl}(nl\rho)\int_{\rho}^{\rho_a}\mathrm{K}_{nl}(nl\xi)d\left(\xi\frac{d\Gamma^*}{d\xi}\right),\quad(10c)$$

where

$$\Gamma_0^* = (i_0 - \beta) t^* \sqrt{1+\rho^2} \Big/ \left(1 + \frac{t^* \sqrt{1+\rho^2}}{4\pi\rho}\right).$$

In (10 *c*) in the first term on the right side the letter Γ_0^* is introduced—that is the specific circulation in the case when the specific induced velocity is replaced by its mean value $\frac{\Gamma^*}{4\pi\rho}$.

This observation leads to a method of solution very much like the method of iterated kernels. A first approximation is obtained by inserting Γ_0^* instead of Γ^* under the integral signs, then, again, a second approximation Γ_2^* by putting Γ_1^* under the integral signs and so on. It will be necessary to assume $t^*(i_0 - \beta)$ so as to become zero at the tip of the blade and at the axis in order to have a good convergence.

c. The third question asking for *maximum thrust* may be treated according to the classical theory of the isoperimetric problem.

Calling λ the Lagrangian factor of the condition of prescribed values of torque M* (eq. (15)), angular velocity ω and speed w_0, the maximum of thrust T* (eq. (15)) demands that

$$\int_0^{\rho a} d\rho \left[\delta\Gamma^* \left\{ \rho(1-\lambda) - \left(\frac{c^*}{c} + \beta\right)(1+\lambda\rho^2) \right\} - \delta\frac{c^*}{c}\,\Gamma^*(1+\lambda\rho^2) \right] = 0.$$

In (15 *a*) the variation $\delta\frac{c}{c}$ is not independent of the variation $\delta\Gamma^*$, but connected to it by (10 *a*) (10 *b*), which show that the change of induced specific velocity $\frac{c^*}{c}$ at any one element of the radius is connected to the changes of specific circulation Γ^* at all elements of the radius along the blades.

For reasons of simplicity and convergence of the necessary summations the two variations $\delta\Gamma^*$ and $\delta\frac{c^*}{c}$

shall both be expressed by the variation of the fictitious source distribution, by using (5 *a*) and changing to dimensionless variables, viz. :

$$\Gamma^*(\rho) = \int_0^{\rho} \frac{d\xi}{\xi} \int_0^{\xi} d\psi \, \psi p^*, \quad . \quad . \quad . \quad . \quad (5\,b)$$

and assuming a change of p^* only at one point ψ

$$\left.\begin{aligned} \delta\Gamma^*(\rho) &= \delta p^* \, \psi \, d\psi \ln\frac{\rho}{\psi}, \quad \psi<\rho, \\ \delta\Gamma^*(\rho) &= 0, \quad \psi<\rho, \end{aligned}\right\} \quad . \quad . \quad . \quad (5\,c)$$

so that a variation of p^* at one point ψ produces changes of Γ^* at all points ρ inside of ψ.

From (10 *b*), then, is deduced

$$\left(\delta\frac{c^*}{c}\right)_{\rho} = (\delta\Gamma^*)_{\rho}\frac{1}{4\pi\rho} - \frac{1}{2\pi\rho}\delta p^*\psi \, d\psi \sum_1^{\infty} [\mathrm{I}_{nl}(nl\psi)\mathrm{K}_{nl}(nl\rho)]_{\psi<\rho} + [\mathrm{K}_{nl}(nl\psi)\mathrm{I}_{nl}(nl\rho)]_{\psi>\rho}.$$

Therefore, observing (5 *c*),

$$\left.\begin{aligned} \left(\delta\frac{c^*}{c}\right)_{\rho>\psi} &= \delta p^*\psi \, d\psi \frac{1}{4\pi\rho}\left[\ln\frac{\rho}{\psi} - 2\sum_1^{\infty}\mathrm{I}_{nl}(nl\psi)\mathrm{K}_{nl}(nl\rho)\right], \\ \left(\delta\frac{c^*}{c}\right)_{\rho<\psi} &= -\delta p^*\psi \, d\psi \frac{1}{2\pi\rho}\sum_1^{\infty}\mathrm{K}_{nl}(nl\psi)\mathrm{I}_{nl}(nl\rho). \end{aligned}\right\} \quad . \quad . \quad . \quad (10\,c)$$

Introducing these expressions for $\delta\Gamma^*$ and $\delta\frac{c^*}{c}$ into (15 *a*) there follows the *Integral equation* of the proposition *of maximum thrust with given torque*, viz. :

$$\begin{aligned} &\sum_1^{\infty}\mathrm{K}_{nl}(nl\psi)\int_0^{\psi}\mathrm{I}_{nl}(nl\rho)\Gamma^*(\rho)\frac{1+\lambda\rho^2}{2\pi\rho}d\rho \\ &+\sum_1^{\infty}\mathrm{I}_{nl}(nl\psi)\int_{\psi}^{\rho_a}\mathrm{K}_{nl}(nl\rho)\Gamma^*(\rho)\frac{1+\lambda\rho^2}{2\pi\rho}d\rho \\ &-\int_0^{\rho_a}d\rho\ln\frac{\rho}{\psi}\left[\rho(1-\lambda)-\left(\frac{c^*}{c}+\beta\right)(1+\lambda\rho^2)\right. \\ &\qquad\left.-\Gamma^*(\rho)\frac{1+\lambda\rho^2}{4\pi\rho}\right]=0. \quad (22) \end{aligned}$$

As to the convergence of the series terms the same observations are valid as in Chapter 5 *a*.

To complete the set of equations determining the functions $\frac{c^*}{c}$ and Γ^* and the constant Lagrangian factor λ, (10 *a*) and the second of equations (15) must be added.

This system of equations (22), (10 *a*), and (15) does not look inviting. Anyhow there exist solutions for the special cases, first the very simple (19) for an infinite number of blades and then the solution of Betz (10 *d*), and Goldstein for profile drag β zero. There is some hope that from these by successive approximation solutions might be found.

Summary.

The paper gives a mathematical treatment of the vortex theory of the air-screw assuming a multiple vortex sheet system of helical symmetry, of infinite axial length and radial distribution of arbitrarily prescribable strength. The principal task consists in determining the field of induced velocities, and especially their distribution at the centre lines of the blades represented as radial vortex lines fixed in space by the blade bodies.

These latter velocities, generated by only the half infinite vortex column are found by the well-known artifice that they have just half of the values generated by the completely infinite column (of course, at all other points, except at infinity along the half infinite field, this utilization of symmetry does not give any help).

The induced velocities are needed to determine the change of angle of attack, the change of inflow, and the induced resistance of the blade profile.

The analytical process for finding the relation between the induced velocities and the vortex distribution is summarized in the introduction to this paper. It may be added that the process can be characterized by the statement that the complete solution for any given thrust distribution is built up from one discontinuous solution arising out of a certain field of sources of saw-like arrangement and a second continuous solution derived from the same source field, but of opposite sign.

The relation obtained in this way is shown to consist of a term giving the velocities for an infinite number of

blades and a series giving along each blade the correction caused by the chosen number of blades.

This relation is then used to build up the theory of the air-screw in three different directions, viz. :—

(1) In choosing an appropriate lift or thrust or circulation or vortex distribution along each blade, in computing the induced velocities, and in using them to determine the blade dimensions and angle settings corresponding to the chosen thrust distribution.

This procedure is fully discussed and illustrated by a numerical example.

(2) In assuming the blade dimensions and their angular positions and obtaining an integral equation for the corresponding circulation function or thrust distribution.

Here a method of solution by iteration is indicated.

(3) In expressing thrust and torque by integrals containing the circulation function, and in formulating the conditions of maximum thrust for given torque with the induced velocity-circulation relation as an accessory condition.

The equations derived from (3) show considerable mathematical difficulties which have not yet been solved, while the problems (1) and (2), although requiring much computation, do not present any real mathematical obstacle.

Finally, in order to anticipate some general criticisms of the vortex theory of the air-screw, we may state some criticisms of our own. It has been said in the introduction that the convergence of the slip-stream caused by the pressure gradient, and a spatial distribution of the fixed vortex lines representing the blade profiles, will be possible and necessary. Another question is if it will turn out to be necessary to take account of the coiling up of the vortex sheet arising out of the (here neglected) action of the induced velocities ; of the inherent instability of every vortex sheet ; and of the internal friction at the places of high velocity gradient. As these phenomena appear only at a certain distance behind the front, and as hitherto all the essential experimental features seem to be covered by the vortex theory of the air-screw and still more by the much more investigated analogous theory of the aeroplane wing, it seems as if the latter demands will require only a theory of secondary corrections.

LXVIII. *Note on the Preferred Orientation of the Crystallites of Electrodeposited Hexagonal Chromium.* *By* W. A. Wood, *M.Sc., Physics Department, National Physical Laboratory, Teddington, Middlesex* *.

[Plates VI. & VII.]

IT was noted during X-ray work on the hexagonal modification of electrodeposited chromium [1] that the crystallites composing the deposit exhibited a pronounced preferential orientation. The present note records the nature of the orientation and the effects of varying thicknesses of deposit and of different base metals.

Specimens.

The deposits were plated on the plane surface of strips of copper, brass, iron, or nickel. The surfaces were initially ground smooth, degreased, and deeply etched. The standard bath was that previously used.

	Per litre.
CrO_3.....	600 gram.
H_2SO_4	0·075 N.
Sugar.....	10 gram.

Temperature 18° C. Normal current density 0·2 amp./cm.^{2}.

The effect of increasing the temperature of the bath (50° C.) was to reduce its efficiency and to bring about deposition of cubic chromium. Variations in acidity about the above value affected the degree of orientation and the brightness; it was concluded that the dullness of such deposits were due to co-deposited foreign material which interfered with the regularity of an oriented growth.

X-ray Spectra.

The spectra were recorded by a cylindrical X-ray camera of radius 5·5 cm. and with chromium K-radiation as incident wave-length. These photographs were supplemented, for determination of the orientation, by transmission photographs through a small flake removed from a thick deposit. For this molybdenum K-radiation was used.

* Communicated by Dr. G. W. C. Kaye.

Effect of Thickness.

It was found that the thin deposits showed least pronounced orientation. The effect is shown in figs. 1, 2, and 3 (Pl. VI.), where the photographs obtained respectively after 1, $4\frac{3}{4}$, and 48 hours deposition on copper are reproduced. It will be seen that the relative intensity of the (101) and (002) planes, indicated on the photographs, changes markedly between figs. 1 and 2 (Pl. VI.), and thereafter remains much the same. The orientation after the first few layers, therefore, appears to settle down to a strongly marked condition. A similar result was given by deposits on other metals. Thus figs. 4 and 5 (Pl. VI.), showing a deposit after half an hour and 17 hours on nickel, indicate the same effect (the extra spots on the thin deposit are from the underlying nickel). These observations are consistent with those obtained by metallographic methods, where it appears that an electrodeposit commonly commences growth from a number of nuclei on the surface of the base metal and, after first branching out in directions over a wide angle, finally settles down to a columnar growth roughly normal to the surface, as a result of the crowding out of the side branches.

Effect of Base Metal.

It will be noted that the spectrum from the deposit on copper shown in fig. 3 (Pl. VI.) shows the same relative intensity of the lines as that of fig. 5 (Pl. VI.) obtained from a deposit on nickel. The type of orientation in the two cases is therefore the same. It was found also that deposits plated on brass, iron, heavily rolled copper (possessing a marked fibre structure), and annealed copper (with a random coarse-grained structure) were also of the same orientation. Further, the orientation was equally highly marked whether the deposit was on a cleaned surface or on one uncleaned and coated with a thin layer of grease. The effect on the deposit of varying the base metal is therefore negligible ; the strikingly pronounced orientation of electroplated hexagonal chromium appears to be an intrinsic property of the material, due probably to the more active rate of crystallization associated with a particular direction in the crystal. This direction follows from the determination of the preferred orientation.

Nature of the Orientation.

It was concluded from the photographs that the preferred orientation was such that the crystallites tended to align themselves with the basal plane of the hexagonal unit cell in the plane surface of the deposit, and with the basal plane rotated at random in that surface. This conclusion was based on the following observations :—

(*a*) The spectra obtained by reflexion from the surface shows an abnormally strong (002) from the basal plane. The calculated relative intensity of the lines (including the effect of the cooperating planes but not that of the angle of reflexion) is compared in the following table with the actual observed intensities :—

Reflexion.	Calculated intensity.	Observed intensity.	Reference.
100	3	Very weak.	Figs. 2, 3, 5.
002	4	Very strong.	,, ,,
101	18	Weak.	,, ,,
102	6	Weak.	,, ,,
110	12	Very weak.	,, ,,
103	18	Very strong.	,, ,,
200	3	Absent.	,, ,,
112	24	Strong.	,, ,,

It will be noted that, whilst in a random orientation the (101) should be very much stronger than the (002) reflexion, in actual practice the reverse is the case. This would only occur if the (002) planes were for the greater part in the plane of the deposit for the small reflexion angles used. Of the other planes, those most nearly parallel to the (002), such as the 103, give an abnormally intense reflexion ; those making a large angle with the (002), such as the prism face (100) and the (110), are characterized by lines of much reduced intensity.

(*b*) A transmission photograph obtained with the incident beam passing normally through a flake, taken from the flat deposit, is reproduced in fig. 6 (Pl. VII.). This has two outstanding characteristics : the (002) diffraction ring is completely absent though all the other possible lines are present ; and the rings show no indication of maxima and minima, but are uniform in intensity around each circumference. The first point confirms that the (002) planes lie in the plane of the deposit, since none of them are sufficiently inclined to form a reflexion

angle. The second point shows that the planes are distributed at random as far as an axis perpendicular to the flake is concerned ; the hexagonal cell may be rotated about the *c*-axis into any position. The incident beam is parallel to an axis of rotation.

(*c*) A further type of transmission photograph was taken by passing the incident beam through a section of a flake in a direction parallel to the original surface of the deposit. Such a photograph is shown in fig. 7 (Pl. VII.). The previous results have shown that photograph obtained from the aggregate was equivalent to that which would be given by a single crystallite rotated about an axis normal to the plane of the deposit. In fig. 7 (Pl. VII.) the incident beam is therefore perpendicular to this axis of rotation, and the diffraction rings should now show maxima and minima. This is the case. The angles on the photographic plate between the line parallel to the axis of rotation (the normal to the flake) and the line joining the centre of the rings to the mid-point of the maxima on each ring are calculated for the case in which the axis of rotation is the *c*-axis of the hexagon.

Plane.	Angle between intensity maxima on plate and the parallel to rotation axis.
100	$\pm 90°$
002	$0°$ and $180°$
101	$\pm 62°$ and $\pm 118°$
102	$\pm 42°$ and $\pm 138°$
110	$\pm 90°$
103	$\pm 27°$ and $\pm 153°$
200	$\pm 90°$

The above angles give the positions which the maxima would occupy as points if the orientation were perfect. The present case is peculiar in that whilst the points are drawn out into arcs, indicating an appreciable latitude in the actual orientation, yet the arcs end sharply and the minima show a perfect absence of reflexions. This contrasts with usual experience of oriented aggregates, which give maxima and minima superposed on a ring which is continuous, and means that the deviations from the ideal orientation are limited to a quite definite angle. This angle appears to be about 30°. The two (100) reflexions then spread on the plate over $\pm(60°–120°)$ and

the (002) over $\pm 30°$ and $180° \pm 30°$; this corresponds with the spread shown on fig. 7 (Pl. VII.). The (101) reflexion at 62° will spread from 32° to 92° and the 118° reflexion from 86° to 148°; these two reflexions will overlap in the neighbourhood of 90° and form in practice a large arc from 32° to 148° approximately. This again agrees with the photograph given by fig. 7 (Pl. VII.) and explains why two arcs instead of four appear on the (101) ring. The same reasoning applies to the (102) ring, which shows a pair of even more extended arcs. On the other hand, the next ring, the (110), possesses maxima which stretch from $\pm(90 \pm 30°)$ and are shorter; similarly the (103) and (200) give less extended maxima; these conclusions are also in agreement with the observed photograph. The above orientation therefore completely accounts for the observed intensity distributions, and particularly the rather curious features that each ring should consist apparently of two maxima only and that for the successive rings these maxima should appear to alternate between the 0° and 90° positions. The result appears to indicate that the columnar structure associated with preferred orientation is composed of crystallites of which the long axis approximates to the hexagonal axis of the atomic structure.

Acknowledgement.

The author is indebted to Dr. G. W. C. Kaye for his interest in the researches of which this is part, and to Mr. M. G. Harwood for assistance in preparing and photographing specimens.

Summary.

An X-ray examination of the hexagonal modification of electroplated chromium has been made in order to determine the orientation of the crystallites composing the deposit. It is found that these tend always to lie with the hexagonal axis of the atomic structure perpendicular to the plane of the deposit. The same highly oriented structure persists whether the deposit is on copper, nickel, brass, or iron, and whether the base metal is cleaned or uncleaned, and thus appears to be an intrinsic property of this form of chromium.

Reference.

(1) W. A. Wood, Phil. Mag. xii. p. 853 (1931).

LXIX. *Thermal Conductivity of Supraconductors in a Magnetic Field. By* K. MENDELSSOHN *and* R. B. PONTIUS, *Clarendon Laboratory, Oxford* *.

THE thermal conductivity of supraconductors has already been subject to a number of investigations carried out in Leiden [1]. These researches have shown that in a pure metal the heat resistance is always higher in the supraconductive than in the normal state, whereas the phenomena are evidently more complicated in the case of alloys. In the course of magnetic and calorimetric experiments on supraconductors carried out in this laboratory in the last few years [2] the destruction and the re-establishment of the supraconductive state in pure metals and alloys has been investigated in detail. It appeared that it would be desirable to learn more about the properties of the so-called "intermediate" state in pure metals and the hysteresis phenomena in alloys. As the Leiden experiments on the thermal conductivity have not been extended to these problems, it was decided to measure the changes of thermal conductivity that occur at the isothermal destruction of supraconductivity by a magnetic field.

Method.

The method of measurements was in principle similar to one used by de Haas and Bremmer [1] but modified for our special requirements. A schematic diagram of the arrangement is given in fig. 1. In the vacuum space of a helium liquefier working on the expansion principle [3] and in thermal contact with the liquid helium, was located a rod R of the sample under investigation The upper end of this sample was autogeneously soldered to the thick walled copper helium container C, through the intermediary of a short bundle of no. 16 s.w.g. copper wires. To the lower end of the sample the copper bulb B of a sensitive helium gas thermometer was attached with Rose metal. Energy could be supplied to the lower end of the specimen by the heating coil H, and the temperature interval between the ends of the specimen was found from the difference between the temperature

* Communicated by Dr. K. Mendelssohn.

given by the vapour pressure of the liquid helium in C and the reading of the gas thermometer.

As our main object was not to determine the absolute

Fig. 1.

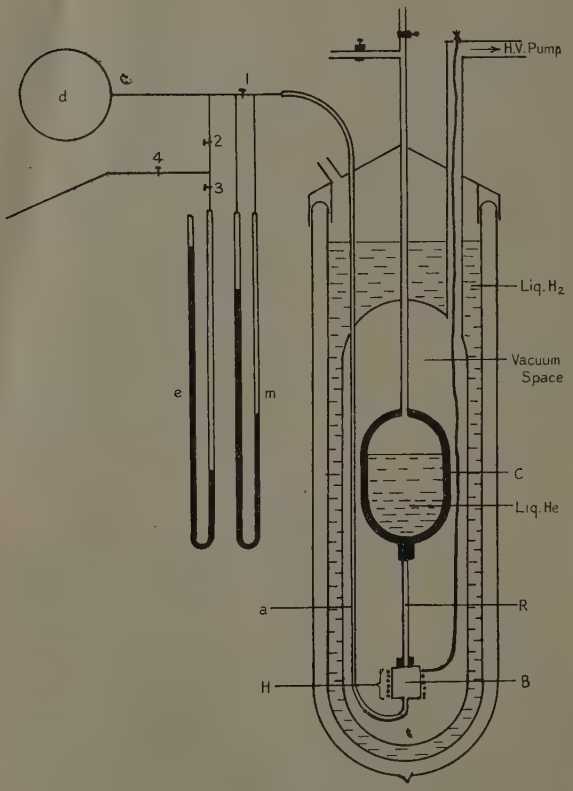

Apparatus.

value of thermal resistance but to measure relative changes very accurately, we employed a special kind of gas thermometer. This was one in which temperature changes resulted in changes of volume and pressure.

The instrument was very simple in construction and operation, and entirely fulfilled its purpose. The thermometer space B is connected through the capillary *a* to the differential manometer *m*, the other side of which is connected with a glass vessel *d* of 3·8 litres capacity. The system can be pumped out and filled with clean helium by tap 4, the pressure of the filling being measured on the mercury manometer *e*. The manometer *m* contains butylpthalate of density 1·289 grams/c.c., which has a vapour-pressure of less than 10^{-3} mm. Hg at room-temperature.

The method of working was as follows: At 4·2° K. (the boiling-point of liquid helium under atmospheric pressure) the gas thermometer was filled with helium gas to about 50 cm. of Hg pressure with taps 1, 2, and 3 open, and the filling pressure read on the mercury manometer *e*. The zero manometer deflexion was obtained by first allowing both sides of the differential manometer to communicate with the gas thermometer reservoir until thermal equilibrium with the liquid helium in C had been obtained through the specimen, then tap 1 was closed. Now the heating current was switched on and the new position of equilibrium obtained, the manometer being read every minute. For every change of field the new equilibrium position was determined in this way. In the case of pure lead a temperature difference between the top and bottom of the specimen of 0·26° (mean temperature 4·36° K.) gave a manometer deflexion of 29·2 cm. Hence a temperature change of 0·001° could still easily be read. The space *d* was always open to the left-hand arm of the manometer, thus maintaining a practically constant pressure on that side. The maximum change in pressure on that side during one experiment was of the order of 0·5 per cent. In order to calculate the temperature interval between the ends of the specimen, corrections to the manometer readings were made for the dead volume and change of pressure; thermal diffusion was neglected, and the correction for the departure of the helium gas from ideality was small, as only a temperature difference was determined. The small correction for heat leakage and radiation was deduced from a blank experiment without a specimen.

Thermal Conductivity in the Intermediate State.

When a supraconductive metal is transformed into the normal state by application of an external magnetic field and does not have the shape of an infinitely long cylinder with its axis parallel to the field, it passes into an "intermediate" state as soon as the field has reached the threshold value (H) at any place on the surface [4]. In this state the induction changes continuously from the value B=O to the value B=H during the increase of the magnetic field. It is in this state also that the electrical resistance of a wire in a transverse field returns in the field interval between $\frac{1}{2}H_c$ and H_c. Hence, in order to investigate the thermal conductivity in this state, we have made use of transverse fields and determined the changes in thermal conductivity in the magnetic transition for the case of pure lead.

A long rod of spectroscopically pure Hilger lead (99·999 per cent. pure, Lab. No. 8334) was made by casting. The transverse external field was produced by a large iron electromagnet giving homogeneous fields over the whole length of the specimen. As the thermal conductivity of pure lead has already been investigated by de Haas and Bremmer [1] in a longitudinal field, no measurements of the absolute values of the conductivity were made by us, but only the relative conductivities with and without fields of strengths up to and somewhat beyond the threshold values. Two curves were taken, one for a mean temperature of 4·36° K. and one for a mean temperature of 5·5° K., both being similar. The first curve is shown in fig. 2, in which the changes in manometer deflexion, which are proportional to the changes in thermal conductivity, are plotted against the external fields. For the curve shown, the temperature difference between the ends of the specimen was 0·256° in zero field.

In fig. 2 a number of interesting features are to be noted. In the first place, up to a definite critical value, the magnetic field has no effect on the thermal conductivity. After this critical value is passed the thermal conductivity increases. Fig. 2 shows that the first change in thermal conductivity occurs at a field of 306 gauss. If we extrapolate the threshold curve of lead (which is known up to 4·25° K.) to the temperature of the warm

end of the specimen (4·49° K.) we arrive at a critical field H_c of 525 gauss. This means that the thermal conductivity in the transverse case is first affected by a field of 0·58 H_c. This does not agree with the expected value 1/2 H_c, but is in agreement with the results of measurements on the electrical resistance [5]. After the critical penetration value of the field has been

Fig. 2.

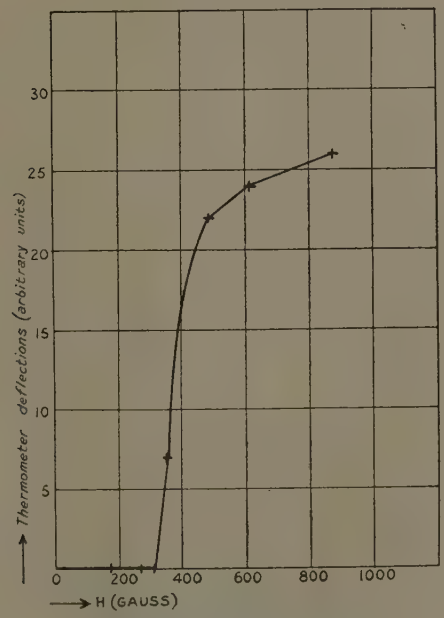

Thermal conductivity of lead.
$T_1 = 4·23°$, $\Delta T = ·256°$, transverse field.

exceeded, the increase of the thermal conductivity seems to proceed regularly without any abrupt changes. We gained the impression from this, and also from the experiment with larger temperature gradients in the specimen (fig. 3), that beyond the threshold value there still remains a slight change of thermal conductivity with field.

Thermal Conductivity of a Supraconductive Alloy.

In order to ascertain the behaviour of an alloy in the region of penetration of an external field, a rod was cast containing by atoms 90 per cent. lead and 10 per cent. bismuth, the metals being both pure "H.S. Brand" Hilger substances. In the case of an alloy one expects a magnetic behaviour different from a pure metal. There

Fig. 3.

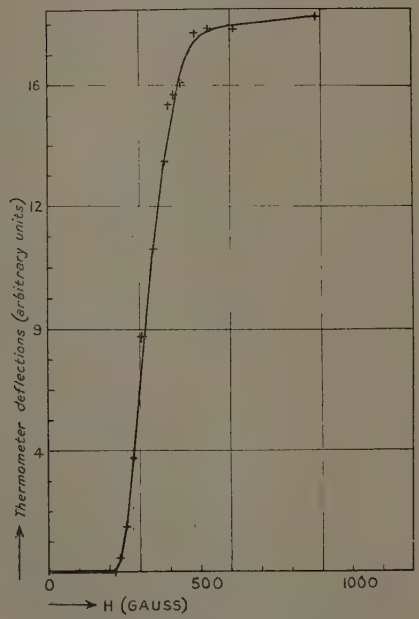

Thermal conductivity of lead.
$T_1 = 4{\cdot}24$, $\Delta T = 2{\cdot}3°$, transverse field.

is an early penetration of the external field, a higher threshold value, and a marked hysteresis or "freezing in" of the flux on decreasing the field [6].

In order to compare the phenomena in induction and thermal conductivity, a magnetic induction cycle was first made with a long ellipsoid (ratio of axes 1 : 10) of the same alloy, the induction being measured by a

flip-coil method previously described [2]. In fig. 4 this cycle is given, where the early penetration of field, high final field, and large residual induction are clearly seen, the " frozen in " flux being close to 38 per cent.

The thermal resistance of this material was then measured in the same apparatus as employed for the pure lead. In order to obtain large deflexions on the gas thermometer, heating currents were used which resulted in temperature intervals of 0·44 to 0·94 degrees. As the

Fig. 4.

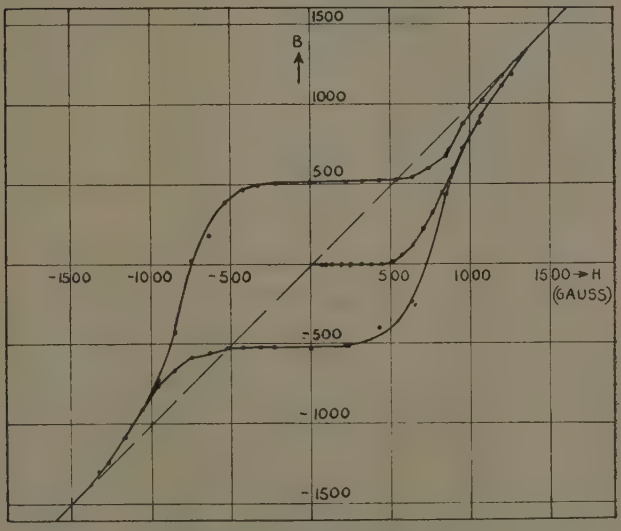

B, H-curve for Pb 90%, Bi 10%.
T=4·31° K., ellipsoid 5·6 : 50.

thermal resistance of the alloy is much greater than that of the pure metal a shorter specimen was employed. The experiments were made on different days with different gas thermometer fillings, and it is not possible to represent the results simply as changes in manometer deflexion proportional to changes in thermal resistance as in figs. 2 and 3. It was therefore necessary to calculate, in each case, the absolute thermal resistance. As now, to make these calculations, a number of measurement errors

must be allowed for, an accuracy to within only 3 per cent. can be claimed for the values of the thermal resistances given. It can be seen, however, from fig. 5, in which a graph of the results is given, that the changes in thermal resistance due to changes of the magnetic field are so large that this accuracy is quite sufficient.

It can be seen that again, up to a definite critical value, there is no penetration of the external field. This value is roughly 210 gauss, approximately half the value for which it began in the induction experiment (where we had to deal with the longitudinal case), and far less than the final threshold field.

The most remarkable facts to be noted here are, however, (*a*) on further application of the field, the thermal resistance increases, and (*b*) after the final threshold value of field has been exceeded and the field reduced to zero again, the thermal resistance remains considerably greater than the virgin value in zero field. In fact, we find a similar hysteresis figure for the thermal resistance as is shown by the induction experiment.

Discussion.

The results for the thermal resistance of a lead wire of circular cross-section in a transverse magnetic field (figs. 2 and 3) bear a great resemblance to change of electrical resistance observed under the same conditions [5]. Here also the first change is observed at a field strength of about $1/2\ H_c$, and a continuous change occurs with further increasing field until H_c is reached. It is probable that the slight increase in thermal conductivity above H_c is linked with the increase in electrical resistance which can be observed in the same region*.

The change in the thermal resistance of the supra-conductive alloy (fig. 5) shows a great similarity to the

* In experiments on the electrical resistance of very pure lead wires in dependence on the magnetic field which have recently been carried out in this laboratory, an increase of resistance with field was observed at fields far above H_c. By more detailed experiments on the thermal resistance in this region one might be able to decide whether this change in electrical resistance is a phenomenon related to supra-conductivity. It seems peculiar that the increase in electrical resistance in this region is accompanied by a decrease in thermal resistance, whereas in general the application of a magnetic field results in an increase of the thermal as well as of the electrical resistance (*e. g.*, E. Grüneisen and J. Gielessen, *Ann. Phys.* 5, xxvi. p. 449 (1936)).

corresponding change in its magnetic induction (fig. 4). The total change is spread over a wide field interval, which evidently means that the magnetic field only penetrates very gradually into the specimen and on the return a strong hysteresis occurs. This is exactly what

Fig. 5.

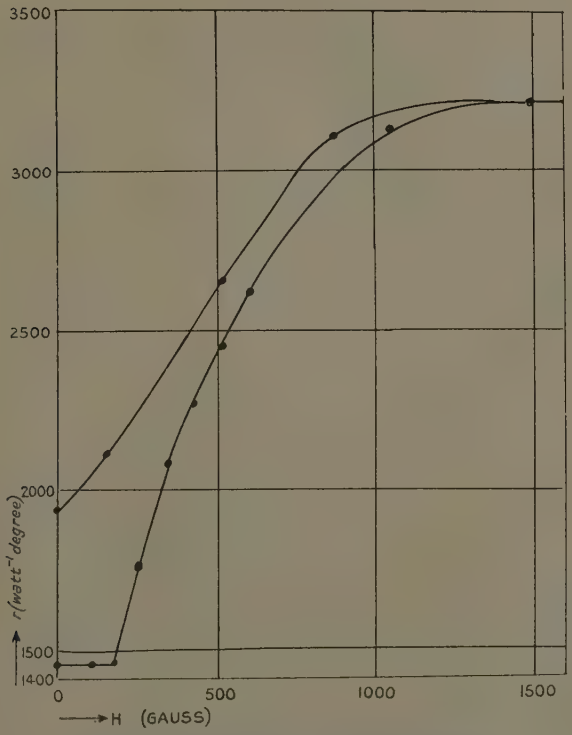

Thermal resistance (r) of Pb 90%, Bi 10%.
$T_1 = 4{\cdot}2°$ K., $\Delta T = {\cdot}44°$–${\cdot}49°$, transverse field.

had to be expected according to our previous experiments on supraconductive alloys. We have compared these alloys with a sponge [2], the meshes of which have high threshold value, whereas the material inside the meshes has roughly the same threshold value as pure metals. In the present experiments again the gradual penetration

of the field indicates the gradual breaking up of the "sponge" in the increasing field. When the field is decreased and the meshes become again supraconductive the magnetic flux inside the meshes is "frozen in," thus preventing part of the metal to return to the supraconductive state. This has the result that the thermal resistance remains on the whole return curve higher than at the corresponding fields of the ascending curve.

R. de L. Kronig [7] has attempted to give an explanation for the drop in thermal conductivity which occurs when a metal becomes supraconductive by assuming that part of the free electrons pass into the supraconductive state and are no longer available for heat transport. Optical experiments on supraconductors carried out by Daunt, Keeley, and Mendelssohn [8] have, however, not shown the effect which de L. Kronig predicted from his assumptions, and the result of the experiments on a supraconductive alloy described in this paper also disagrees with de L. Kronig's view. It is evident that if the supraconductive electrons did not take part in heat conduction this should result in an increased heat resistance in an alloy as well as in a pure metal, whereas the experiment shows clearly that the heat resistance of the alloy *decreases* when it becomes supraconductive.

In order to remove the difficulty which arises out of the fact that the supraconductor shows a lower heat conductivity than the normal state in a pure metal, and a better conductivity than the normal in an alloy, we suggest the following tentative explanation: the electrons in the supraconductive state take part in the heat transport, but conduct, as the experiment shows, heat not as good as the electron "gas" in the normal state. The scattering of electrons at lattice disturbances, which diminishes heat conduction, however, is stronger in the normal than in the supraconductive state, owing to the higher degree of order [9] of the latter. (This is also shown by the change in electrical conductivity.) The addition of a second constituent to the metal creates lattice disturbances, and accordingly higher scattering and decreased heat conduction in the normal state, whereas the supraconductive electrons are not similarly affected. If our assumption is right, it should be possible to trace all intermediate stages between a pure supraconductor and an alloy in thermal conductivity, and

one should be able to make a metal which shows no change in heat conduction at all when passing from the normal to the supraconductive state. Experiments on the difference in behaviour of solid solutions and intermetallic compounds may also yield interesting results.

Summary.

The change of thermal conductivity of supraconductors in a transverse magnetic field has been investigated.

For a pure metal the change in thermal conductivity is similar to the corresponding change in electric conductivity.

For an alloy the change in thermal conductivity shows a hysteresis and is similar to the change in magnetic induction in an external field. The result is in good agreement with our previous assumptions on the constitution of supraconductive alloys.

An explanation for the effect of a magnetic field on supraconductive pure metals and alloys has been suggested.

References.

(1) W. J. de Haas and H. Brenmer, *Comm. Leiden*, 214 *d*, 220 *b*, 220 *c*.
(2) See, *e. g.*, K. Mendelssohn, Proc. Roy. Soc. A, clii. p. 34 (1935); *ibid.* clv. p. 558 (1936). T. C. Keeley and K. Mendelssohn, *ibid.* cliv. p. 378 (1936).
(3) F. Simon and E. Ahlberg, *Z. Physik*, lxxiii. p. 482 (1933).
(4) R. Peierls, Proc. Roy. Soc. A, clv. p. 613 (1936). F. London, *Physica*, iii. p. 450 (1936).
(5) See, *e. g.*, W. J. de Haas and J. Voogd, *Comm. Leiden*, 212 *c*.
(6) K. Mendelssohn, J. R. Moore, and R. B. Pontius, VII. Int. Cong. du Froid, the Hague, 1936.
(7) R. de L. Kronig, Proc. Roy. Soc. A, clii. p. 16 (1935).
(8) J. G. Daunt, T. C. Keeley, and K. Mendelssohn, Phil. Mag. vii. pp. 23, 264 (1937).
(9) J. G. Daunt and K. Mendelssohn, Proc. Roy. Soc. A, clx. p. 127 (1937).

LXX. *Threshold Values of Supraconductors of Small Dimensions.* *By* R. B. Pontius, *Clarendon Laboratory, Oxford* *.

Introduction.

CONDUCTIVITY experiments on alloys have shown that for these supraconductivity persists in field strengths much greater than the threshold fields for pure

* Communicated by Dr. K. Mendelssohn.

metals, whereas it is evident from magnetic experiments that in these alloys the induction deviates from the value zero in field strengths far below the threshold fields. In this connexion, with regard to a large number of experiments on supraconductive alloys, it was pointed out by Mendelssohn [1] that the high threshold value in alloys is probably confined to regions of very small dimensions, and that small dimensions of a supraconductor and the high threshold value are causally connected. This view is rendered plausible by the electrodynamic considerations of Becker, Sauter and Heller [2], and the Londons [3], who have shown that a magnetic field will penetrate below the surface of a supraconductor *, the depth of this penetration depending on the number of supraconducting electrons, and being of the order of 10^{-6} cm. if there are as many supraconducting electrons as atoms. With regard to our previous experiments, we have suggested that the effect of the depth of penetration on small supraconductive regions might be to increase their magnetic threshold, and thus account for the high threshold values found for alloys [4]. It follows that supraconductivity might persist in higher field strengths in a very thin wire than in a thick wire of the same material at the same temperature [5]. Theoretical treatments of small supraconductive regions by Gorter [6] and H. London [7] indicate the same possibility.

A number of experiments carried out in Toronto on thin tin and lead films by Misener, Grayson Smith, and Wilhelm [8] actually indicate such an effect. In these experiments, however, the film was deposited on a core of non-supraconducting metal, and, as the possibility of an alloy being formed at the boundary surface could not be excluded, the effect of the film thickness on the threshold value was not altogether certain It was therefore decided to carry out experiments on thin wires of a pure metal which were made as free as possible from the disturbing effects of impurities.

Method.

Lead was chosen for these experiments, as it has already at 4·2° K. a high threshold value. Hilger

* This surface penetration is for field strengths less than the threshold value, and is quite independent of the penetration which occurs in the magnetic transition or " intermediate state."

" H.S. Brand " lead (Lab. no. 8334, 99·999 per cent. pure) was used, and wires were made by the Taylor process by drawing in carefully cleaned pyrex capillaries in an oxygen flame. After being drawn the wires were annealed for twelve hours at 230° C., and the pyrex then dissolved off with hydrofluoric acid. The most uniform samples were selected and their average diameters measured by means of a microscope with calibrated eyepiece.

In mounting the small wires great care was necessary to prevent breakage, and, as soldering was found unreliable, the end connexions were finally made by electroplating with copper. Thin strips of mica were prepared with strips of copper foil bent around near the ends of the mica and soldered with pure bismuth. To these copper strips on the underside of the mount the current and potential leads of no. 40 s.w.g. copper were soldered, also with pure bismuth. The tops of the copper strips were carefully cleaned with acid and acetone, and the wire specimen laid on and between the two copper strips. The copper electroplating was now done by using the copper foil as the cathode and bringing up an external anode, a drop of copper sulphate serving as the electrolyte. After plating on a layer of copper of 50 to 150 μ thickness, depending on the specimen, the copper sulphate was drained away with filter paper and the plating washed with several drops of distilled water. Afterwards the whole specimen was protected by means of a mica shield supported about 0·5 mm. above but not touching the wire. The largest specimens were 4 to 5 cm. long the smallest 0·5 cm. The specimens were allowed to lie a little slack as a precaution against breakage. The connexions at the ends introduced a small resistance which did not vanish when the specimen became supraconductive, but this could be allowed for in the measurements.

By this method of preparing and mounting the wires small specimens of high purity could be produced. This is indicated by transition curves, which show approximately the same breadth for small and large wires, and by the magnetic induction curve (fig. 3) made with a compact bundle of such wires. This latter shows a rather sharp transition and exceedingly small amount of " frozen in " flux, both characteristics of a high purity, as previous experiments have proved [4]. As the contact

resistance of the ends was small compared with the total resistance of the wire (in the normal state), this did not introduce any disturbing influence on the measurements.

Finally, the specimens were fastened to the end of a long, thin glass tube, by means of which they could be dipped into liquid helium *, the current and potential leads running out through the glass tube. A wire of large (60 to 160 μ) and one of small diameter were always mounted together, so that the transitions of both could be compared simultaneously.

The potential drop through the specimen was measured by means of a sensitive galvanometer, with which changes of resistance of the order of 10 micro-ohms—that is, about 0·07 per cent. of the normal resistance at 4·2° K.—could be detected. The longitudinal external field was produced by a long solenoid, homogeneous to within 1 per cent. over the length of the specimen. The field could be kept constant to 0·2 per cent. A change of threshold value of 0·2 per cent. could therefore be determined.

Results.

The first series of measurements were made at the normal boiling-point of helium, which, owing to the variation of the barometric pressure, was slightly different on different days, although the maximum departure from the mean temperature of 4·213° K. on any measurement was only 0·03° K. The results for wire sizes ranging from 127·1 μ to 5·6 μ are given in Table I., and the transition fields—that is, the field strengths at which resistance first *appears*—plotted against wire size in fig. 1. It is seen from the table that no increase of threshold value above that for the large wires was observed † except in specimens of 19·7 μ or smaller. The first actual change probably occurred at about 25 μ, as can be seen from fig. 1. The maximum increase of threshold value

* The liquid helium was produced in an apparatus which will be described elsewhere, in which, after the helium had been liquefied by expansion, it could be opened to the outside and the specimens inserted one after another. The helium so used lasted ordinarily about six to eight hours for a moderate expansion.

† It must be emphasized that in each case a thick wire of the order of 60 μ or greater was mounted and tested under identical conditions as the thin wire, so that a direct control was obtained.

for the smallest wire measured, 5·6 μ, was 4·08 per cent. greater than the value for the thick wires.

TABLE I.

Threshold Fields of Lead Wires of different sizes.

Diameter in microns.	Measuring current in milli-amperes.	Surface field due to current, in Gauss.	Temperature in degrees Kelvin.	Threshold field in Gauss.
127·2	20	0·6	4·24	539
61·8	20	1·3	4·21	539
46·5	20	1·7	4·20	539
35·3	20	2·3	4·20	539
34·1	5	0·6	4·24	539
19·7	10	2·0	4·23	542
14·2	10	2·8	4·21	545
14·2	5	1·4	4·21	545
9·6	20	8·35	4·21	548
9·6	5	2·1	4·21	551
5·8	2·4	1·65	4·21	558
5·6	3	2·1	4·21	561

Fig. 1.

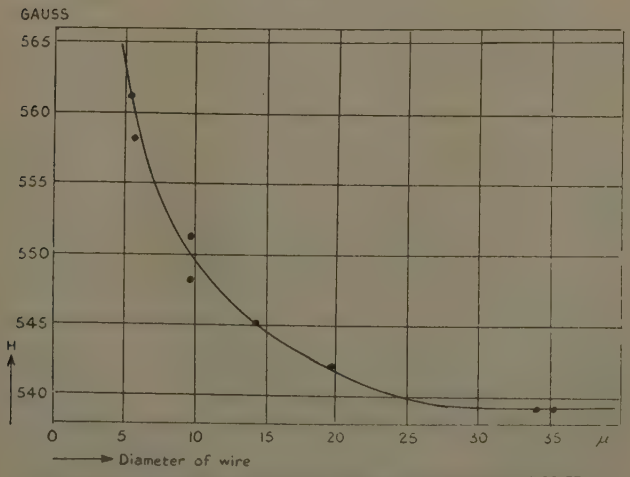

Threshold fields of lead wires of different diameter at 4·2° K.

The actual transition, of course, was influenced by the field at the surface of the wire produced by the measuring current itself. Since the vector of the current field was

at all times perpendicular to the vector of the external field these two had to be added vectorially to find the resultant. However, a surface field of 2·5 gauss due to a current would make a difference of only 0·01 per cent. in a threshold value of 539 gauss. Therefore measuring currents small enough to give a surface field of the order of 2·5 gauss were chosen in most cases, this being small enough to neglect without materially reducing the accuracy of the results.

In the case of the transition to the supraconductive state by reducing the field, for the smallest wires it was found that supraconductivity did not necessarily occur

TABLE II.

Threshold Fields of Thin Lead Wires at different temperatures.

Temp. ° K.	Threshold field.		Ratio of threshold fields.
	5·8 μ.	34·1 μ.	
4·24	565	542	1·042
3·49	660	640	1·031
2·57	749	723	1·035
1·67	796	772	1·032

at the same field strengths at which it had disappeared, but that normal conductivity persisted to far lower fields. This hysteresis, however, did not have the same form for the same specimen in different experiments, and could be reduced by commutating the current after each reading.

The effect of size was further compared for two wires at lower temperatures. For this comparison a 5·8 μ and a 34·1 μ wire were mounted side by side, and their transition fields found at four different temperatures, the results being shown in Table II. and fig. 2. It can be seen that, roughly, the relative increase in threshold for the smaller wire was independent of the temperature, only the sharpness of the transition decreased, as is indicated by the transition curves drawn in fig. 2.

Finally, this effect was correlated with ordinary induction measurements. A large number of thin wires were

drawn, annealed, the pyrex partly dissolved off, and all packed tightly in a small bundle of a length, roughly, ten times the diameter. Of the total number of wires present in the bundle approximately 10 per cent. were of a diameter less than 30 μ and 1 per cent. of a diameter less than 10 μ. The induction was measured at 4·23° K. by a method described by Mendelssohn [9]. The results are given in fig. 3.

It can be seen that the induction (B) was zero nearly up to the threshold value and only began slowly to rise at 480 gauss. This was evidently due to the fact that some

Fig. 2.

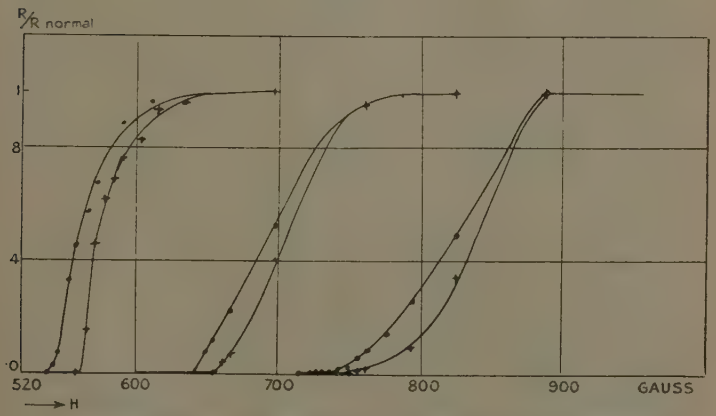

Transition curves of a wire of 34·1 μ (·) and of 5·8 μ (+) diameter at 4·24°, 3·49°, and 2·57° K.

of the wires were not quite straight. The rapid increase in induction occurred at 540 gauss, the normal value being reached at 558 gauss, the induction curve "tailing off" at the end. This "tail" was quite reversible. When the field was reduced practically no flux was "frozen in," which indicated the wires were of high purity and in good crystalline state.

It is instructive to compare this result with the threshold value for a solid sphere of the same lead. The sharp "tailles" transition for this at the same temperature was found by Daunt and Mendelssohn in induction experiments to be 539 gauss [10]. This means the small

size of the specimens was responsible for the "tail" of the induction curve, and agrees with the results of the resistance measurements.

In order to estimate the depth of penetration it would be necessary, according to the theory of H. London [7], to determine the ratio of the current threshold and external field threshold values. However, in every case the wires burned out inconsistently at comparatively low

Fig. 3.

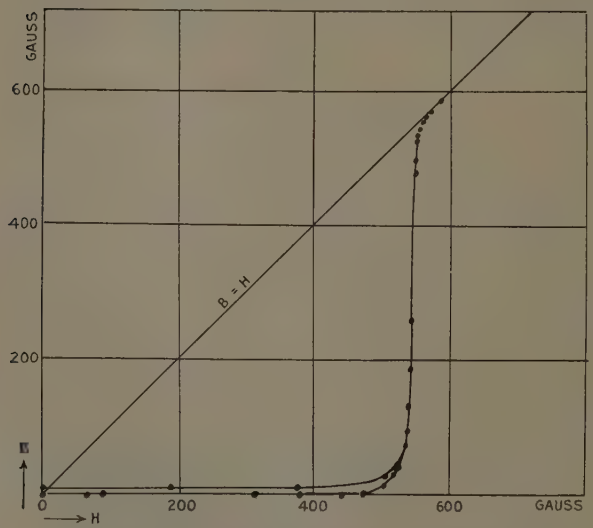

B, H curve of a bundle of thin lead wires at 4·23° K.

current densities. This was probably due to the fact that the current threshold value was first exceeded at the place where the wires made contact with the copper base, and hence no reliable estimate of the current threshold values can be given.

Discussion.

In these experiments the effect of size on threshold values, which had been predicted by Mendelssohn from

considerations of the high threshold values in alloys and pure tantalum, is clearly shown. This effect in these experiments is obviously not due to impurity or strains in the specimen, and gives a clear indication of the rôle which the depth of penetration of the field and current into the supraconductor must play in the magnetic transition. At constant temperature the threshold increases rapidly with decreasing size of wire below a certain critical diameter, while at lower temperatures the relative increase for constant wire size is independent of the temperature. This latter shows that the effect of the depth of penetration is substantially not dependent on the temperature, as one would expect if the number of supraconduction electrons does not change materially with decreasing temperature. Although one cannot give a definite value for the depth of penetration this must be of the order of magnitude of 10^{-5} to 10^{-6} cm., which would yield a value for the number of supraconduction electrons of the order of the number of ions. Unfortunately, reliable current threshold values, which could settle this question, are lacking.

The resistance measurements are entirely confirmed by the induction experiment on the bundle of fine wires, which further shows that in all cases wires of exceptional purity were being dealt with. In particular, the small "tail" is exactly what one would expect for the case of an alloy; while the fact that the induction curve is definitely that of a pure material is proved by the very small amount of "frozen in" flux obtained on decreasing the external field.

In the light of these experiments, the origin of the high threshold fields of alloys can be accounted for. Mendelssohn has postulated [1] a supraconducting "sponge," the skeleton of which possesses a high threshold value, although occupying only a small fraction of the total volume of the alloy. This fine partition of small regions, which may originate from defects in the lattice, chemical or physical, must possess, according to the experiments described in this paper, a much higher threshold value than the bulk of the material. It can be seen from an examination of fig. 1 that, in order to account for the enormously high threshold values of some alloys, it is not necessary to assign exceedingly small dimensions to the skeleton of the "sponge."

Summary.

In order to ascertain the effect of the depth of penetration on the threshold value of a pure supraconductor lead wires of a diameter of nearly the same order as the depth of penetration have been investigated at several temperatures. Wires of high purity were made by the Taylor process and their resistance and induction threshold values investigated in a longitudinal field. The results show an increase of threshold value with decreasing size of wire below $20\,\mu$, indicating a depth of penetration of the order of 10^{-5} to 10^{-6} cm., and corresponding to this a number of supraconduction electrons of the same order as the number of atoms. This result confirms Mendelssohn's assumption that supraconductors of small dimension show a higher threshold value than the bulk material, and the high threshold values observed in alloys are interpreted in terms of this effect.

Acknowledgment.

In conclusion, I wish to express my thanks to Prof. F. A. Lindemann, F.R.S., for kind permission to work in his laboratory and for his continual interest in my work, and to Dr. K. Mendelssohn, who suggested this research, for his encouragement and help in carrying out the experiments. I wish also to acknowledge the assistance of Dr. R. V. Jones in preparing the fine wires, and of Mr. J. G. Daunt in carrying out the experiments. I am especially grateful to the Rhodes Trustees, who, by a special grant, made this research possible for me.

References.

(1) K. Mendelssohn, Proc. Roy. Soc. A, clii. p. 34 (1935).
(2) R. Becker, Heller, and Sauter, *Z. Physik.* lxxxv. p. 772 (1933).
(3) F. and H. London, Proc. Roy. Soc. A, cxlix. p. 71 (1935).
(4) K. Mendelssohn, J. R. Moore, and R. B. Pontius, VII. Congr. Int. du Froid, the Hague, 1936.
(5) K. Mendelssohn and J. R. Moore, Phil. Mag. 7, xxi. p. 532 (1936).
(6) C. J. Gorter, 'Physica,' ii. p. 449 (1935).
(7) H. London, Proc. Roy. Soc. A, clii. p. 650 (1935).
(8) Misener, H. Grayson Smith, and J. O. Wilhelm, Trans. Roy. Soc. Canada, 3, xxix. p. 13 (1935); Canad. J. Research, xiv. p. 25 (1936).
(9) K. Mendelssohn, Proc. Roy. Soc. A, clv. p. 558 (1936).
(10) To be published shortly.

LXXI. *The Adsorbed Moisture Films on the Surface of Glazed Porcelain.* *By* F. W. Johnson, *M.Sc., Ph.D., Lecturer in Electrical Engineering, Denbighshire Technical Institute, Wrexham* *.

Introduction.

THE moisture films which form on the surface of most insulating materials are of great importance. That they are of a very complex nature is known. Their behaviour under the influence of alternating voltage stresses has been studied. The films are not stable under these conditions, but the laws of change can be definitely defined, and are all of exponential character. The present paper deals with the coordination of results obtained upon a glazed porcelain surface, with regard to the changes which occur in these films under the influence of alternating voltage stresses and surface temperatures. All the physical properties of the films are interrelated.

Humidity and the Surface Film.

Under steady conditions of humidity and temperature the surface film is stable and has a definite fixed value for the surface resistivity r_0. There are then two factors operating on the film. There must be deposition of moisture particles from the air on to the surface at a rate proportional to the humidity, that is counterbalanced by the evaporation of an equal number of particles from the surface.

When an alternating voltage is applied across the film a current passes and energy is dissipated. When the voltage applied is e, and the resistivity per square centimetre of surface is r, the energy dissipated per square centimetre of the surface is e^2/r, and this produces evaporation of the film at a rate of $\mathrm{K}e^2/r$ per unit mass of moisture on the surface. This effect is counterbalanced by a deposition of moisture particles from the surrounding air at a rate of A per unit mass of moisture on the surface. The factors K and A are termed the rate of evaporation and rate of deposition of moisture per unit mass of moisture respectively. It has been shown † that the

* Communicated by Prof. W. M. Thornton.

† Phil. Mag. xviii. (July 1934).

film then alters its resistivity in an exponential manner, and finally reaches a second equilibrium state when its resistivity becomes equal to some value r_∞ after infinite time.

The change is according to

$$r = r_0 + (r_\infty - r_0)(1 - \epsilon^{-At}),$$

and is increasing for $r_\infty > r_0$, decreasing for $r_\infty < r_0$; and there is no change for the special condition $r_\infty = r_0$. This condition only occurs once for any range of humidity and one type of surface of the insulating material. This change leads to the condition $A \lessgtr Ke^2/r_0$ for the initial state and $A = Ke^2/r_\infty$ at the second equilibrium state.

The relations between the two equilibrium values of r_0 and r_∞ and the humidity h are both exponential in character. The change of the final resistivity r_∞ with the humidity h is expressed by

$$r_\infty = r_{\infty_{100}} \epsilon^{k_3(1-h)},$$

while that between the initial resistivity r_0 and the humidity is more complex, probably of the form

$$r_0 = r'_{0_{100}} \epsilon^{k_4(1-h)+c\,\epsilon^{k_5(1-h)}},$$

where $r_{\infty_{100}}$ and $r'_{0_{100}}$ refer to the values of the resistivity at 100 per cent. humidity.

The rate of deposition factor A per unit mass of moisture on the surface varies exponentially for a fixed voltage with the humidity, $A = A_{100} \epsilon^{k_2(1-h)}$. The actual value of A depends upon the square of the voltage applied to the film. The evaporation factor K is also an exponential function of the humidity, $K = K_{100} \epsilon^{k_1(1-h)}$. The value of K depends only on the surface conditions, and is not affected by the voltage values. And from the relation $A = Ke^2/r_\infty$, since A, K, and r_∞ are exponential functions of the humidity, the indices k_1, k_2, and k_3 are related by $k_1 + k_2 = k_3$.

It has been shown * that the surface resistivity depends on the surface conditions, and small changes of the surface state have marked effects on the values of the surface resistivities r_0 and r_∞. But at zero humidity

* *Ibid.*

the surface state has little or no effect on the value of the resistivity r_{∞_0} finally reached under the influence of voltage.

These expressions have led to the suggestion that the surface films on insulating materials are partly an adsorbed film and partly a solution of the insulator surface in the film.

Surface Conditions.

If the surface film is of the nature of a partly adsorbed film and partly a solution of the insulator surface in the surface film it should show physical properties dependent on the concentration and proportions of these two states. The surface solution will be saturated, since the mass of the solute is much in excess of the solvent, and deposition of foreign matter on the surface will affect only the composition of the surface solution. The change produced will depend on the relative solubilities of the deposit and the surface materials, but the surface solution will always remain saturated. The composition of the surface solution is therefore constant for one surface condition irrespective of the humidity. For a stable film at any humidity the two parts of the film must be in equilibrium with each other, and there will be a definite proportion between them. The deposition of matter on the surface, affecting only the surface solution, will not affect the adsorbed film unless it is capable of changing the whole nature of the surface. The equilibrium between the two portions of the film is a mass equilibrium between the amounts of moisture held in these parts, and is independent of the composition of the surface solution. Changes in the resistivity of the surface film are caused by changes in the surface solution, unless the deposit can change the nature of the insulator surface.

When the humidity is changed the equilibrium states between the surface film and the water vapour of the surrounding air and between the two portions of the film are disturbed. Evaporation or deposition of moisture will take place initially with respect to the surface solution, and this is followed automatically by a transference of moisture between the constituent parts of the surface film to maintain the equilibrium states. For any given humidity therefore the proportions of the surface film are constant, and its physical properties which are dependent

on its composition are also constant. Over a range of humidities the proportionate composition of the film for a fixed surface condition must remain constant, for only under this condition can the physical properties show exponential relations with respect to humidity, and throughout the changes of resistivity caused by the passage of a current through the film.

The amount of energy K required to evaporate a unit mass of moisture from the surface depends on the humidity and the composition of the surface film. If the composition is constant the rate of evaporation K depends on the humidity. The changes produced in the rate of evaporation K by change of humidity if the rate is high are less than those produced if the rate is low. Hence the index k_1 of the expression $K=K_{100}\epsilon^{k_1(1-h)}$ depends inversely on the value of K.

For any given type of surface the resistivity cannot increase indefinitely, for the film must reach a minimum thickness. Hence there must be a maximum value for K_0 at which k_1 is zero. Taking the other limiting values of K_{100} at 100 per cent. humidity, a range of values of K_{100} is possible, and for each case the expression relating K to the humidity is $K=K_{100}\epsilon^{k_1(1-h)}$. At zero humidity this gives $K_0=K_{100}\epsilon^{k_1}$. At zero humidity the surface solution will have disappeared, although it is known that part of the adsorbed film remains *. The values of the physical properties of the film at zero humidity will therefore be constant: so K_0 is a constant, a maximum value for all surface conditions, and when K_{100} equals K_0 the index k_1 is zero. Therefore the value of K_{100} for each surface condition is a function of the index of change k_1. Thus $K_{100}=K_0\epsilon^{-k_1}$ for all cases, and the value at any other humidity may be calculated.

The final resistivity r_∞ is also a function of the composition of the film and the humidity. The value of r_{∞_0} at zero humidity is a constant maximum value for all surface conditions, and for any surface condition $r_{\infty_{100}}=r_{\infty_0}\epsilon^{-k_3}$. Correlation of this is obtained through the relations existing between the final resistivity r_∞, the rate of evaporation K, and the rate of deposition A, which are all constants at a given humidity. The indices of change, k_1, k_2, and k_3, are also definitely related by the

* Warburg and Ihmori, Wiedemann's *Annalen*, xxvii. (1886).

expression $k_1+k_2=k_3$. Hence all values of r_∞ can be found from the maximum value r_{∞_0}. Similarly the indices k_4, k_5, and c of the expression

$$r_0=r'_{0_{100}}\epsilon^{k_4(1-h)+c\epsilon^{k_5(1-h)}}$$

must be functions of the initial and final resistivities r_0 and r_∞.

If the values of $r_{\infty 100}$ and K_{100} greater than the fixed values r_{∞_0} and K_0 are possible for any type of surface the indices k_1 and k_3 will become negative; but since these values are bound up with the rate of deposition of moisture on the surface A, whose change with respect to humidity gives the indices relation $k_3=k_1+k_2$, negative values of k_1 and k_3 are not possible. The values of k_1 and k_3 are decreasing in value, and k_2 is always positive and of a definite value for one applied voltage. Values greater than r_{∞_0} are not possible for any one type of surface material.

Experimental Results.

During tests on a glazed porcelain surface, six different surface conditions were obtained. Values for the initial resistivity r_0, the final resistivity r_∞, the rate of evaporation factor K, and the rate of deposition factor A were measured. From these the equations given above were derived.

TABLE I.

Values obtained for the Rate of Evaporation Factor K. Standard form of equation: $K=K_{100}\epsilon^{k_1(1-h)}$.

Surface condition.	Value of K_{100}.	Value of index k_1.	Value of K at zero humidity K_0.	Value of $r_{\infty 100}$.
1	1·858	4·257	131·3	$5·52\times10^8$
2	0·7474	5·169	131·4	$2·22\times10^8$
3	1·353	4·582	131·4	$4·02\times10^8$
4	2·383	4·017	131·4	$7·08\times10^8$
5	18·18	1·963	129·6	$5·40\times10^9$
6	0·4104	5·776	132·5	$1·22\times10^8$

These results give a maximum value for the rate of evaporation factor K_0 at zero humidity; for this particular

porcelain surface it is 131·1. Plotting these results, fig. 1 the indices k_1 to a base of the logarithm of K_{100} for each surface condition gives a linear relation. Thus $K_{100} = K_0 \epsilon^{-k_1}$ for all the surface conditions.

Fig. 1.

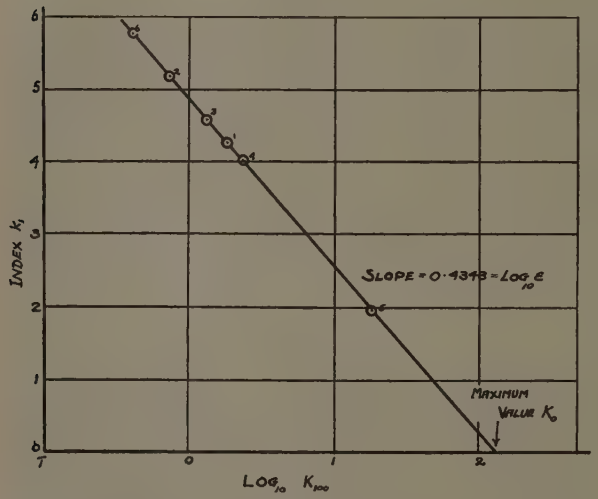

Showing the linear relation between the indices k_1 to a base of the logarithms (to the base 10) of the values K_{100} for the corresponding surface conditions, indicated by the numerals 1, 2, 3, etc.

Table II.

Values obtained for the Final Resistivity r_∞.
Standard form of equation : $r_\infty = r_{\infty\,100}\, \epsilon^{k_3(1-h)}$.

Surface condition.	Value of $r_{\infty\,100}$.	Value of index k_3.	Value of r_∞ at zero humidity $r_{\infty\,0}$.
1	$5{\cdot}52 \times 10^8$	7·456	$9{\cdot}548 \times 10^{11}$
2	$2{\cdot}22 \times 10^8$	8·366	$9{\cdot}543 \times 10^{11}$
3	$4{\cdot}02 \times 10^8$	7·769	$9{\cdot}548 \times 10^{11}$
4	$7{\cdot}08 \times 10^8$	7·206	$9{\cdot}548 \times 10^{11}$
5	$5{\cdot}40 \times 10^9$	5·174	$9{\cdot}537 \times 10^{11}$
6	$1{\cdot}22 \times 10^8$	8·966	$9{\cdot}550 \times 10^{11}$

These results give a maximum value for the final resistivity r_{∞_0} at zero humidity for this particular porcelain surface of $9{\cdot}548 \times 10^{11}$ ohms per centimetre square of surface. Plotting the results the indices k_3 to a base of the logarithms of $r_{\infty_{100}}$ gives a linear relation. Thus $r_{\infty_{100}} = r_{\infty_0} \epsilon^{-k_3}$ for all the surface conditions.

Fig. 2.

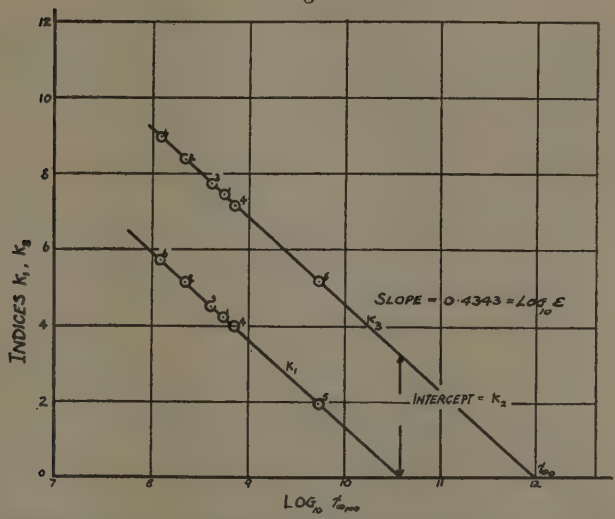

Showing the linear relation between the indices k_3 to a base of the logarithms (to the base 10) of the values of the final resistivity $r_{\infty_{100}}$ for the corresponding surface conditions.

On fig. 2 are also plotted the indices k_1 of the rate of evaporation factor K. The lines are parallel, the intercept being the index k_2 of the rate of deposition factor A, viz., 3·189 at 3000 volts. The lines do not appear to come to zero together, but as the factors r_∞ and K are related by the expression $A = Ke^2/r_\infty$, if e is constant A is proportional to e^2, hence K is proportional to r_∞. That there is a linear relation between K and r_∞ is shown by fig. 3. The curves indicate that the value K_0, that is the maximum value of the evaporation factor, is reached before $r_{\infty_{100}}$ equals r_{∞_0}. This must be the maximum possible value at 100 per cent. humidity for the one type of surface. Hence when K and r_∞ reach

their maximum values k_1 and k_3 are zero together. There can be no deposition of moisture at zero humidity.

Fig. 3.

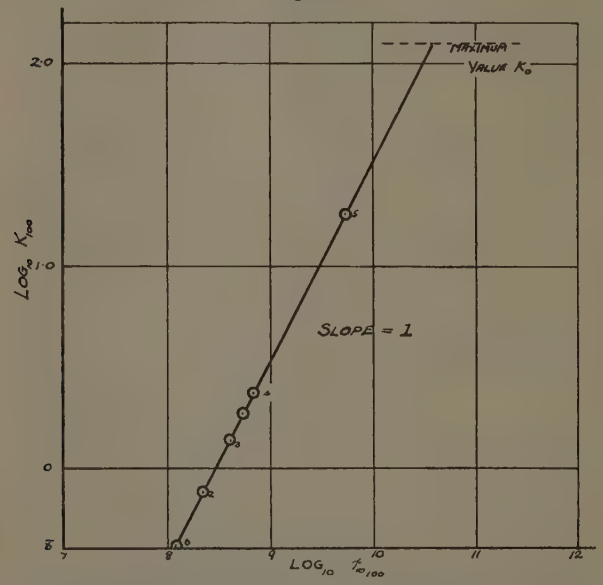

Showing the linear relation between the values of K_{100} and the final resistivity $r_{\infty 100}$. Logarithmic values are plotted for convenience.

Table III.

Values obtained for the Initial Resistivity r_0.

Standard form of equation : $r_0 = r'_{0_{100}} \epsilon^{k_4(1-h)} + c\,\epsilon^{k_5(1-h)}$.

Surface condition.	Value of $r'_{0_{100}}$.	Values of indices.		
		k_4.	k_5.	c.
1	$2{\cdot}134 \times 10^8$	3·773	8·465	0·2158
2	$0{\cdot}820 \times 10^8$	4·723	8·0	0·1759
3	$1{\cdot}337 \times 10^8$	4·173	8·25	0·1980
4	$3{\cdot}066 \times 10^8$	3·232	8·68	0·2776
6	$0{\cdot}403 \times 10^8$	5·975	7·65	0·1443

These results are given in fig. 4, which clearly shows that there are relations between the indices and the values of the resistivity r_0 for which they occur.

In a similar manner it can be shown that all the indices and the values of K, r_0, r_∞ are interrelated by exponential functions, indicating that the physical properties of the film remain constant for each surface condition.

Fig. 4.

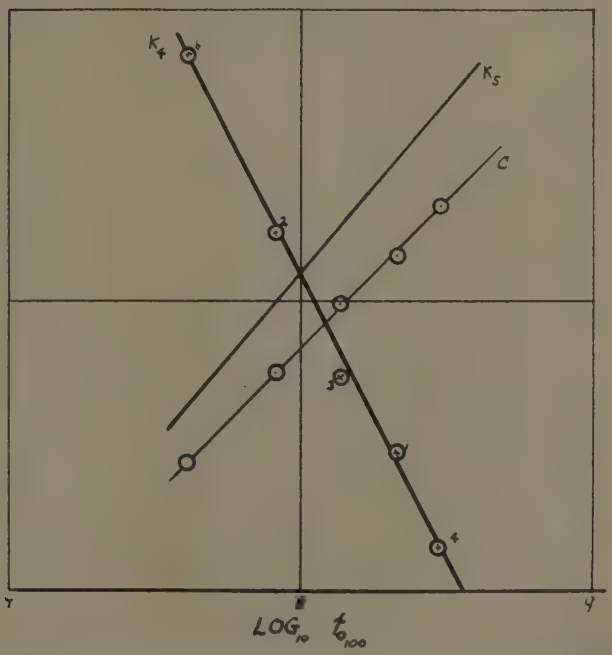

Showing the relations between the indices k_4, k_3, c, and the values of the initial resistivity at which they occur.

Surface Temperature.

Under stationary conditions of humidity, surface state, and temperature the surface film is stable and has fixed physical properties. There is a constant rate of deposition of moisture A and a constant rate of evaporation K from the surface. Raising the surface temperature is equivalent to establishing conditions of varying

humidity close to the film, due to the evaporation caused by the temperature changes, while the surrounding air maintains the fixed humidity value and A is constant. A small change of surface temperature dT produces a small equivalent change in the surface film such as that which would be caused by a small change of humidity dh, and over a small comparative range of temperatures, $d\mathrm{T}/dh =$ a constant. Changes in the rate of evaporation factor K which are produced by a change of humidity dh are also produced by a change of temperature dT. And as the relation between K and the humidity is expressed by the equation $\mathrm{K}=\mathrm{K}_{100}\epsilon^{k_1(1-h)}$, changes in K due to changes of surface temperature are expressed by $\mathrm{K}_{\mathrm{T}_1}=\mathrm{K}_{\mathrm{T}_0}\epsilon^{m(\mathrm{T}_1-\mathrm{T}_0)}$, for as the temperature T_1 increases $\mathrm{K}_{\mathrm{T}_1}$ will increase in value. m is a constant whose value has yet to be determined experimentally.

Under the conditions expressed by $\mathrm{A}=\mathrm{K}e^2/r_\infty$ if the humidity of the surrounding air and the applied voltage are constant A and e are constant. So for a small change of surface temperature the relation becomes $\mathrm{A}=e^2/r_\infty \times \mathrm{K}_{\mathrm{T}_0}\epsilon^{m(\mathrm{T}_1-\mathrm{T}_0)}$, or $r_\infty = \dfrac{\mathrm{K}_{\mathrm{T}_0}e^2}{\mathrm{A}}\epsilon^{m(\mathrm{T}_1-\mathrm{T}_0)}$. But $\dfrac{\mathrm{K}_{\mathrm{T}_0}e^2}{\mathrm{A}} = r_{\infty\mathrm{T}_0}$, the value of the final resistivity at the temperature T_0, so $r_{\infty\mathrm{T}_1} = r_{\infty\mathrm{T}_0}\epsilon^{m(\mathrm{T}_1-\mathrm{T}_0)}$, and the value of r_∞ will increase exponentially with the surface temperature.

The expression $\mathrm{A}\lessgtr\mathrm{K}e^2/r_0$ leads to the establishment of the relation $\mathrm{K}e^2/r_0=\mathrm{BA}$, where B is a constant for each case. The value of B will be $1\geqslant\mathrm{B}\geqslant 0$, depending on the humidity and the surface state. From this $r_0 = \dfrac{\mathrm{K}_{\mathrm{T}_0}e^2}{\mathrm{BA}}\epsilon^{m(\mathrm{T}_1-\mathrm{T}_0)}$ and r_0 varies exponentially with the surface temperature.

From tests on the surface of glass Smail, Brooksbank, and Thornton * have given the law of change of the surface resistivity with respect to the surface temperature in the form $r=r\epsilon^{m(\mathrm{T}_1-\mathrm{T}_0)}$. The values given are those for the initial resistivity r_0.

Conclusion.

The above experimental results and their analyses show clearly that the leakage film, if continuous, has two

* Journ. I. E. E. lxix. (1931).

components, one adsorbed and the other a surface solution. The proportional equilibrium between these two parts remains constant throughout the changes produced by voltage stress and by changes of temperature. The very definite exponential characteristics are direct evidence of this condition.

The research was carried out in the Electrical Engineering Laboratory at Armstrong College, Newcastle-on-Tyne, and the author wishes to thank Professor Thornton for his constant advice and interest.

LXXII. *Conditions under which Functions are Measurable, Integrable, and Differentiable.* By W. Fabian, *M.A.*, *Ph.D.**

1. *Introduction.*

TO obtain conditions under which functions of a complex variable are measurable, differentiable, and integrable in the sense of Lebesgue †, we introduce here the notions of absolute continuity and bounded variation, used so far for functions of a real variable.

Let L be a bounded simple curve joining z_0 and Z, which is defined by

$$z=x+iy=x(t)+iy(t)$$

in the finite interval $(t_0 \leqslant t \leqslant \mathrm{T})$; where $z=z_0$ when $t=t_0$, and $z=\mathrm{Z}$ when $t=\mathrm{T}$.

Definition of Absolute Continuity.

A function $f(z)$, defined on L, will be said to be absolutely continuous on L, if, corresponding to an arbitrarily chosen positive number ϵ, another positive number η can be so determined that, in every enumerable or finite set of non-overlapping intervals (t_r, t_r') in (t_0, T) and such that the total measure of the intervals is less than η, the sum, or limiting sum,

$$\sum_{r=1} \left| f(z_r)-f(z_r') \right| < \epsilon,$$

* Communicated by the Author.

† Fabian, Phil. Mag. ser. 7, vol. xxii. pp. 523–534, 1117–1122 (1936); vol. xxiv. pp. 256–262 (1937).

where z_r and z'_r are points on L of t-parameters t_r and t'_r respectively.

Definition of Bounded Variation.

Let (t_0, T) be divided into a number of parts (t_0, t_1), (t_1, t_2), ... (t_{r-1}, t_r), ... (t_{n-1}, t_n), where $t_n = T$, these parts forming a net of closed meshes. If

$$\sum_{r=1}^{n} | f(z_r) - f(z_{r-1}) |$$

is less than some fixed positive number, for all possible nets, where z_r and z_{r-1} are points on L of t-parameters t_r and t_{r-1} respectively, then $f(z)$ will be said to be of bounded variation on L.

The following two theorems follow almost immediately :—

Theorem 1.—*The necessary and sufficient conditions that* $f(z)$ *may be absolutely continuous on* L *are that the real and imaginary parts of* $f(z)$ *should be absolutely continuous in* (t_0, T).

Theorem 2.—*The necessary and sufficient conditions that* $f(z)$ *may be of bounded variation on* L *are that the real and imaginary parts of* $f(z)$ *should be of bounded variation in* (t_0, T).

For, on L let $f(z) = \theta(t) = \theta_1(t) + i\theta_2(t)$, where $\theta_1(t)$ and $\theta_2(t)$ are real. Then, for any set of intervals (t_r, t'_r) in (t_0, T),

$$\sum_{r=1} | \theta_1(t_r) - \theta_1(t'_r) | \leqslant \sum_{r=1} | \theta(t_r) - \theta(t'_r) |$$

$$\leqslant \sum_{r=1} | \theta_1(t_r) - \theta_1(t'_r) | + \sum_{r=1} | \theta_2(t_r) - \theta_2(t'_r) |$$

and

$$\sum_{r=1} | \theta_2(t_r) - \theta_2(t'_r) | \leqslant \sum_{r=1} | \theta(t_r) - \theta(t'_r) | .$$

From these inequalities the above two theorems follow.

2. *Conditions under which Functions are Measurable, Integrable, and Differentiable.*

Throughout all that follows in the present paper the curve L is to be such that it can be broken up into a finite number of bounded simple curves, for each of which $x(t)$ and $y(t)$ are monotonic functions of t.

A. *Theorem* 3.—*The necessary and sufficient condition that a function* F(z) *may be an indefinite integral along* L *is that it should be absolutely continuous on* L.

Proof.—I. To prove the above condition necessary, suppose that, on L,

$$F(z)=F(z_0)+\int_{z_0}^{z} f(z)dz,$$

where the Lebesgue integral, taken along L, exists everywhere on L. By a previous theorem *,

$$F(z)=F(z_0)+\int_{t_0}^{t} f(z)\frac{dz}{dt}\,dt,$$

where the integral is taken over (t_0, t) in (t_0, T).

The real and imaginary parts of F(z) can now be seen to be indefinite integrals in (t_0, T), and hence † are absolutely continuous in (t_0, T). By Theorem 1, F(z) is absolutely continuous on L.

II. To prove the condition sufficient, suppose that F(z) is absolutely continuous on L. By Theorem 1, the real and imaginary parts of F(z) are absolutely continuous in (t_0, T), and hence † are indefinite integrals in (t_0, T). Therefore, for all points z on L,

$$F(z)=F(z_0)+\int_{t_0}^{t} \phi(t)dt,$$

where the integral of $\phi(t)$ is taken over (t_0, t) in (t_0, T). By a previous theorem ‡,

$$F(z)=F(z_0)+\int_{z_0}^{z} \phi(t)\frac{dt}{dz}\,dz,$$

where the integral is taken along L.

The theorem is proved.

Theorem 4.—*A function of bounded variation on* L *has a finite differential coefficient along* L *almost everywhere on* L.

Proof.—Let $f(z)=P+iQ$, where P and Q are real, have bounded variation on L. Then, by Theorem 2, P and Q have bounded variation in (t_0, T). Hence $\frac{dP}{dt}$ and $\frac{dQ}{dt}$, and

* Fabian, Phil. Mag. ser. 7, vol. xxiv. p. 256 (1937).

† Hobson, ' Theory of Functions of a Real Variable,' vol. i. p. 545 (1921).

‡ Fabian, Phil. Mag. ser. 7, vol. xxiv. p. 256 (1937).

consequently $\frac{df(z)}{dt}$, exist as finite numbers almost everywhere in (t_0, T).

Now, $\frac{df(z)}{dt} \cdot \frac{dt}{ds} \cdot \frac{ds}{dz}$ (along L) $= \frac{df(z)}{dz}$ (along L),

where s is the length of the arc $(z_0 z)$ of L. Since t, $x(t)$ and $y(t)$ are monotonic functions of s on the s-segment corresponding to L, therefore $\frac{dt}{ds}$, $\frac{dx(t)}{ds}$, and $\frac{dy(t)}{ds}$ exist as finite numbers almost everywhere on this s-segment.

Since $$\frac{ds}{dz}(\text{along L}) = \frac{1}{\frac{dx}{ds} + i\frac{dy}{ds}},$$

where $\left(\frac{dx}{ds}\right)^2 + \left(\frac{dy}{ds}\right)^2 = 1$, it follows that $\frac{ds}{dz}$ (along L) is never infinite on L, and it exists almost everywhere on L, since, as shown, $\frac{dx(t)}{ds}$ and $\frac{dy(t)}{ds}$ exist almost everywhere on the s-segment corresponding to L.

The conclusion follows.

Theorem 5.—*If a function is continuous on* L *for variations of* z *along* L, *and has a finite differential coefficient along* L *almost everywhere on* L, *then this differential coefficient along* L *is measurable on* L.

Proof. $$\frac{df(z)}{ds} = \frac{df(z)}{dz} \cdot \frac{dz}{ds}(\text{along L}),$$

where s is the length of the arc $(z_0 z)$ of L.

Thus it can be seen that

$$\frac{df(z)}{ds} \equiv \frac{dP}{ds} + i\frac{dQ}{ds},$$

where P and Q are real, exists almost everywhere on the s-segment corresponding to L. And since P and Q are continuous on this s-segment, therefore * $\frac{dP}{ds}$ and $\frac{dQ}{ds}$, and hence $\frac{df(z)}{ds}$, are measurable on this s-segment.

* Hobson, ' Theory of Functions of a Real Variable,' vol. i. p. 538 (1921).

Now

$$\frac{df(z)}{dz}\ (\text{along L}) = \frac{df(z)}{ds}\cdot\frac{ds}{dz}\ (\text{along L})$$

$$= \frac{df(z)}{ds}\left(\frac{dx}{ds} - i\frac{dy}{ds}\right).$$

Since $x(t)$ and $y(t)$ are continuous functions of s on the s-segment corresponding to L, therefore * $\frac{dx}{ds}$ and $\frac{dy}{ds}$ are measurable on this s-segment. Since, as shown, $\frac{df(z)}{ds}$ is also measurable on this s-segment, therefore $\frac{df(z)}{dz}$ (along L) is so, and hence the conclusion.

Theorem 6.—*If* F(z) *is continuous on* L *for variations of z along* L, *and is of bounded variation on* L, *then* $\frac{dF(z)}{dz}$ (*along* L) *is integrable along* L.

Proof.—Let $F(z)=u+iv$, where u and v are real. Then u and v are continuous in (t_0, T), and, by Theorem 2, are of bounded variation in (t_0, T). Consequently, $\frac{du}{dt}$ and $\frac{dv}{dt}$ exist almost everywhere in (t_0, T), and

$$\int_{t_0}^{T}\frac{du}{dt}\,dt + i\int_{t_0}^{T}\frac{dv}{dt}\,dt = \int_{t_0}^{T}\frac{dF(z)}{dt}\,dt,$$

taken over (t_0, T), exists as a finite number †. By a previous theorem ‡

$$\int_{t_0}^{T}\frac{dF(z)}{dt}\,dt = \int_{L}\frac{dF(z)}{dt}\cdot\frac{dt}{dz}\,dz$$

$$= \int_{L}\frac{dF(z)}{dz}\,dz,$$

whence the conclusion follows.

---

* Hobson, ' Theory of Functions of a Real Variable,' vol. i. p. 538 (1921).

† Hobson, ' Theory of Functions of a Real Variable,' vol. i. p. 543 (1921).

‡ Fabian, Phil. Mag. ser. 7, vol. xxiv. p. 256 (1937).

We wish also to state the following :—

Theorem 7.—An indefinite integral along L *is measurable and of bounded variation on* L.

For, if $F(z)=F(z_0)+\int_{z_0}^{z} f(z)dz$ be an indefinite integral along L, then, by a previous theorem *,

$$F(z)=F(z_0)+\int_{t_0}^{t} f(z)\frac{dz}{dt}\,dt,$$

where the integral is taken over $(t_0,\ t)$ in $(t_0,\ T)$. The real and imaginary parts of $F(z)$, being indefinite integrals and continuous functions in $(t_0,\ T)$, are therefore measurable and of bounded variation in $(t_0,\ T)$. The conclusion follows by previous theorems †.

B. Let l be an arc (z_0Z') of L, for which $x(t)$ and $y(t)$ are monotonic functions of t. Let $G(l)$ be a fixed measurable set of points on l, and let $E(l)$ be that component which consists of all points of $G(l)$ on the arc corresponding to $(t_0,\ t)$. Let Ω be the curve traced out in the w-plane by the point

$$w=\pm m(E_x)\pm im(E_y),$$

as $E(l)$ varies simply ‡ in $G(l)$ with respect to t ; where $m(E_x)$ and $m(E_y)$ are the measures of E_x and E_y, the sets of points corresponding to $E(l)$ on the x- and y-segments respectively ; the positive or negative signs in $\pm m(E_x)$ are taken, according as $x(t)$ is a non-diminishing or non-increasing function of t on the t-segment corresponding to l, and the positive or negative signs in $\pm im\ (E_y)$ are taken, according as $y(t)$ is a non-diminishing or non-increasing function of t on this t-segment.

A function $f(z)$, defined in $G(l)$, will be said to be absolutely continuous in $G(l)$, if the function $\chi(w)=f(z)$ is absolutely continuous on Ω.

A function $f(z)$, defined in $G(l)$, will be said to be of bounded variation in $G(l)$, if the function $\chi(w)=f(z)$ is of bounded variation on Ω.

* Fabian, Phil. Mag. ser. 7, vol. xxiv. p. 256 (1937).
† *Loc. cit.*
‡ Fabian, Phil. Mag. ser. 7, vol. xxii. p. 528 (1936).

We have shown* that, if $f(z)$ is measurable in $G(l)$ †, then

$$\int_{E(l)} f(z)dz = \int_0^w \chi(w)dw,$$

taken along Ω, where $f(z)=\chi(w)$, if either of these integrals exists.

Also, we have defined ‡ the generalized differential coefficient $D\phi\{E(l)\}$ of a function $\phi\{E(l)\}$ with respect to $E(l)$ by

$$D\phi\{E(l)\} = \frac{d\psi(w)}{dw} \text{ (along } \Omega),$$

where $\phi\{E(l)\}=\psi(w)$, if the latter differential coefficient exists.

It will now be seen that, with the previous results obtained § with regard to Ω, theorems 3 to 7 in the present paper, established here for the curve L, can be extended to hold for the set $G(l)$ by applying these theorems to the curve Ω.

Doing this, we obtain :—

Theorem 8.—*The necessary and sufficient condition that a function* $\phi\{E(l)\}$ *may be a generalized indefinite integral over* $E(l)$ *in* $G(l)$ *is that it should be absolutely continuous in* $G(l)$.

Theorem 9.—*A function* $\phi\{E(l)\}$ *of bounded variation in* $G(l)$ *has a finite generalized differential coefficient with respect to* $E(l)$ *almost everywhere in* $G(l)$.

Theorem 10.—*If* $\phi\{E(l)\}$ *is a continuous function of* $E(l)$ *in* $G(l)$, *and has a finite generalized differential coefficient with respect to* $E(l)$ *almost everywhere in* $G(l)$, *then this generalized differential coefficient is measurable in* $G(l)$.

Theorem 11.—*If* $\phi\{E(l)\}$ *is a continuous function of* $E(l)$ *in* $G(l)$, *and is of bounded variation in* $G(l)$, *then* $D\phi\{E(l)\}$ *is integrable over* $G(l)$.

Theorem 12.—*The generalized indefinite integral* $\phi\{E(l)\}$ *of a measurable function over* $E(l)$ *in* $G(l)$ *is measurable and of bounded variation in* $G(l)$.

* Fabian, Phil. Mag. ser. 7, vol. xxii. p. 531 (1936).
† This condition could have been omitted in the enunciation.
‡ Fabian, Phil. Mag. ser. 7, vol. xxii. p. 532 (1936).
§ Fabian, Phil. Mag. ser. 7, vol. xxii. pp. 528–532 (1936).

LXXIII. *On Einstein's Gravitational Field Equations.* *By* Ludwik Silberstein, *Ph.D.*†

I. *Non-Existence of Variable Radially Symmetrical Solutions in Empty Space.*

THE purpose of Part I. of this paper is to prove that Einstein's field-equations in empty space ($T_{\iota\kappa}=0$) do not admit any radially (spherically) symmetrical solutions varying in time; in other words, that the solutions of this kind are necessarily statical ‡.

The most general radially symmetrical line-element can be reduced to the form

$$ds^2=g_1dr^2-r^2(d\phi^2+\sin^2\phi\,d\theta^2)+g_4dt^2, \quad . \quad . \quad (1)$$

where g_1 and g_4 are functions of r and t.

Write $h_1=\log(-g_1)$, $h_4=\log g_4$. Then, coordinating the indices 1, 2, 3, 4, with r, ϕ, θ, t respectively, the only surviving components $R_{\iota\kappa}$ of the contracted curvature tensor are R_{11}, R_{22}, R_{33}, R_{44}, and R_{14}, to wit,

$$R_{11}=(R_{11})+\frac{1}{2}\frac{g_1}{g_4}\left\{\frac{\partial^2h_1}{\partial t^2}+\frac{1}{2}\frac{\partial h_1}{\partial t}\frac{\partial(h_1-h_4)}{\partial t}\right\},$$

where (R_{11}) is the well-known value of R_{11} when $g_{11}g_4$ are independent of t, and

$$-g_1R_{22}=-\frac{g_1}{\sin^2\phi}R_{33}=1+g_1+\frac{r}{2}\frac{\partial}{\partial r}(h_4-h_1),$$

$$\frac{g_1}{g_4}R_{44}=R_{11}+\frac{1}{r}\frac{\partial}{\partial r}(h_1+h_4), \qquad R_{14}=-\frac{1}{r}\frac{\partial h_1}{\partial t}.$$

Thus, Einstein's field-equations in empty space (except at the centre $r=0$) become

$$(R_{11})+\frac{g_1}{2g_4}\left\{\frac{\partial^2h_1}{\partial t^2}+\frac{1}{2}\frac{\partial h_1}{\partial t}\frac{\partial}{\partial t}(h_1-h_4)\right\}=0, \quad . \quad (a)$$

$$1+g_1+\frac{r}{2}\frac{\partial}{\partial r}(h_4-h_1)=0, \quad . \quad . \quad . \quad . \quad (b)$$

† Communicated by the Author.

‡ I have communicated this result, with its derivation, to Dr. Einstein in a private letter of December 1933.

$$\frac{1}{r}\frac{\partial}{\partial r}(h_1+h_4)=0, \quad \ldots\ldots \quad (c)$$

$$\frac{\partial t}{\partial h_1}=0. \quad \ldots\ldots \quad (d)$$

By (c), $h_1+h_4\equiv\log(-g_1g_4)=f(t)=\log \mathrm{F}(t)$, say, whence

$$g_1=-\frac{\mathrm{F}(t)}{g_4}, \quad \ldots\ldots \quad (2)$$

where $\mathrm{F}(t)$ is an undetermined function of t. Since $\frac{\partial h_1}{\partial r}=-\frac{\partial h_4}{\partial r}$, (b) becomes $\frac{\partial}{\partial r}\log[rg_4-r\mathrm{F}(t)]=0$, whence

$$g_4=\mathrm{F}(t)+\frac{1}{r}\mathrm{G}(t), \quad \ldots\ldots \quad (3)$$

where $\mathrm{F}(t)$, $\mathrm{G}(t)$ are to be determined from (a) or, more simply, from (d), which gives $\partial g_1/\partial t=0$. Thus, by (2),

$$\frac{\partial}{\partial t}[g_4/\mathrm{F}(t)]=0,$$

i. e., by (3),

$$\frac{\mathrm{G}(t)}{\mathrm{F}(t)}=\text{const.}=-2\mathrm{L}, \text{ say.}$$

Thus $\quad g_4=\mathrm{F}(t)\left(1-\frac{2\mathrm{L}}{r}\right), \quad g_1=\left(1-\frac{2\mathrm{L}}{r}\right)^{-1}, \quad \ldots \quad (4)$

where $\mathrm{F}(t)$ remains a perfectly arbitrary function of t and $\mathrm{L}(=\mathrm{M}/c^2$, say) an arbitrary *constant*.

Equation (a) can now be shown to be satisfied identically by (4), no matter what the form of $\mathrm{F}(t)$.

This, then, *i. e.* (4) with (1), is the most general radially symmetrical field in empty space. The remarkable result is that $\mathrm{G}(t)/\mathrm{F}(t)$ is necessarily a constant.

Introducing $\tau=\int\sqrt{\mathrm{F}(t)}\,dt$ as time, we now have

$$ds^2=\left(1-\frac{2\mathrm{L}}{r}\right)d\tau^2-\left(1-\frac{2\mathrm{L}}{r}\right)^{-1}dr^2-r^2(d\phi^2+\sin^2\phi\,d\theta^2), \quad \ldots \quad (5)$$

i. e., a *statical* field (Schwarzschild-field) around a mass centre of necessarily *constant mass* $c^2\mathrm{L}$.

This is the announced result, a peculiar property of Einstein's field equations. The field around our Sun, for instance, whose mass decreases every second by several millions of tons, cannot be represented by Einstein's equations, unless one wished to fill the surrounding space with "matter," possibly the energy of its own radiation.

No such excuse or remedy, however, is possible in the axially symmetrical case, to be treated in Part II.

At any rate, the remarkable result is that Einstein's theory admits no variable field in empty space around a spherical body. On the classical, Newtonian theory, a field of potential $M(t)/r$, where M is any function of the time, offers no difficulty, just as one with M=const. By Einstein's theory, no such field, reducing approximately to $M(t)/r^2$, is provided.

A somewhat similar state of affairs prevails in the more general case of axial symmetry, as will be shown in Part II. of this paper.

II. *Non-Existence of Variable Axially Symmetrical Solutions, of Form* (1*), *in Empty Space.*

Let us first recall that the most general *statical* axially symmetrical solution, in empty space, has been proved by Levi-Civita and others to be of the form

$$ds^2=e^{2\nu}dt^2-e^{-2\nu}[e^{2\lambda}(dx_1^2+dx_2^2)+x_1^2dx_3^2],$$

where ν, λ are functions of x_1, x_2 only, the former any solution of Laplace's equation $\nabla^2\nu=0$ and the latter satisfying the conditions

$$\frac{\partial\lambda}{\partial x_1}=x_1\left[\left(\frac{\partial\nu}{\partial x_1}\right)^2-\left(\frac{\partial\nu}{\partial x_2}\right)^2\right] \quad \text{and} \quad \frac{\partial\lambda}{\partial x_2}=2x_1\frac{\partial\nu}{\partial x_1}\frac{\partial\nu}{\partial x_2}.$$

Now, without asserting that this line-element, but with ν, λ depending on t also, represents the most general axially symmetrical field, I propose to investigate all solutions of the field-equations outside of matter, of the form

$$ds^2=e^{2\nu}dt^2-e^{2(\lambda-\nu)}(dx_1^2+dx_2^2)-x_1^2e^{-2\nu}dx_3^2, \quad . \quad (1^*)$$

where ν and λ are functions not only of x_1, x_2, *but also of the time* t or x_4 ($c=1$).

Of the ten components of the curvature tensor three vanish identically, and the remaining seven, R_{11}, R_{22}, R_{33}, R_{44}, R_{14}, R_{24}, R_{12}, equated to zero, give for the two unknown functions

$$g_{44} \equiv g_4 = e^{2\nu} \quad (h_4 = \log g_4 = 2\nu)$$

and $$g_{11} \equiv g_1 = e^{2(\lambda-\nu)} \quad [h_1 = \log(-1) + 2\lambda - 2\nu],$$

the following seven differential equations :

$$\frac{\partial\lambda}{\partial x_1} = \frac{x_1}{4}\left[\left(\frac{\partial h_4}{\partial x_1}\right)^2 - \left(\frac{\partial h_4}{\partial x_2}\right)^2\right], \quad . \quad . \quad . \quad (11)$$

$$\frac{\partial\lambda}{\partial x_2} = \frac{x_1}{2}\frac{\partial h_4}{\partial x_1}\frac{\partial h_4}{\partial x_2}, \quad . \quad . \quad . \quad . \quad . \quad . \quad (12)$$

$$\nabla^2 h_1 + \left(\frac{\partial h_4}{\partial x_2}\right)^2 + \frac{\partial}{\partial x_4}\left(\frac{g_1}{g_4}\frac{\partial h_1}{\partial x_4}\right) = 0, \quad . \quad . \quad (22)$$

$$\nabla^2 h_4 + \frac{g_1}{g_4}\left\{\frac{\partial^2 h_1}{\partial x_4^2} + \frac{1}{2}\left(\frac{\partial h_1}{\partial x_4}\right)^2\right\} = 0, \quad . \quad . \quad (33)$$

$$\frac{\partial^2(h_1 - h_4)}{\partial x_4^2} + \frac{1}{2}\left[\frac{\partial(h_1 - h_4)}{\partial x_4}\right]^2 + \frac{1}{2}\left(\frac{\partial h_4}{\partial x_4}\right)^2 = 0, \quad (44)$$

$$\frac{\partial\lambda}{\partial x_4} = \frac{x_1}{2}\left[\frac{\partial h_4}{\partial x_1}\frac{\partial h_4}{\partial x_4} + \frac{\partial^2(h_1 - h_4)}{\partial x_1 \partial x_4}\right], \quad . \quad . \quad (14)$$

$$\frac{\partial h_4}{\partial x_4}\frac{\partial h_4}{\partial x_2} + \frac{\partial^2(h_1 - h_4)}{\partial x_2 \partial x_4} = 0, \quad . \quad . \quad . \quad (24)$$

where

$$\nabla^2 = \frac{\partial^2}{\partial x_1^2} + \frac{1}{x_1}\frac{\partial}{\partial x_1} + \frac{\partial^2}{\partial x_2^2}.$$

The equations (11) and (12) are exactly the same as in the statical sub-case.

The identity $\frac{\partial}{\partial x_2}(11) = \frac{\partial}{\partial x_1}(12)$ gives, after simple reductions, $x_1 \nabla^2 h_4 = 0$, *i. e.*, outside the axis at least,

$$\nabla^2 h_4 = 0. \quad . \quad . \quad . \quad . \quad . \quad . \quad . \quad (2)$$

We have also, from (11) and (12),

$$\nabla^2 h_1 + \left(\frac{\partial h_4}{\partial x_2}\right)^2 = 0. \quad . \quad . \quad . \quad . \quad . \quad (3)$$

In virtue of (2) and (3) our seven equations can now be written, more conveniently,

$$\text{(I.)}\quad \frac{\partial\lambda}{\partial x_1}=\frac{x_1}{4}\left[\left(\frac{\partial h_4}{\partial x_1}\right)^2-\left(\frac{\partial h_4}{\partial x_2}\right)^2\right];$$

$$\text{(II.)}\quad \frac{\partial\lambda}{\partial x_2}=\frac{x_1}{2}\frac{\partial h_4}{\partial x_1}\frac{\partial h_4}{\partial x_2};$$

$$\text{(III.)}\quad \frac{\partial}{\partial t}\left(\frac{g_1}{g_4}\frac{\partial h_1}{\partial t}\right)=0;$$

$$\text{(IV.)}\quad \frac{\partial^2 h_1}{\partial t^2}+\frac{1}{2}\left(\frac{\partial h_1}{\partial t}\right)^2=0;$$

$$\text{(V.)}\quad \frac{\partial^2}{\partial t^2}(h_1-h_4)+\frac{1}{2}\left[\frac{\partial}{\partial t}(h_1-h_4)\right]^2+\frac{1}{2}\left(\frac{\partial h_4}{\partial t}\right)^2=0;$$

$$\text{(VI.)}\quad \frac{\partial\lambda}{\partial t}=\frac{x_1}{2}\left[\frac{\partial h_4}{\partial x_1}\frac{\partial h_4}{\partial t}+\frac{\partial^2(h_1-h_4)}{\partial x_1\partial t}\right];$$

$$\text{(VII.)}\quad \frac{\partial h_4}{\partial t}\frac{\partial h_4}{\partial x_2}+\frac{\partial^2(h_1-h_4)}{\partial x_2\partial t}=0.$$

The equations (2) and (3) are consequences of (I.) and (II.).

In the first place one would naturally look for solutions representing the case of two or more mass-centres moving along the axis. Now, the Laplacean equation (2) can be satisfied by

$$h_4=-\frac{2L_1}{r_1}-\frac{2L_2}{r_2}-\ldots,$$

where L_1, L_2, etc., may be constants or, also, functions of the time, while r_1, r_2, etc., are the distances of a general field-point from centres moving along the axis of symmetry ($x_1=0$). Their motion, one might think, should be determinable by the remaining equations. But here one finds oneself strangely disappointed.

In fact, consider, *e. g.*, the case of two mass-centres. Let their coordinates be $x_1=0$ and $x_2=a(t)$ and $x_2=b(t)$, *i. e.*,

$$2v\equiv h_4=-\frac{2L_1}{r_1}-\frac{2L_2}{r_2},\quad r_1^2=x_1^2+(x_2-a)^2,$$
$$r_2^2=x_2^2+(x_2-b)^2,$$

where a and b are to be determined as functions of the time.

Now, by (IV.), we have either $\partial h_1/\partial t=0$ or

$$h_1 \equiv 2(\lambda-\nu)+\text{const.}=2\log(t+\gamma)+\zeta, \quad . \quad . \quad (4)$$

where γ, ζ are functions of x_1, x_2.

On the other hand, we can write down λ and thence h_1 at once so as to satisfy (I.) and (II.) with the above h_4, namely, as in a previous paper †, but adding now an arbitrary function of t alone, and writing $D^2=(a-b)^2$,

$$h_1=\frac{2L_1}{r_1}+\frac{2L_2}{r_2}-x_1^2\left(\frac{L_1^2}{r_1^4}+\frac{L_2^2}{r_2^4}\right)+\frac{4L_1L_2}{D^2}\left(\frac{r_1^2+r_2^2-D^2}{2r_1r_2}-1\right)+\Psi(t).$$

But this cannot be made compatible with the form (4) of the function h_1 claimed by (IV.), unless $\partial h_1/\partial t=0$; but then also $\partial h_4/\partial t=0$, and we are thrown back upon the statical case.

We thus see that even the three equations (I.), (II.), (III.) alone are compatible with each other only for fixed, not for moving mass-centres.

In fine, the case of moving mass-centres *cannot be represented by any solution of the form* (1*). This result itself seems to be noteworthy.

But it is not at all difficult to find *the most general* field (λ, ν) satisfying all seven equations, (I.) to (VII.). In other words, this apparently formidable system of non-linear partial differential equations can be completely integrated.

In fact, by (III.),

$$\frac{g_1}{g_4}\frac{\partial h_1}{\partial t}=\alpha(x_1, x_2), \quad . \quad . \quad . \quad . \quad [\text{III.}]$$

and by (IV.), unless $\partial h_1/\partial t=0$,

$$\frac{\partial h_1}{\partial t}=\frac{2}{t+\beta(x_1, x_2)}, \quad . \quad . \quad . \quad . \quad [\text{IV.}]$$

where α, β are some functions of x_1, x_2. Thus,

$$\frac{g_1}{g_4}=\frac{\alpha}{2}.(t+\beta), \quad . \quad . \quad . \quad [\text{III., IV.}]$$

† L. Silberstein, Phys. Review, Feb. 1, 1936, formula (10).

whence $h_4=\log\gamma(x_1, x_2)\pm\log(t+\beta)$ and, correspondingly, either

$$g_4=\gamma.(t+\beta)$$

or

$$g_4=\gamma/(t+\beta),$$

where γ depends only on x_1, x_2, and by [III., IV.], either

$$g_1=\frac{\alpha\gamma}{2}(t+\beta)^2$$

or

$$g_1=\alpha\gamma/2.$$

But the latter is incompatible with (IV.), so that we are left with the former g_1-value only. Thus (VI.) becomes

$$\frac{x_1}{\gamma}\frac{\partial\gamma}{\partial x_1}=3,$$

whence

$$\gamma_1=x_1{}^3\,.\,\delta(x_2), \quad . \quad . \quad . \quad . \quad . \quad \text{(VI.)}$$

where δ is a function of x_2 only.

Equation (VII.) now gives, after some straightforward developments,

$$\frac{\partial\beta}{\partial x_2}+(t+\beta)\left[\frac{\delta'(x_2)}{\delta(x_2)}+\frac{1}{2}\frac{\partial\alpha}{\partial x_2}(t+\beta)\right]=0,$$

which is possible only if

$$\delta=\text{const. and } \alpha=\alpha(x_1), \text{ and thus also } \beta=\beta(x_1). \quad \text{(VII.)}$$

Notice that equation (V.) is identically satisfied by the above $\partial h_1/\partial t$ and h_4 (which gives $\partial h_4/\partial t=1/(t+\beta)=\frac{1}{2}\partial h_1/\partial t$).

Thus, and since without loss to generality we can put $\delta=1$, we have

$$\left.\begin{aligned} g_1&=\tfrac{1}{2}\alpha x_1{}^3\,.\,(t+\beta)^2, \quad \alpha=\alpha(x_1),\\ g_4&=x_1{}^3\,.\,(t+\beta), \qquad\quad \beta=\beta(x_1).\end{aligned}\right\} \quad \text{[III. to VII.]}$$

It remains to satisfy (I.) and (II.). Now, since $2\frac{\partial\lambda}{\partial x_2}=\frac{1}{\alpha}\frac{\partial\alpha}{\partial x_2}$ and $\partial h_4/\partial x_2=0$, (II.) becomes

$$\frac{\partial\alpha}{\partial x_2}=0, \quad \alpha=\alpha(x_1),$$

which we already know, so that, ultimately,

$$\text{(A)} \quad \left\{\begin{aligned} g_1&=\tfrac{1}{2}\alpha(x_1)x_1{}^3[t+\beta(x_1)]^2,\\ g_4&=\chi_1{}^3[t+\beta(x_1)],\end{aligned}\right\} \quad \text{[II. to VII.]}$$

a physically useless solution, viz,. *depending only on* x_1, t. Equation (I.), which now becomes

$$\frac{\partial \lambda}{\partial x_1} = \frac{x_1}{4}\left(\frac{\partial h_4}{\partial x_1}\right)^2,$$

would impose only a condition upon α and β as functions of x_1, which offers no interest. What matters is that (unless $\partial h_1/\partial t = 0$) *the field is independent of* x_2, the coordinate measured along the axis of symmetry.

The only alternative left is $\partial h_1/\partial t = 0$, *i. e.*

$$g_1 = g_1(x_1, x_2).$$

Then (III.) and (IV.) are satisfied identically. Equation (VI.) becomes, after simple reductions,

$$\frac{1}{\beta}\frac{\partial \beta}{\partial x_1} = \frac{1}{x_1},$$

whence

$$\beta = x_1 \gamma(x_2), \quad \ldots\ldots \quad \text{(VI.)}$$

and equation (VII.) gives at once $\partial\beta/\partial x_2 = 0$, so that also $\gamma = \text{const.}$, say $\gamma = 1$. Hence $\beta = x_1$ and

$$g_4 = \frac{x_1}{\alpha - t}, \quad \alpha = \alpha(x_1, x_2).$$

So far equations (III.), (IV.), (VI.), and (VII.), are taken care of.

It remains to satisfy the equations (I.), (II.), and (V.), which now are reduced to

$$\frac{\partial h_1}{\partial x_1} = \frac{x_1}{2(\alpha - t)^2}\left[\left(\frac{\partial \alpha}{\partial x_1}\right)^2 - \left(\frac{\partial \alpha}{\partial x_2}\right)^2\right] - \frac{1}{2x_1}, \quad \text{[I.]}$$

$$\frac{\partial h_1}{\partial x_2} = \frac{x_2}{(\alpha - t)^2}\frac{\partial \alpha}{\partial x_1}\frac{\partial \alpha}{\partial x_2}, \quad \ldots\ldots \quad \text{[II.]}$$

and

$$\frac{\partial^2 h_4}{\partial t^2} = \left(\frac{\partial h_4}{\partial t}\right)^2 \ldots\ldots \quad \text{[V.]}$$

But since $\partial h_1/\partial t = 0$, we have, by [II.], either $\partial\alpha/\partial x_1 = 0$ or $\partial\alpha/\partial x_2 = 0$, and by [I.], $\left(\frac{\partial \alpha}{\partial x_1}\right)^2 = \left(\frac{\partial \alpha}{\partial x_2}\right)^2$; hence $\frac{\partial \alpha}{\partial x_1} = \frac{\partial \alpha}{\partial x_2} = 0$, in fine, $\alpha = \text{const.}$, $\partial h_1/\partial x_2$, and

$$\frac{\partial h_1}{\partial x_1} = -\frac{1}{2x_1}, \quad h_1 = -\log \sqrt{x_1} + \text{const.},$$

i. e., $g_1 = \mathrm{A}/\sqrt{x_1}$, where A is a constant.

Equation (V.) is satisfied identically by the last-found function $g_4=x_1/(\alpha-t)$.

Ultimately, then, the assumption $\partial h_1/\partial t=0$ leads necessarily to

$$g_1=\frac{A}{\sqrt{x_1}}, \quad g_4=\frac{x_1}{\alpha-t}, \quad . \quad . \quad . \quad . \quad (B)$$

where A and α are constants, and the line-element in our present notation is

$$ds^2=g_1(dx_1^2+dx_2^2)-\frac{x_1}{g_4}dx_3^2+g_4\,dt^2. \quad . \quad . \quad (1')$$

In fine, we have either (A) or (B), and both are physically useless solutions, since they represent fields depending on t and x_1 only (not on x_2). If a field of the forms (1*) or (1′) is to depend on x_1 and x_2 as well, we must have both

$$\frac{\partial h_1}{\partial t}=0 \quad \text{and} \quad \frac{\partial h_4}{\partial t}=0,$$

i. e., *a statical field.*

And since the solutions (A) and (B) are physically inadmissible †, we may as well formulate our net result by saying that *the most general axially symmetrical field of the form* (1*) *in empty space is necessarily statical.*

We have, in Part I., derived the same result (without any restriction as to form) for spherically symmetrical fields, but the situation in the present case is more acute. For whereas a variable spherical field implies necessarily a centre of varying mass, which can be brought about only by mass streaming or radiation, and this excludes an empty surrounding, a variable cylindrical field can be associated, *e. g.*, with two centres of *constant* masses moving along their straight join (say, two dark stars), and the space surrounding them need not, therefore, contain any trace of matter or energy.

Toronto.
November, 1937.

† Not only because they would represent fields extending monotonously to infinity in both senses of the axis of symmetry, but also because, in (A), g_1 and g_4 increase indefinitely with t and, in (B), $g_1=\infty$ all along the axis and $g_4=\infty$ for $t=\alpha$.

LXXIV. *On the Calculation of Surface Tension from the Measurement of Sessile Drops.* *By* ALFRED W. PORTER, *D.Sc., F.R.S., Emeritus Professor in the University of London* *.

IN a paper by me on "The Calculation for Surface Tension from Experiment," the calculation was made by means of a correction curve for measurements of a sessile drop (see fig. 2 of that paper, Phil. Mag. (7) xv. p. 168). The portion for the correction curve from $\frac{h^2}{r^2}=0$ to $\frac{h^2}{r^2}=\cdot 14$ was determined by one of the usual approximate formulæ and the remainder was intercalated graphically between it and the values of Bashforth and Adams. I was unaware at the time that the whole of the "large drop" region can be derived from an important paper by C. H. Bosanquet (Phil. Mag., Feb. 1928), who employed a method more expeditious than that of Bashforth and Adams. This paper is not a particularly lucid one, and may easily be overlooked. By aid of it I have calculated the following table :—

$\frac{h^2}{r^2}$.	$\frac{1}{2}\frac{h^2}{r^2}-\frac{\beta^2}{r^2}$.	$\frac{\beta^2}{r^2}$.
·016965	·000639	·007843
·028017	·001316	·012692
·038173	·002037	·017050
·054954	·003286	·024191
·085153	·005402	·037174
·14470	·00752	·064819

These numbers cover a range of drop-width from infinity to the beginning of the tables of Bashforth and Adams.

It is important to notice that no gap is left to be filled in by graphical intercalation. Thus the value of Δ is determined with precision for all values of $\frac{h^2}{r^2}$ from zero to infinity, or, in other words for all sizes of drops.

The values of Δ which I previously adopted for the middle region of the curve turn out to be in defect at most by ·0006.

* Communicated by the Author.

LXXV. *Notices respecting New Books.*

Eclipses of the Sun and Moon. By Sir Frank Dyson and R. v. d. R. Woolley. International Series of Monographs on Physics. [Pp. i–vii+1–160.] (Oxford: Clarendon Press, 1937. Price 15*s*.)

AT first sight the inclusion of a book on eclipses of the sun and moon in a series of monographs on physics may well appear odd. Nevertheless, the chief interest of these phenomena to-day is probably physical because of the information about the state of matter in the sun's outer layers which total eclipses provide. Thus Sir Frank Dyson and Dr. Woolley have devoted less than half of their book to purely astronomical questions such as the calculations of the dates of eclipses, of the tracks on the earth's surface of solar eclipses, of the moon's secular acceleration, etc. The remainder is given up to a detailed study of the sun's chromosphere and corona based on the observations of their spectra and luminosities made during the few seconds of totality occurring in a total solar eclipse. The evidence for and against the various theories of the structure and composition of these solar regions is clearly and objectively presented. For the chromosphere, the authors themselves prefer M'Crea's turbulence theory to Milne's theory of radiation pressure. Similarly, they incline to Grotrian's dust-particle theory of the corona, whilst frankly recognizing its shortcomings. Their treatment of these and other matters will interest not only specialists but all those who, without following the mathematical arguments in detail, are curious to know something of the constitution of the sun and of the many problems its structure still presents.

[*The Editors do not hold themselves responsible for the views expressed by their correspondnets.*]

Fig. 1.

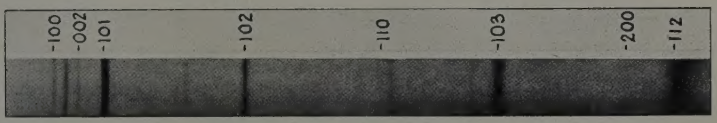

Fig. 2.

Fig. 3.

Fig. 4.

Fig. 5.

Figs. 1, 2, & 3.—X-ray spectra of hexagonal chromium plated on copper, showing changing intensity of lines due to orientation : least marked after 1 hr. (fig. 1), strong after $4\frac{3}{4}$ hrs. (fig. 2), and thereafter constant up to 48 hrs. (fig. 3).

Figs. 4 & 5.—Plated on nickel, showing final orientation after 17 hrs. (fig. 5), same as on copper.

Fig. 6.

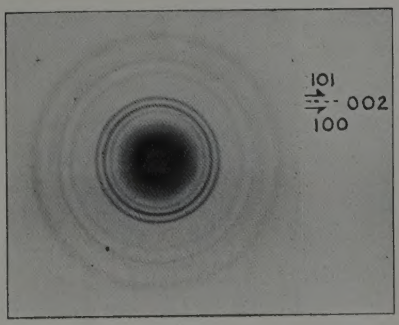

Fig. 7.

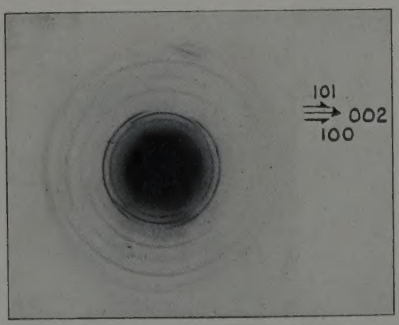

Fig. 6.—Transmission photograph, with incident beam normal to surface of deposit. Note (002) plane absent.

Fig. 7.—Transmission, with beam parallel to surface of deposit. Note, now, formation of maxima on rings.

These show orientation is random only about normal to surface of deposit with (002) in that surface.